Fabrication, Functionalities and Applications of Transparent Wood: A Review

Xin Hu[1a, b], Rujun Yu[1a, b], Faming, Wang[c], Zunfeng Liu[d], Hongyu Yang[e], Chaoji Chen[f], Yangling Li[g], Nuruzzaman Noor[a, b]*, Bin Fei [a, b]*

a Materials Synthesis and Processing Lab, School of Fashion and Textiles, The Hong Kong Polytechnic University, Hung Hom, Kowloon, Hong Kong SAR, China.

b Research Centre for Resources Engineering towards Carbon Neutrality, The Hong Kong Polytechnic University, Hung Hom, Kowloon, Hong Kong SAR, China.

c Department of Biosystems Engineering, Faculty of Bioscience Engineering, KU Leuven, Leuven, 3001, Belgium.

d State Key Laboratory of Medicinal Chemical Biology, Key Laboratory of Functional Polymer Materials, College of Chemistry, Nankai University, Tianjin, 300071, China

e College of Materials Science and Engineering, Chongqing University, Chongqing, China.

f School of Resource and Environmental Sciences, Hubei Biomass-Resource Chemistry and Environmental Biotechnology Key Laboratory, Wuhan University, Wuhan, 430079, China

g School of Textile Materials & Engineering, Wuyi University, Jiangmen, 529020, China

Email: nzmnoor@outlook.com *, bin.fei@polyu.edu.hk*

Abstract

Transparent wood (TW)-based materials have increasingly become the focus of researchers worldwide owing to their superior physico-chemical-optical properties, sustainable nature, as well as the fact that they are highly accommodating frameworks that can act as building blocks to readily explore a vast range of potential functionalities, holding great potential to displace glass and plastics in their various respective applications. The integration of multiple functionalities into TW has been undertaken to fulfill the demands of prospective sophisticated applications through the utilization of functional fillers or coatings. Herein, we comprehensively summarize the up-to-date foundational developments and reports concerning emergent TW composites and coatings from a perspective of fabrication-functionality-application, with a particular focus on seven specific functionalities; i) solar control; ii) chromically-responsive, iii) electrically-conductive, iv) shape-memory active; v) flame-retardant; vi) electromagnetic interference shielding; and vii) aesthetics. The potential applications of TW with these functionalities are also discussed. Finally, we address the current challenges with TW, as well as the future developments required for eventual real-world application.

Keywords: Transparent wood, Sustainable materials, Multifunctional wood, Wood coatings and composites, Bio-composites

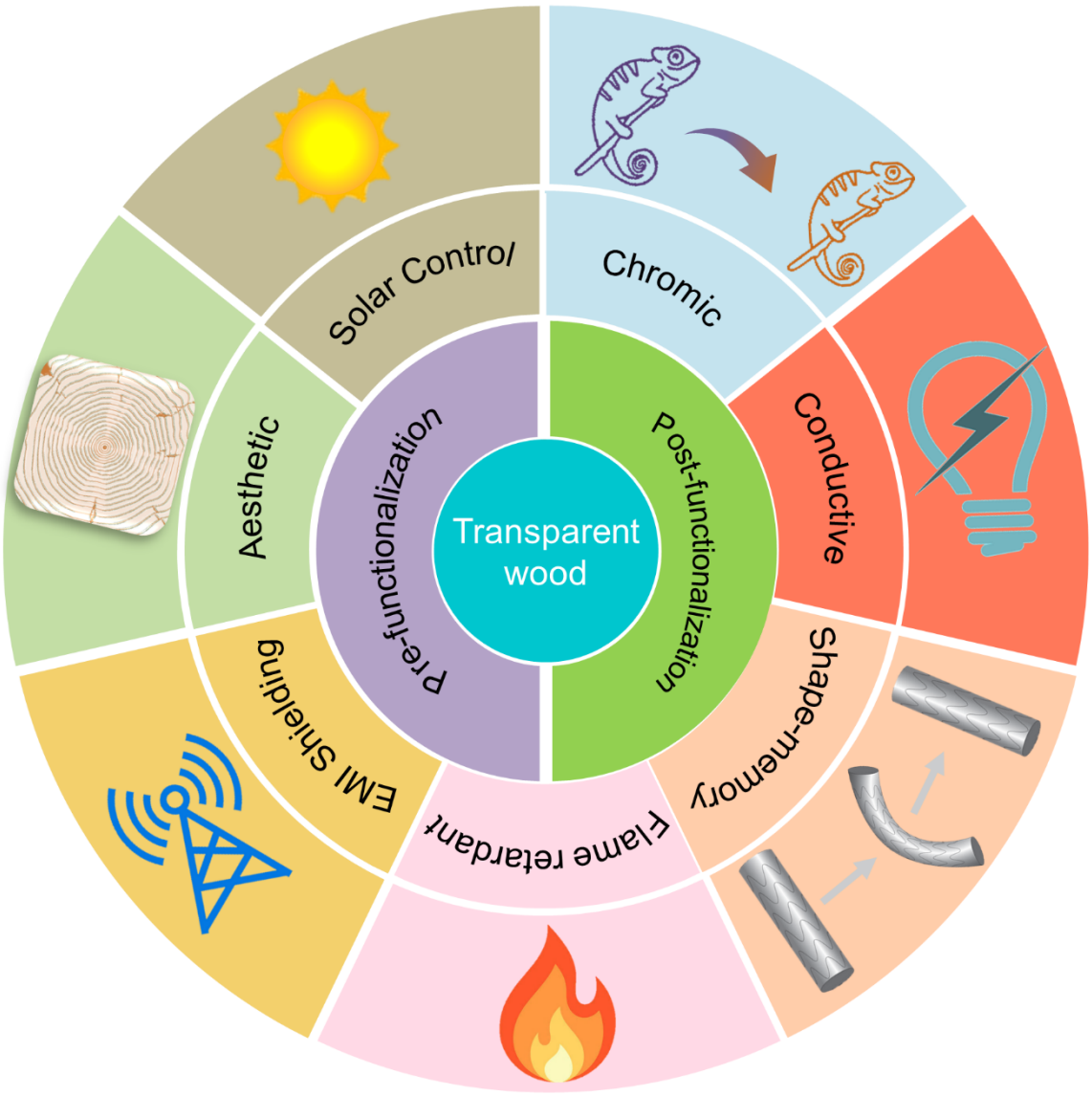
Transparent wood
Pre-functionalization
Post-functionalization
Solar Control
Chromic
Conductive
Shape-memory
Flame retardant
EMI Shielding
Aesthetic

Outline

1. Introduction

A green revolution of energy and materials consumption patterns is being undergone in almost every sector of global industry. Anthropomorphic overexploitation of natural resources and the resultant environmental problems associated with the use of petroleum-based chemicals and materials, as well as inefficient energy consumption patterns in contemporary industrial processes and materials, have resulted in a slew of global issues that must be presently addressed [1]. For example, residential building energy usage currently accounts for nearly 40% of the total energy consumption [2]. This, in turn, has motivated the development of new energy-saving building materials with good light transmittance and thermal insulating properties, offering substantial cost savings up-front, as well as a plethora of longer-term environmental benefits, contributing to a more carbon-neutral society (e.g., worldwide net-zero 2050 goals). In recent years, sustainable materials have reported unique and increasingly reliable materials properties (e.g., super plasticity, enhanced machinability, and superior strength and/or toughness) compared to established comparators (usually petroleum-based), combined with the increasing efficiency and variety of production technologies for mass production of these 'green' products. Such sustainable materials and processes are critical for achieving the UN Sustainable Development Goals by the 2030 target [3].

Given its renewable and biodegradable nature, wood may play an essential role in this green revolution. Natural wood has been intensively used since the beginning of human civilization due to its ease of processing, broad availability, low thermal conductivity and excellent mechanical performance [4]. However, with developments of application requirements, natural wood has yet to be able to fully cater to contemporary human needs. This has contributed to the rise of petro-plastics, glass, metals, concrete and other industries – all of which are highly energy-intensive and environmentally damaging. If wood-based materials could realistically compete with modern industrial materials, it could once again offer a viable route to new industrial materials that are less costly to the environment and more beneficial to quality of life. To this end, various wood-based materials with additional or enhanced functionality have been developed in recent years via chemical or physical treatment, to better cater to the needs of different applications spanning energy saving, radiative cooling, energy harvesting, energy storage, electronic devices, hydrogel devices, and photonic devices [5]. Among various wood-based materials, transparent wood (TW) has been intensively studied recently due to its unique performance.

TW is generally prepared via a discoloration process (i.e., delignification or lignin-modification) followed by polymer impregnation or a compressing process (top-down process). The primary TW prepared from the top-down process holds great potential for replacing traditional plastic materials due to the intrinsic high visible transparency and haze, low thermal conductivity and excellent mechanical properties. TW can also derive from nanocellulose that originated from trees, plants, cotton and even bacterial (bottom-up process). A special TW (named transparent fiber wood) can be created by mixing wood nanofibers (obtained from the delignification of wood particles) and the refractive index (RI) matched polymers [6]. Another strategy for creating transparent composite of nanofibers and polymer is directly assembling the cellulose nanofibers (obtained from the fibrillation of wood pulp or bacterial) into a thin film, which was then impregnated by acrylic resin under vacuum [7]. Although bottom-up processes have been implemented to achieve optical transparency, the resulting products have exhibited significant deviations in their microstructure from that of natural wood. Cellulose based transparent composites prepared from such bottom-up process will not be addressed in this review. Thus, the focus of this review is limited to TWs obtained through top-down processes.

Though the original TW-substrates have been considered as good exploratory materials for many applications[8], such substrates have yet to achieve sufficiently satisfactory properties for applications that required special functionalities. Functional TWs with enhanced or added value properties were developed using different techniques, enabling TW to find use in many other emerging fields such as smart buildings,

smart windows and optoelectronic devices. The functional TW can be prepared through either pre-functionalization or post- functionalization methods. Pre-functionalization refers to treatments before or during the impregnation, such as incorporating the functional component with the impregnating polymers, selecting impregnating polymers with special functions, special treatments on the wood scaffold [9]. Post-functionalization refers to treatments of TW after impregnation via surfacing engineering and coating [10]. Progress on TW has been comprehensively summarized, such as Berglund and coworkers for foundational transparent wood reports [11], Zhang *et al* for processes and procedures [12], as well as specific architectural applications by Wang and Zhu [13]. However, there has been a lack of comprehensive reviews on functional TWs that specifically emphasize their various functionalities. Very recently, Zhu *et al* summarized transparent wood-based functional materials, emphasizing process-structure-property-application relationships [14]. However, some functionalities, such as electromagnetic interference shielding and shape memory, that explored by researchers have not been well illustrated in their review. Therefore, there might be enough room to review functional TWs from a fabrication-functionality-application perspective with a specific focus on various functionalities.

For the first time we systematically summarized the functional TWs from a fabrication-functionality-application perspective. A focus is placed on seven specific functionalities that have shown promising development and reports in the TW composites and coatings fields, including i) solar control; ii) chromically-responsive, iii) electrically-conductive, iv) shape-memory active; v) flame-retardant; vi) electromagnetic interference shielding; and vii) aesthetic. In general, this review outlines the challenges and extraordinary opportunities afforded by functional TW from the standpoint of coatings and/or composites. This will include the foundational literature from the nascent TW field, as well as associated literature from overlapping and adjacent fields. In cases where the topic falls outside the purview of the TW composites and coatings focus, we refer the readers to other excellent recent literature reviews for more information [5d, 11-15].

2. Transparent Wood: From Opacity to Transparency

TW and its various coatings and/or composites have been made optically transparent (i.e., highly optically transmissive over visible light wavelengths; ~350-780 nm), by impregnating the porous structure with various clear polymers and/or fillers that match the RI of the wood scaffold. Thus, at the fundamental level, TW composite combines the functional aspects of wood, with the optical aspects of a clear polymer. Although TW was first reported in 1992 by Siegfried Fink[16], ostensibly to better understand wood anatomy – it was the more recent report in ~2016 by Li *et al*[17] and Zhu *et al* [18], that sparked the rush of interest in the area of functional TW composites and coatings. We will start with a brief overview of wood anatomy to provide a better overall understanding of TW substrates.

2.1 Wood Anatomy

Wood is the most used bio-based, renewable material in buildings, furniture, and a whole host of other applications (e.g., wearables and/or decorative) [19]. It is sustainable (including low energy input manufacturing practices), biodegradable and environmentally friendly [20]. Wood offers excellent mechanical properties, including reaction and alteration of the wood substrate's physico-chemical properties, when used for other applications. The architectures and compositions for natural wood (NW) at different levels of magnification are shown in the Fig. 1, a typical tree trunk mainly includes pith, heartwood, sapwood (secondary xylem), and bark (secondary phloem and cork). NW typically exhibits a porous structure, aiding the chemical or physical modification, and all tracheids contain both primary, secondary walls, and middle lamella [21]. On the molecular scale, wood consists of the three natural biomacromolecules - cellulose, hemicellulose and lignin [22]. Generally, the cellulose microfibrils, containing both crystalline and amorphous regions, are embedded in the matrix of hemicellulose and lignin [23]. Obviously, NW shows directional variance in terms of structural and chemical composition.

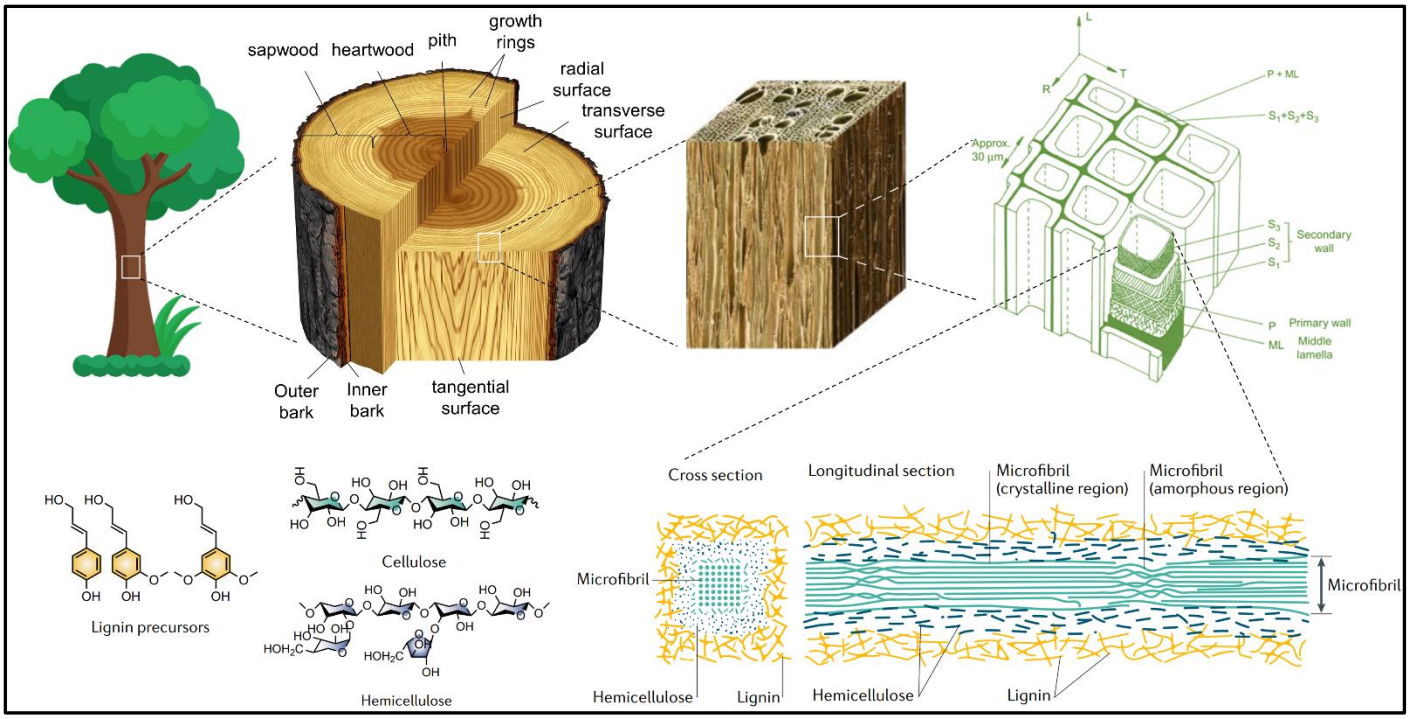

Figure 1. A general overview of wood architectures and compositions at different levels of magnification. Reproduced with permission, Copyright 2018, Elsevier[24]; Copyright 2020, Springer Nature [25].

Aside from being a natural material with intrinsic directional variance, wood is also an orthotropic-type of anisotropic material with marked variation in directional properties (e.g., strength) [26]. Briefly, the three main directions of wood property variance are; longitudinal (i.e., along the grain), as well as radial and tangential (both of which are perpendicular to the grain). For most purposes, the differences between the radial and tangential forms are considered minimal, although e.g., tangential shrinkage can be up to twice as high as radial shrinkage, due to reasons including variations in lignin presence, cell wall thicknesses, etc. [27]. Thus, the main differentiators in terms of physico-chemical properties tend to broadly be between parallel and perpendicular to grain. In addition, all woods have two broad zones: the inner core of darker heartwood hat contains the majority of living components of wood, and an outer ring of lighter sapwood, which is predominantly dead cells that only serve a supportive function [28].

In terms of material variation, the configuration and orientation between and even within species have marked influences on strength, and shrinkage, which is exacerbated by minor structural variations between different wood types, e.g., the longitudinal cells in softwood are usually shorter than those in hardwood. Because the longitudinal axes typically confer considerably higher strength than perpendicular axes – the strength of wood along the fibers is approximately ten times higher than the strength across the fibers, while the limiting strains across the fibers are significantly higher than along the fibers [29]. This anisotropy continues to be an issue after TW is formed, with orientation having marked effects on optical and mechanical properties [18]. To a certain extent, multilayer TW could improve the mechanical strength and overcome some issues with material anisotropies, depending on element orientation and load direction [30]. Further differences in property are due to the range of variations of compositional factors such as cellulose-hemicellulose-lignin compositions, the crystalline:amorphous character, the cellulose allomorphs present (cellulose I:cellulose II (α:β): cellulose IV), the presence of nodes, the arrangements of fibrils, the size of pores among many other factors [31].

Generally, wood can be broadly classified into two main groups: softwoods (e.g., cedar, pine, Douglas fir) and hardwoods (e.g., balsa, mahogany, oak). These primarily differ in their cellular structure. Softwoods are generally made up of two types of cells; 1) tracheids (~90% of the cell composition, measuring ~30-50 µm diameter, aligned longitudinally along the trunk), which tend to give a tree support, and conduct water, as

well as; 2) rays (~10%, located in the radial–longitudinal (RL) plane), involved in support and transport (e.g., water and minerals) functions [24, 32]. The cells are smaller in size, and are arranged more relatively uniformly than their hardwood counterparts. The limited and more uniform cell types can make softwoods more difficult to differentiate from one another.

Hardwoods, have a denser, more complex arrangements of cells with thicker cell walls, including a normally larger heartwood zone, which gives rise (generally) to greater compressive strength, weight and tensile stiffness [33]. This includes a structure comprising vessels (i.e., ~50-500 μm diameter, pore-like structures that yield a more noticeable grain) for sap, water and mineral transport, as well as much thinner fiber tracheids, which comprise the thick walls around vessels that support the tree [34]. Some hardwoods however may even be softer and lighter than softwoods, e.g., balsa is a relatively soft hardwood, while Douglas fir is a relatively hard softwood [35]. Nevertheless, the mechanical properties and fracture behaviors of wood structure are typically determined by fiber length, fibrillar structural orientation, density, chemical composition, and morphology. For example, birch has a greater energy absorption than pine, both along and across the fibers [29]. It is due to the retention of this structural array from the original wood to the TW, that many of these parent properties often translate into their TW-based composites and determines many of the subsequent mechanical properties of the system, similar to carbonization processes for carbonaceous materials [36].

Beyond the brief treatment given here, the anatomy of wood is a vast topic area that is beyond the scope of this review, and we refer the readers to the cited references for further information [37].

2.2 TW Fabrication Process

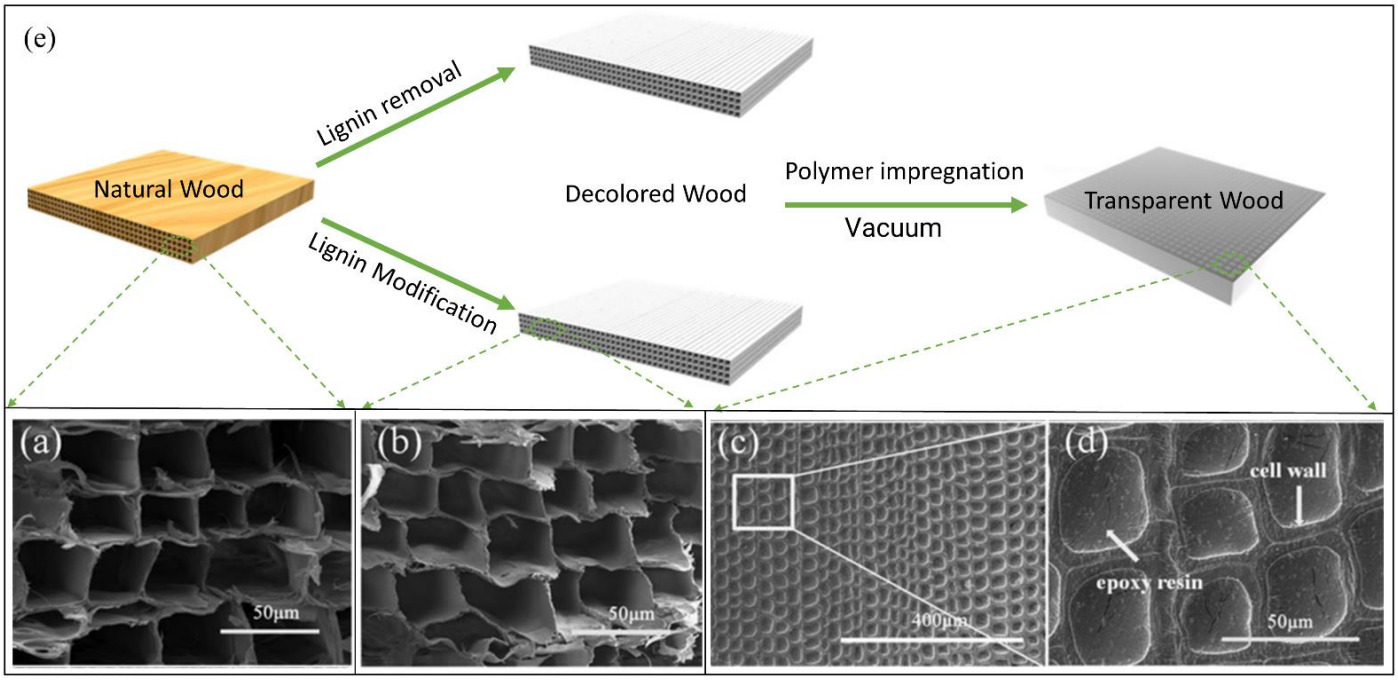

Figure 2. A general fabrication process of TW and corresponding SEM images at different fabrication stages Reproduced with permission. Copyright 2020 American Chemical Society[9b].

The general fabrication process of TW involves two steps: wood discoloration and polymer impregnation (Fig. 2e). Discoloration can be achieved by two methods: lignin modification and/or delignification, which are quite similar to those used for chemical pulping, involving treating and compressing stages – most commonly by adopting the already proven bleaching chemicals and processes from such industries [38]. Though, enzymes are widely used in chemical pulping, there appear to be no reports of enzyme-based

bleaching routes to TW to-date [39]. However, in addition to the decoloration effect resulted from delignification and lignin modification, such treatments frequently result in some (usually undesired) loss of the hemicellulose components of wood. There are four different delignification recipes that are most frequently used to fabricate TW:

i) NaOH-Na_2SO_4-H_2O_2 system: Wood blocks or strips are immersed in boiling (80-100°C) aqueous solutions containing sodium hydroxide (NaOH) and sodium sulfite (Na_2SO_4) for ~12 hours, followed by boiling hydrogen peroxide (H_2O_2) for ~6 hours [18].

ii) $NaClO_2$-CH_3COOH system: The pH of $NaClO_2$ solution is adjusted to ~4.6 by CH_3COOH, then wood strips are immersed in the mixture at ~80°C for several hours (until completely white, depending on the sample size) [17].

iii) NaClO system: Wood strips are directly immersed in NaClO solution for more than 12 hours [40].

iv) Peracetic acid (PAA)-NaOH system: Delignification is performed using an aqueous PAA solution (4 wt.%) at a pH of 4.8 (adjusted with sodium hydroxide) for several hours (until completely white, depending on the sample size) [41].

Partial or complete removal of the cell wall lignin-component leads to voids in the lignin-rich cell wall corner and a general thinning of cell walls[17]. It is worth noting that the natural porous structure of wood is generally reserved (at least at the micron level, Fig. 2a & 2b). Broadly, the loss of lignin has negative impacts on the mechanical properties of TW, but a positive impact on achieving a high level of transparency. While lignin removal is usually desirable for obtaining TW, in order to obtain the maximum value of visible transparency and mechanical performance simultaneously, alternative lignin modification processes have also been developed. In these processes, the chromophores of lignin are selectively eliminated while the aromatic skeleton remains intact. Li *et al* (2017) have reported a high lignin content TW (up to 80% lignin retention, TW-lignin) variant that exhibited transmittance of 83% (slightly lower than that (86%) of TW based on the delignified wood template (TW-delign) at the thickness of 1.5 mm) and a haze of 75% (an increase of 7% when compared to TW-delign at the thickness of 1.5 mm). [42]. Though a comparison of TW-lignin and TW-delign in terms of mechanical properties was not presented in this study, the comparison of the mechanical properties of the two wood templates (delignification method and lignin modification method) were conducted. For both parallel and perpendicular direction of birch, pine, and ash, the wet strength of lignin modified samples was much higher than that of delignified samples.

Two lignin modification systems are commonly used for wood decoloration: thermal alkaline/H_2O_2 and ultraviolet-H_2O_2. The general recipe for alkaline/H_2O_2 lignin modification solution usually includes sodium silicate, sodium hydroxide, magnesium sulfate, diethylenetriaminepentaacetic acid (DPTA), and H_2O_2. Wood slides are immersed in such solution mixtures (usually below 100°C) until they become completely white. Typically, this requires less processing time (1-2 hours) than the delignification process (usually more than 10 hours). Alternatively, Xia *et al* [5f] also introduced an in-situ lignin modification method with the assistance of ultraviolet (UV). The natural wood was treated with a small quantity of a 10% NaOH solution prior to the addition of a 30% H_2O_2 solution. The pre-treated wood was then placed under UV light. This process also shows excellent patternability by directly brushing the H_2O_2 on the NaOH pre-treated wood surface [43]. In this manner, most of the "binder" was preserved, providing a robust wood scaffold for polymer infiltration while drastically reducing chemical and energy consumption as well as processing time.

After wood discoloration, the decolored wood is usually stored in a low boiling point solvent (e.g., ethanol, acetone, etc.) to avoid densification. The water and chemicals remaining in the wood channel after

the decoloration process will be displaced by the low boiling point solvent over time. In the final stage, an alternative polymer (e.g., epoxy, acrylic, poly (vinyl alcohol), polyvinylpyrrolidone, polyimide, thiol-ene, vitrimers, poly (limonene acrylate), melamine formaldehyde, etc.) is allowed to permeate into the wood matrix under vacuum (Fig.2c &, 2d). At this point, the substrate turns clear due to the reduced light scattering afforded by this new, interpenetrating, index-matched polymer [9b, 44]. Such a configuration allows for the complete infiltration and long-term retention of the polymers as compared to conventional surface coating processes, in which only the surface cavity was impregnated with resin. One inconspicuous but very important point to ensure the decolored wood is fully immersed in the impregnation polymers. The density of decolored wood is even lower than that of natural wood, and it may float on the surface of polymer mixtures during impregnation if proper precautions are not taken. Once floatation occurs, the infiltration process can fail, leading to the failure of the entire fabrication process.

2.3 Transparency Mechanism

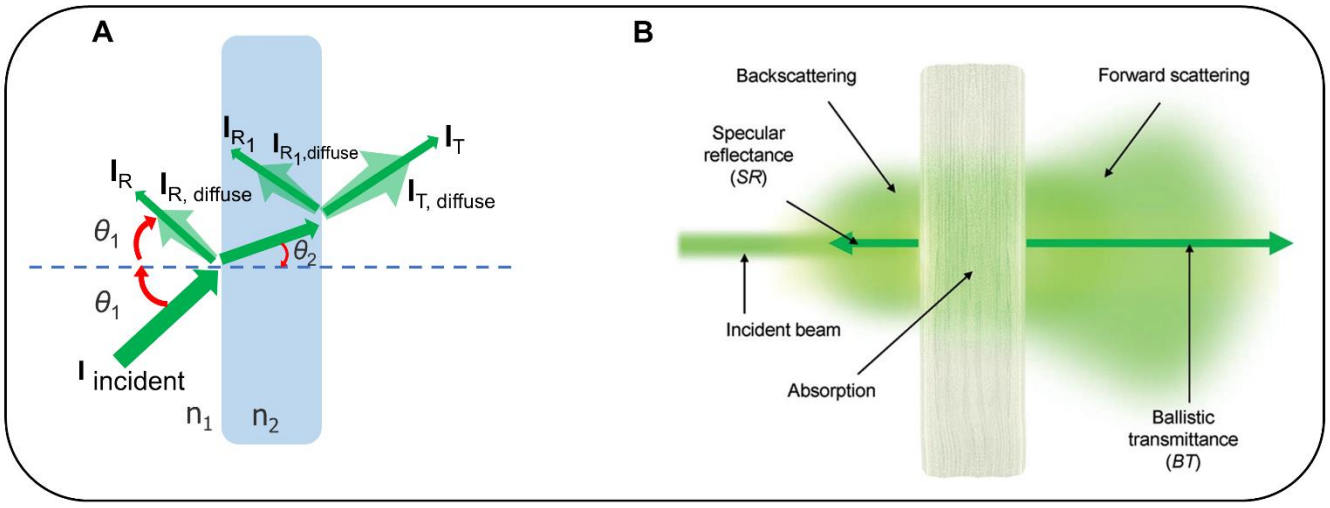

Figure. 3 A) Sketch Illustration of light-solid object(RI, n_1) interaction in a medium (RI, n_2), where $I_{incident}$ (incident light intensity), I_R (intensity of specular reflection) $I_{R,\ diffuse}$ (diffusely reflected light intensity), I_T (ballistically transmitted light intensity), $I_{T,diffuse}$(diffusely transmitted light intensity), θ_1(incident angle) and θ_2 (refracted angle) are presented. B) Measurable photon budget components. Reproduced with permission. Copyright 2022, Wiley-VCH[45].

The light-solid object interaction is crucial to comprehending the mechanism of transparency. As shown in Fig. 3A, when light interacts with a solid object (n_1) in a medium (n_2), it may be reflected backwards at the solid-medium interface, or it may propagate forwards for refraction and/or absorption, and the refraction is governed by Snell's law:

$$n_1 \sin\theta_1 = n_2 sin\theta_2 \qquad (1)$$

Where n_1 is the RI of the medium, n_2 is the RI of solid object, θ_1 is the angle of incidence, θ_2 is the angle of refraction. Generally, the bigger the difference between n_1 and n_2, the stronger the light scattering. The transmittance of this solid object can be determined by the ratio of transmitted light intensity (both ballistically transmitted and diffusely transmitted) to incident light intensity. Haze is calculated using the ratio of diffused transmitted light intensity to the intensity of transmitted light (both ballistically transmitted and diffusely transmitted). Wood is usually composed of cellulose (RI of 1.52), hemicellulose (RI of 1.53), and lignin (RI of 1.61) – a light-absorbing (accounting for 80–95% of the light absorption) structural polymer that serves as a 'glue' for the wood framework[16, 46]. Since wood has a naturally multiscale porous structure (micro- and nanoscale) and its lumen space is fully filled with air (RI of 1.00). Therefore, the RI contrast between the wood

cell walls (1.52-1.61) and the air-filled lumen space (1.00) and the presence of light absorption content (lignin) lead to strong scattering and absorption when light interacts with the wood at all air-cell wall interfaces. In order to make wood transparent, both absorption and scattering effects, which arise predominantly due to lignin and RI contrast, need to be reduced or eliminated.

Therefore, the preparation of TW usually involves two steps: decoloration (removing/modifying the light-absorption content) and impregnation (reducing the light scattering). The air-filled lumen is filled with RI-matched polymers. Such impregnating polymers subsequently enables the production of TW-composites to in addition to a variety of other advantageous mechanical and optical properties. Chen et al. [45] investigated the photo walk in TW, with the measurable photon budget components is shown in Fig. 3B. Their results suggested that light scattering is dominated by forward scattering if there are no voids within the sample (e.g., nano-voids inside wood cell wall or air gaps between cell wall and polymer). In other words, the majority of the photons can pass through TW, despite the fact that the ratio of ballistically transmitted photons to total transmitted photons (forwards scattering and ballistically transmitted) varies with different sample thickness. Therefore, the resultant composite appears "transparent" after impregnation. The resultant material is also less frequently (but perhaps more correctly), as 'translucent wood'. In addition to the standard impregnating resins, a whole host of other materials could be alternatively or concurrently be inserted into the porous wood framework for enhanced functionality. This will be explored in greater depth in this review. The light-TW interaction is further complicated when functional fillers or coatings are involved.

2.4 General Characteristics of TW

TW has unique optical, mechanical and thermal properties, resulting from intrinsic structural properties, such as the cellulose volume fraction, cellulose microfibril orientation, chemical interactions at the cell wall interfaces, thickness, porosity and anisotropic structure of TWs. Table 1 provides an up-to-date summary of all experimental reports of such structural variations and their effects on physical and optical properties.

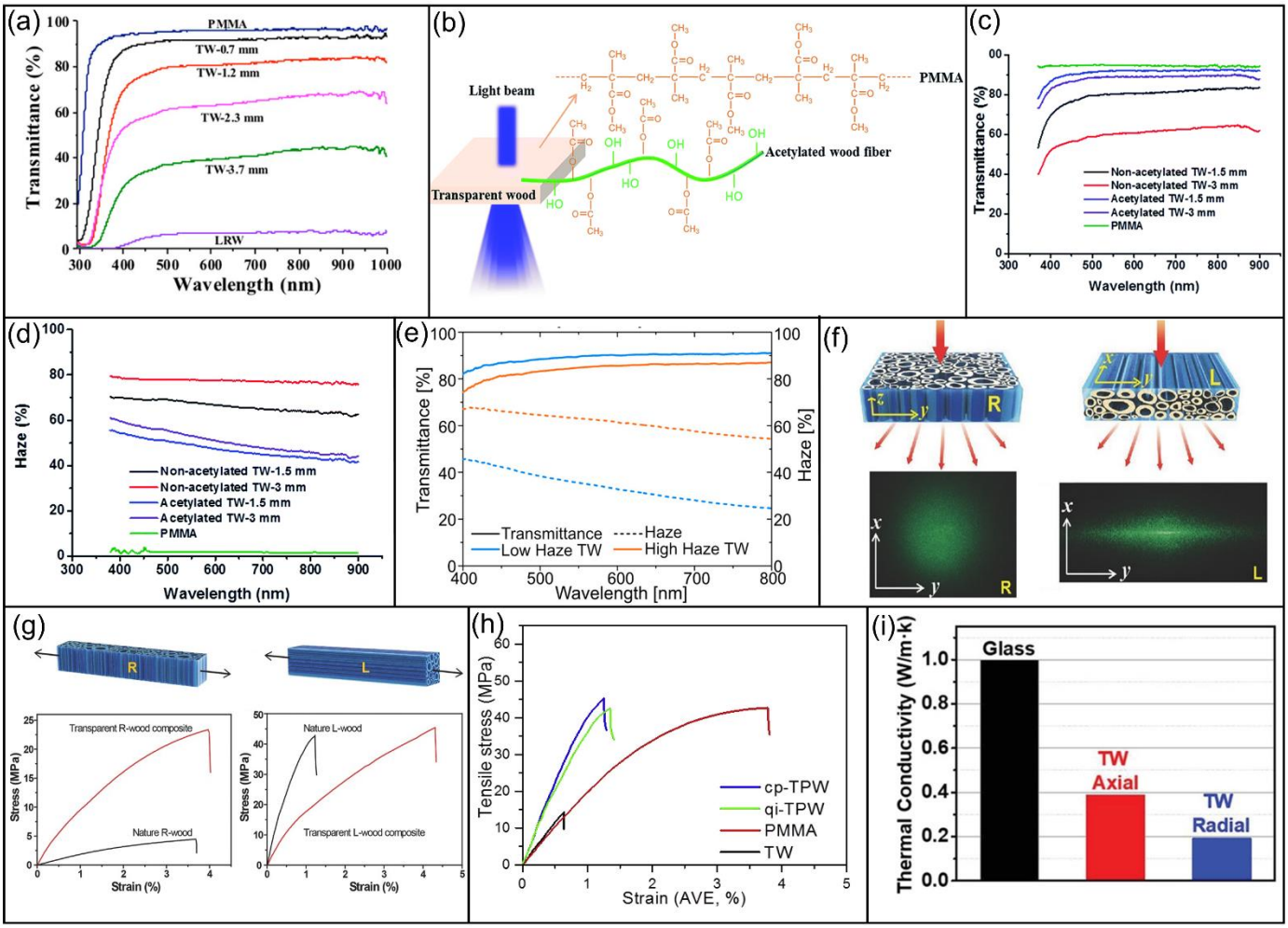

Figure.4 General performance of TW. (a) Transmittance of transparent wood samples with different thicknesses. Reproduced with permission, Copyright 2016 American Chemical Society [17]. (b) The Illustration showing the interactions between acetylated wood substrate and PMMA. (c & d) The transmittance(c) and haze(d) of acetylated TW and non-acetylated TW at the thickness of 1.5mm and 3mm. (b-d): Reproduced with permission, Copyright 2018, Royal Society of Chemistry[47]. (e) Optical transmittance and haze of TW specimens at the thickness of 1.2 mm. Reproduced with permission, Copyright 2020 American Chemical Society [48]. (f) Photo images of scattering patterns from different direction. (g) Stress–strain curves for the nature R/L-wood and transparent R/L-wood. (f & g): Reproduced with permission, Copyright 2016, Wiley-VCH [18]. (h) Typical stress-strain curves of the tensile test in transverse direction. Reproduced with permission, Copyright 2018, Elsevier [30b]. (i) The thermal conductivity of the transparent wood was measured at the axial and radial heat transfer direction and the comparison with glass. Reproduced with permission, Copyright 2019, Wiley-VCH [49].

Table 1 Summary of optical, mechanical and thermal properties of TWs

Sample	Wood Species	[a]Decoloration Method	[b] Wood scaffolds Vol/%	Thick-ness /mm	Optical		Mechanical				Thermal	Direc tion	Ref
					T[c]/%	H[d]/%	E/Gpa	σ/Mpa	ε/%	Tn[e]/MJ·m^{-3}	Tc[f]/W·m^{-1}K^{-1}		
[g] DW/PMMA	Balsa	$NaClO_2$/Acetate	\	0.7	90	48	\	\	\				
			5	1.2	85	70	2.05	38	2.2				
			19	1.2	78	75	3.59	90.1	3.8	\	\	\	[17]
			65	1.2	34.	78	\	\	\				
			\	3.7	40	~80	\	\	\				
DW/EP	Basswood	NaOH-Na_2SO_4-H_2O_2	\	3	90	\	1.22	23.38	\	0.59	\	⊥	[18]
				3	~80		2.37	45.38		1.2		//	
DW/PVA	Balsa	NaClO	\	0.8	91	15	3.85	143	4.2	3.03	0.39	//	[49]
				0.8	\	\	3.1	67	3.7	1.06	0.19	⊥	
DW/EP	Balsa	$NaClO_2$/Acetate	\	2	77	\	\	69.13	\	\	\	//	[50]
				2	\			6.06				⊥	
	Basswood			2	64			75.12				//	
				2	\			8.17				⊥	
DW/PMMA	Balsa	$NaClO_2$/Acetate	\	1.5	86	68	\	\	\	\	\	\	[42]
[h] LMW/PMMA		Alkaline/H_2O_2[f]		1.5	83	75		100.7	2.18				
DW/thiol-ene	Balsa	$NaClO_2$/Acetate	5	1.2	85	63	3.2	53.7	2.1	\	\	\	[48]
LMW/thiol-ene		Alkaline/H_2O_2	4.3	1.2	90	36	3.4	59	2.5				
DW/LIMA	Birch	PAA-NaOH	26	0.7	88	49	12.6	146.6	1.2				
SA-DW/LIMA	Birch			0.7	92	44	17.3	173.3	1.0				
DW/LIMA	Balsa		12	1.2	87	46	\	\	\	\	\	\	[41]
SA-DW/LIMA				1.2	89	41							
DW/LIMA				2.0	80	62							
SA-DW/LIMA				2.0	87	45							
DW/LIMA				3.0	71	65							
SA-DW/LIMA				3.0	81	51							
DW/PMMA	Balsa	PAA-NaOH	6.4	2.0	70.6	76.3	4.8	41.4	\	\	\	//	[51]
DW/PMMA				2.0			2.9	11.4				⊥	
SA-DW/PMMA			6.2	2.0	83.8	66.9	4.5	61.7				//	
SA-DW/PMMA				2.0			2.9	12.8				⊥	
IA-DW/PMMA			6.5	2.0	76.6	76.2	4.3	54.9				//	
IA-DW/PMMA				2.0			3.3	33.2				⊥	
MA-DW/PMMA			6.0	2.0	79.5	73.6	4.3	46.2				//	
MA-DW/PMMA				2.0			3.1	18.0				⊥	

To be continued

Table 1 (continued)

DW/PEAG DW/EP	Balsa	$NaOH-Na_2SO_4-H_2O_2$	\	\	93 82	98 \	2.2 \	153.6 \	\	\	\	// //	[52]
Compressed single DW/PVP (STW)	Balsa	$NaClO_2$/Acetate	40.25	0.48	70.4	31.9		99.5					[53]
Double layer-same direction laminated (DSTW)			41.15	\	59.6	41.4		\					
Double layer-same-direction laminated (DCTW)			40.75	\	50.0	58.1	\	88.3	\	\	\	\	
Trible layer-same-direction laminated (TSTW)			40.45	1.32	44.3	50.5		134.0					
Trible layer-cross-direction laminated (TCTW)			40.97	1.32	43.5	65.6		125.3					
DW/PMMA	Balsa	$NaClO_2$/Acetate	\	1.5	83	70	\	\	\	\		\	[47]
Acetylated-DW/PMMA			5%	1.5	92	50	4	78.9	2.2	1.0		⊥	
Acetylated-DW/PMMA			\	3	89	53	\	\	\	\	\	⊥	
Acetylated-DW/PMMA			\	7	71	74	\	\	\	\		⊥	
Acetylated-DW/PMMA			\	10	60	76	\	\	\	\		⊥	
DW/PMMA/PEG	Birch	$NaClO_2$/Acetate	\	0.5	84	74	\	\	\	\	\	\	[54]
DW/PMMA/PEG				1.5	68	77	14.9	70.5			0.3		
DW/EP(Clear)	Basswood	NaClO	2.54	0.7	90	10	\	43.39	19.14	6.10	0.35	//	[55]
DW/EP(Clear)		NaClO	\	\	\	\	\	33.29	16.30	3.96	\	⊥	
DW/EP(Haze)		$NaClO_2$/Acetate	\	\	90	80	\	\	\	\	0.24	\	
LMW/EP	Balsa	UV-H_2O_2-NaOH	\	1	90	60	\	46.2	3.4	1.64	\	//	[43]
LMW/EP				1.5	\	\		31.4	7.4	0.93		⊥	
DW/MF	Balsa	Alkaline/H_2O_2	11	1.1	65	92	\	\					[56]
LMW/MF	Balsa	$NaClO_2$/Acetate	8.5	1.2	68	90	\	\	\	\	\	\	
LMW/MF	Birch	Alkaline/H2O2	25	1.2	74	66	11.1	60					

[a] All decoloration recipes can be found in Section 2.2

[b] wood scaffold vol%: Depending on the decoloration methods, this value refers to the sum of cellulose vol%, hemicellulos vol%, and lignin vol% or cellulose vol%.

[c] Transmittance; [d] Haze; [e] Toughness; [f] Thermal conductivity; [g] Delignified wood; [h] Lignin modified wood

//: The direction of the light propagation, applied stress and heat transferring is parallel to the wood channel. ⊥: The direction of the light propagation, applied stress and heat transferring is perpendicular to the wood channel.

2.4.1 Optical Properties of TW

The two most important measures of TW optical properties are transmittance and haze. As discussed in Section 2.3, the transmittance of TW is determined by the ratio of transmitted light intensity (both ballistically transmitted and diffusely transmitted) to incident light intensity. The transmittance is generally measured with an integrating sphere, which collects a total cone of scattered light consisting of ballistic and randomly scattered photons (forward scattering, Fig.3b). Though the transmittance can reach as high as 93%[52], the main contribution comes from diffusely transmitted light (forward scattering) rather than ballistic transmission. This also makes TW appear inconsistent with human's general perception to transparency. Another important parameter is haze, referring to the ratio of the ratio of diffused transmitted light intensity to the intensity of transmitted light (both ballistically transmitted and diffusely transmitted). Haze is measured according to ASTM D1003[57], and is defined as the percentage of transmitted light that is scattered with a direction deviating more than a specified angle (2.5°) from the direction of the incident beam. An insightful discussion about transmittance and haze measurements has been given by Li et al[11b]. Though TW normally exhibits at high transmittance and high haze, a wide range of tunable transmittance (10-93%) and haze (10-98%) can be achieved depending on several factors, including wood species, thickness, cellulose volume fraction and microstructure. Based on the careful modulation of these factors, several strategies have been proposed to tailor the haze and transmittance of TW.

Thickness is a critical factor in on the optical properties of TW. The quantity of polymer/wood interface is highly thickness-dependent. The interfaces between the wood substrate and the polymer increases within the increase of sample thickness, thereby, resulting in a lengthened light propagation path. As a result, the transmittance will decrease and haze will increase. This trend has been observed for balsa-based (Fig.4a)[17], beech-based[58] and birch-based[54] TWs. The quantitative relationship between the total transmittance (T_{total}) and thickness of TWs can be expressed by the anisotropic photon diffusion equation (Equation (1)), demonstrating that T_{total} decays exponentially with increasing TW thickness[59].

$$T_{total} = exp(-\alpha d) \quad (2)$$

where α is the attenuation coefficient, and d is the sample thickness.

Interface tailoring is an effective strategy to control the optical properties of TW. Light scattering in TW is normally dominated by forward scattering from RI mismatch between the cell wall and the polymer. Nonetheless, if the air-filled voids caused by multiscale porous structural combination of micro, meso- and macropores and polymer shrinkage during polymerization cannot be minimized, such voids will completely dominate scattering in TW[45]. Thus, a good surface compatibility is crucial to the desired optical properties of TW. To date, surface manipulation (e.g., surface esterification and use of compatibilizer) has been explored to minimize the air-filled voids caused by the poor compatibility between the polymers and decolored scaffold[41, 47, 51, 60]. By using compatibilizers, such as KH-550, epoxy resin and the decolored wood scaffold can be successfully coupled, resulting in an improved interfacial compatibility, consequently, improved optical performance [60b]. Another strategy is to graft acetyl groups onto the cellulose microfibrils to improve the interfacial compatibility of the wood scaffold and PMMA (Fig.4b). Due to the improved interfacial compatibility, acetylated TW shows higher transmittance (92%) and lower haze (50%) than non- acetylated TW (transmittance ~83% and haze ~70%) at a thickness of 1.5 mm due to the improved interfacial compatibility (see Fig. 4c&d). Compatibility issues can also be caused by polymer shrinkage during polymerization. This can be resolved by selecting polymers with smaller shrinkage ratios. A novel impregnating system (i.e., thiol–ene) with a low volume shrinkage ratio (~4%) was introduced for the preparation of TW [48, 61]. Compared to normal PMMA based TW, the scattering from air voids and the

corresponding haze are significantly reduced due to the low polymer shrinkage, resulting in improved optical performance (high transmittance and low haze, Fig. 4e).

The optical properties of TW are highly direction-dependent due to the anisotropic structure of wood. The wood fibers can either direct light along the axial direction or cause significant anisotropic scattering, depending on the alignment of the material direction and the incident light. When light travels parallel to the wood fiber direction, the polymer-filled lumen can be regarded as broadband waveguides with high propagation scattering losses [44], showing an isotropic scattering (Fig.4f, left). While the light propagates perpendicular to wood fiber direction (Fig.4f, right), the x-direction-aligned wood fibers are expected to affect the light scattering in the y-direction, resulting in nonsymmetric intensity distribution in two perpendicular planes. Anisotropy influences the transmittance and haze, based on the orientation of the incident beam relative respect to the direction of wood fibers. The transmittance and haze of R-wood are both higher than that of L-wood due to the high propagation scattering as light travelling in the vertically aligned channels of R-wood[18, 62]. Despite the special advantages of anisotropic light scattering, the even distribution of light is often desired. Lamination is an effective way to turn the optical properties of TW from anisotropic to isotropic. Fu et al. [30b] studied a five-layer structure of transparent plywood with varying fiber orientations. Unlike the compressed parallelogram-shaped scattering pattern observed in single-ply TWs, a nearly circular scattering pattern was observed in the quasi-isotropic transparent plywood, which exhibited approximately 75% transmittance and 80% haze. The laminated fiber in the transparent plywood structure confined the light, resulting in isotropic light scattering behavior. Similar anisotropic-to-isotropic transition has been reported by Wu et al [30a, 63].

Berglund's group[17, 45, 47-48, 51, 59, 62b, 64], has provided excellent illustrations of the relationship between the optical properties, the nano- and microscale structure, and the decoloration process and light-TW interaction. We refer the readers to these works for more detailed information about the TW substrate. However, the functional fillers and coting for TW are likely to introduce uncertainty to the current models. Further investigations about the impact of functional filler and coting on optical properties of TW should be conducted in future to better understand and control the optical properties of functional TW from a synthesis-structure-property perspective.

2.4.2 Mechanical Properties of TW

Mechanical properties are crucial to many practical applications of TW. Similar to the optical properties, the mechanical properties are highly dependent upon the wood species, wood scaffold volume, decoloration methods, polymer identities, sample thickness and microstructure (corresponding summary can be found in Table 1). Several strategies can effectively enhance the mechanical performance of TW, including interface manipulation, densification of the wood scaffold and lamination.

The presence of air voids between the wood scaffold and polymers not only influence the optical properties, but also contribute to the formation and propagation of cracks under stress. Reduction of air voids through improvement of interfacial compatibility can enhance the mechanical properties of TW. For example, Montanari et al. prepared bio-based TW by impregnating cyclic anhydrides esterified delignified wood scaffold with PMMA[51]. Esterification of the delignified wood scaffold allows molecular-scale interface manipulation with tunable interfacial adhesion, improved optical transmittance and enhanced mechanical strength. Compared to the TW prepared from un-esterified wood scaffold, TW from succinic anhydride esterified wood scaffold shows improved tensile strength (from 41.4 MPa to 61.7 MPa. Table 1). Similar to the control of optical properties, higher mechanical performance can also be achieved by selecting impregnating polymers with lower polymerization shrinkage[48]. Other interface design based on the surface

modification of wood scaffold, such as acetylation, also permit improved control of the wood/polymer interfacial compatibility, achieving improved mechanical performance[47].

Another strategy to improve the TW mechanical properties is to adjust the wood scaffold volume fractions (V_f), which can be controlled by compressing the wood scaffold prior to impregnation. Compression increases the V_f accordingly, leading to enhanced mechanical performances. Densification by compression was reported by Li et al[17]. TW from the compressed wood scaffold shows much higher mechanical properties ($V_f = 19\%$, $E = 3.59$ GPa and $\sigma = 90$ MPa) than TW from un-compressed wood scaffold ($V_f = 19\%$, $E = 2.05$ GPa and $\sigma = 38$ MPa). Similar results can be found in Yu et al.'s and Wang et al.'s reports[9a, 65]. The enhanced mechanical properties might be attributed to the hierarchical and longitudinally oriented cellulose nanofiber structure, which not only improves modulus, but also provides a strong synergistic strength improvement. Some researchers also attributed these enhancements to the formation of additional hydrogen bonds between the cellulose microfibrils of the densified wood cells after compression[14]. The mechanical properties of TW are also anisotropic due to the intrinsic anisotropic structure of wood. As shown in Fig. 4g, the tensile strength (45.4 MPa) of L-wood is twice that of transverse TW (23.4 MPa, R-wood). However, in many cases, the isotropic mechanical performance is desirable. Similar to the methods for regulating optical properties, lamination is an effective method to obtain TW with isotropic mechanical properties. Transparent balsa veneer plies were laminated with control over the wood fiber direction and thickness to create an isotropic TW. The resulting transparent plywood exhibited an increase in ultimate strength from 15 MPa to 45 MPa (Fig. 4h) under transverse loading[30b]. The resultant elastic moduli and tensile strengths after lamination might be predicted by classical lamination plate theory and simple rule of mixtures, respectively [53].

One significant justification for the potential of TW to replace common glasses is its toughness (~3.2 MJ/m^3), which can be 30 times higher to that of common glass (~0.1 MJ/m^3)[66]. Unlike common silica-based glass, TW will not shatter into sharp pieces in case of strong sudden impact, eliminating potential safety issues. The high toughness of TW might relate to the identity of the impregnating polymer and the wood structure[11b]. Though the toughness of TW is crucial for practical applications, especially for building applications, little research has been expended on this topic. Recently, Jungstedt et al.[67] investigated the transverse fracture toughness of TW. Their results indicated that the fracture toughness of TW might be highly related to the intercellular peeling energy, which may decrease during the delignification process (removal of the lignin-rich middle lamella between fibers). Therefore, two possible strategies for improving the fracture toughness were proposed[67]. One is impregnating polymers into the delignified interfiber region. Another is selecting other methods for selectively degrading the chromophores rather than delignification. These strategies might require additional validation in future research.

2.4.3 Thermal Properties of TW

Thermal insulation is an essential component of buildings, particularly those designed for energy conservation, with its efficacy primarily dependent on thermal conductivity. The thermal conductivity of a material is influenced by various factors, including pore structure (pore size and porosity), the volume fraction of the solid wood scaffold, and the anisotropy of the wood structure.

TW's thermal conductivity is anisotropic (e.g., 0.357W/(m·K) axial direction; 0.190 W/(m·K) radial direction, Fig.4h) due to the alignment of the wood cellulose fibers[49]. This can be explained by the fact that heat propagation perpendicular to the highly aligned lumens (Fig. 4i, radical) is expected to yield greater phonon scattering than heat propagation along the lumens (Fig. 4i, axial). The nanoscale pores in the wood scaffold also against the heat propagation, leading to the low thermal conductivity of TW. This thermal

conductivity is lower than conventional silica glass, implying that it is more thermally insulating. As a result, TW can intrinsically (i.e., without coating or any other additive) help keep a building at more consistent temperature, making it easier to reach higher energy efficiency. For example, TW glazing could reduce space conditioning energy consumption by ~25-33% in medium and large office spaces [68]. A further potential TW benefit stems from this thermal conductivity anisotropy; thin electronic devices require efficient heat dissipation and TW's directional dependence properties imply that TW is a potential substrate for dense loading of multiple devices with thermal interference between heat sources in close proximity being minimized due to the directional heat dissipation effects [69].

The thermal conductivity of TW is also affected by the wood scaffold volume fraction. The thermal conductivity of haze wood (prepared from $NaClO_2$/acetate decoloration method, 0.24 $W \cdot m^{-1}K^{-1}$) is lower than that of clear wood (prepared from NaClO decoloration method, 0.35$W \cdot m^{-1}K^{-1}$) [55]. The reduction in thermal conductivity can be attributed to the fact that the $NaClO_2$/acetate decoloration method (V_f~18.4%) provides higher wood scaffold volume fraction than the NaClO system (V_f~2.9%), resulting in more nanoscale pores. The increased nanoscale pores may pose more blocking or confinement (i.e., the increased phonon scattering) to heat propagation when phonons travel through the wood cell walls [44]. Therefore, manipulation of the wood scaffold volume fraction and heat transfer direction offers a potential method for achieving the desired thermal insulating performance.

3. Functional Transparent Wood: From Transparency to Functionality

Besides the unique intrinsic properties, TW also shows a great potential for extra functionalization via functional fillers and coatings. Different functional fillers can be combined with TW substrate during the polymer impregnation process. The large surface area TW polymer composite substrates can be employed as carrier matrices for functional coatings (e.g., active metal oxide components, silver nanowires, etc.). Immobilization on such substrates likely occurs predominantly via adsorption at the solid substrate surface, in addition to physical entrapment [70]. As such, TW offers a vast range of possibilities for functionalization via composites or coatings routes for a multitude of potential applications.

3.1 Solar-control Transparent Wood

TW was originally designed as glazing materials for building applications due to its high optical transmission and low thermal conductivity. However, neat TW substrates may not be able to displace conventional advanced glazing materials (i.e., solar control glass). Solar control composites and coatings primarily control the passage and interactions of ultraviolet (UV), visible and near-infrared (IR) radiation on transparent substrates to better control, for example, the amount of natural daylight, glare and interior temperature of a room, when used for glazing applications. In order to make TW a more promising candidate for windows materials, many efforts had been made into TW with solar (200- 2500 nm) control functionalities, such as UV blocking and near infrared (NIR i.e., 780-2500 nm) shielding.

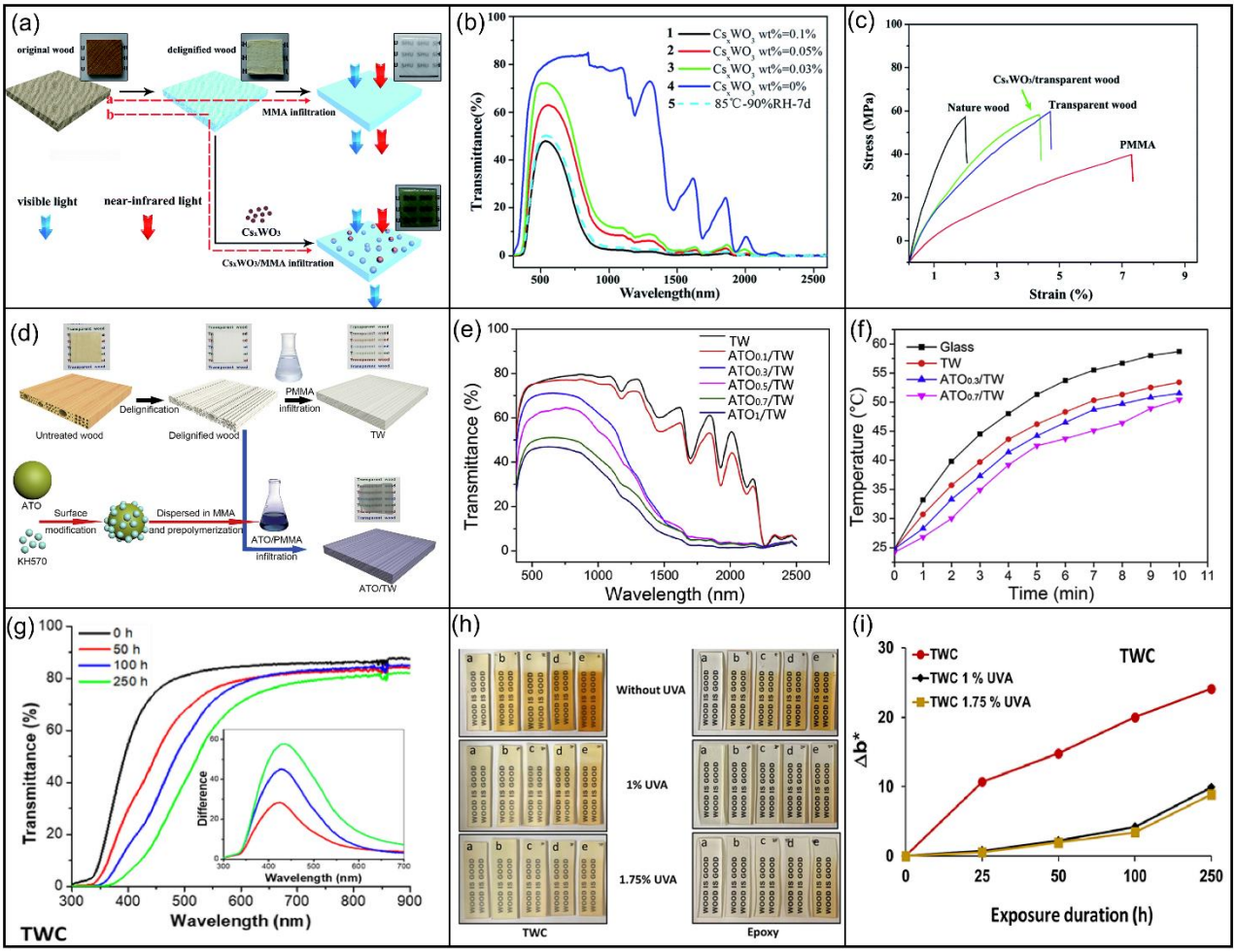

Figure.5 Demonstration of solar control TW. (a-c), Reproduced with permission, Copyright 2017, Royal Society of Chemistry[9a]: (a) Fabrication route and sample image of the Cs$_x$WO$_3$/transparent wood; (b) Transmittance spectra of Cs$_x$WO$_3$/transparent wood at different concentrations (0 %. 0.03%,0.05%, and

0.1%); (c) stress–strain curves in uniaxial tension for nature wood, PMMA, transparent wood, and Cs_xWO_3/transparent wood; (d-f), Reproduced with permission, Copyright 2019, Elsevier [9c]:(d) Illustration for the preparation of TW and ATO/TW; (e) Transmittance spectra of ATO/TW composites at different concentration (0.1%, 0.3%, 0.5%, 0.7%, and 1%); (f) Temperature-time curves inside the box undergoing infrared light irradiation of different samples; (g-i), Reproduced with permission, Copyright 2021, Elsevier [71]:(g) Effect of UV irradiation on transmittance spectra of TWC; (h) Images of effect of light irradiation on TWC and epoxy without and with Btz-UVA (Conc. 1.0% and 1.75%); (i) Changes in yellowness (Δb) of TWC without and with Btz-UVA (conc. 1 and 1.75%) after UV exposure.*

The first solar-control TW was seemingly reported by Yu et al in 2017 [9a]. The heating shielding TW were prepared by infiltrating Cs_xWO_3 nanoparticles with polymerized methyl methacrylate (PMMA) into the delignified wood scaffold (Fig. 5a). The final Cs_xWO_3/TW retained high visible light transparency (~72% transmittance at 550 nm) at Cs_xWO_3 content of 0.03 wt.%. More interestingly, optical transmittance was increased slowly across the visible range (400-800 nm) after 7 days, though the authors did not provide any explanations. The transmittance of Cs_xWO_3/TW in NIR range was significantly reduced compared to neat TW (clearly from the images), but no specific solar shielding values were offered (Fig. 5b). The strength of Cs_xWO_3/TW was slightly decreased (from 60.1 MPa to 59.8 MPa, (Fig. 5c)) compared to pure TW, while the modulus was increased moderately (from 2.67 GPa to 2.72 GPa). The model simulations showed that the temperature of the doll house equipped with Cs_xWO_3/TW increased from 21.6 to 26.8 °C, while the temperature of the doll house equipped with normal glass increased from 21.5 to 41.5 °C after 10 mins of simulated solar radiation, indicating a great potential for energy saving applications.

Another research exploring NIR shielding effect was reported by Qiu *et al* in 2019[9c]. Antimony-doped tin oxide (ATO) nanoparticles combined with PMMA were impregnated into delignified wood scaffold to prepared ATO/TW with excellent mechanical properties, thermal performance and NIR shielding effect (Fig. 5d). The 0.3 wt.% incorporation of ATO improved the interfacial bonding between PMMA and wood scaffold, leading to a higher fracture strength of 96.4 MPa and modulus of 4.27 GPa compared to pure TW (93.0 MPa and 3.38 GPa). The thermal conductivity of ATO/TW remained at ~0.2 W/(m·K), suggesting considerable thermal insulation. ATO/TW exhibited excellent UV blocking and NIR shielding effect due to the introduction of ATO, which also lowered the visible transmittance (~40-70% at 550 nm, varying with the ATO content). The transmittance of ATO/TW across the infrared region (780–2500 nm) and UV range (300-400 nm) were decreased remarkably compared to that of TW (Fig. 5e). The model experiments showed that the rising rate of the temperatures inside the doll house using ATO/TW as glazing materials was constantly lower than that of the doll house equipped with TW or glass (Fig. 5f). Under the protection of ATO/TW, *A. niger* retained high bioactivity after 1 hour of UV radiation, indicating excellent UV blocking performance. This is of great significance for extending the service life of indoor items. Zhang *et al* also observed similar results by using W-Doped VO_2 nanoparticles as the functional fillers [9b].

Though a high UV blocking effect for indoor items can be achieved, UV radiation may cause appearance deterioration, chemical degradation, microstructure breakdown and mechanical property loss of the impregnated polymers when exposed to solar light[72]. Priya Bisht *et al* prepared UV-resistant TW by impregnating epoxy resin and an UV absorber (2-(2H-benzotriazol-2-yl)-4, 6-di-tert-pentylphenol) into the lignin-modified scaffold [71]. The transmittance loss of UV-resistant TW at 550 nm after 250 hours of UV irradiation was close to zero (1.43%), while this figure soared to 27.46% when it comes to pure TW (Fig. 5g). The obvious color changes (yellowness) were observed in all samples after exposure to UV, indicating the high UV sensitivity of TW. However, the color changing speed of TW with UV absorber (UVA) was much

lower than that of TW without UVA (Fig. 5h & 5i). Such results suggested that the prepared TW has high UV stability due to the presence of the UV absorber.

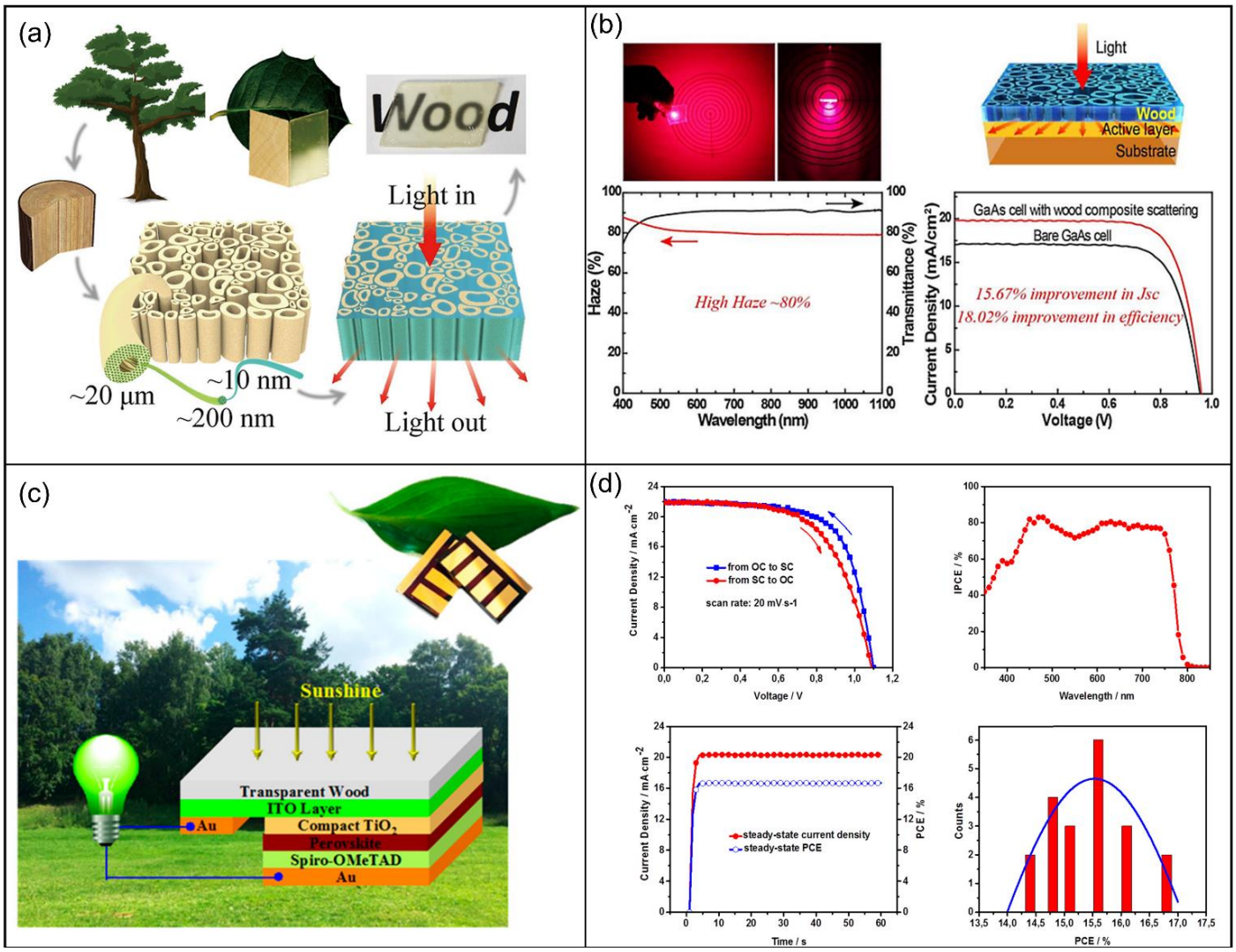

Figure.6 Composite image of adapted images comprising; a transparent wood (TW)-based gallium arsenide (GaAs) thin film solar cell construction that yielded enhanced power conversion efficiency as well as short circuit current densities (a & b). Reproduced with permission, Copyright 2016, Elsevier [73]; The solar cell structure based on TW (c) and a further performance advance of GaAs cells based on TW substrates, with the associated optical and current-voltage properties (d). Reproduced with permission, Copyright 2019, American Chemical Society [74].

Solar control is also crucial to solar cells. Two TW photovoltaic (TW-PV) systems are introduced here, though no extra functionalities were involved in a typical TW based solar cell. Zhu *et al.* first demonstrated that TW can be used for GaAs solar cells in 2016, where an 18% efficiency improvement versus bare GaAs cells (from 12.21% to 14.41%) was obtained as well as a J_{SC} (short-circuit current density) of 19.78 mA/cm^2, a V_{OC} (open-circuit voltage) of 0.968 V and fill factor (FF) of 76%, due to the high optical transmittance (~90%) and concurrent high haze (~80%) over a broad wavelength range between 400-1100 nm (Fig. 6a & 6b) [73]. This was followed up in 2019, by Berglund and co-workers, who reported the first perovskite solar cells constructed on ITO-coated TW substrates [74]. The assembled solar cell structure is shown in Fig. 6c. Such TW-PV cells showed the highest power conversion efficiency up to 16.8%, at 100 mW/cm^2 AM 1.5 G simulated irradiation with a J_{SC} of 21.9 mA/cm^2, a V_{OC} of 1.09 V, and an FF of 70.2%. These values are only marginally lower than that of FTO-glass based PV (power conversion efficiency of 18.9%, Jsc of 24.2

mA/cm^2, V_{OC} of 1.10 V, FF of 71.1%, shown in Fig. 6d). Such devices could retain 77% of the initial performance after 720 h of aging, showing a good long-term stability. Further, through surface control of the TW substrate, variations in transmittance and haze should be obtainable at the low coating temperatures.

Reports on TW-PV are still in the early stages, and despite recent lab advances, further development is needed to compete with established technologies. For example, industrially-produced crystalline silicon PV cells have conversion efficiencies of 18-22%, whereas LONGi achieved a world-record conversion efficiency of 26.81% with a silicon heterojunction architecture, which is approaching the practical limit for a single-junction silicon cell[75]. This is also the case for thin-film based comparators, e.g., gallium-arsenide (GaAs) PV technologies can show similarly high conversion efficiencies, often in conjunction with light-concentrating optics, while the best-reported lab-based report to-date has been as high as 68.9% (by the *Fraunhofer ISE* team in 2021) – many multiples of the best-reported TW-PV system [76]. Alternatively, other novel architectures, competing with TW-PV, such as $AgBiS_2$ nanocrystals, also show great promise (current density of 27 mA/cm^2, a power conversion efficiency of 9.17% (8.85% certified) and high stability under ambient conditions) [77].

3.2 Chromic Transparent Wood

The static and fixed optical properties of conventional TW may not suffice for smart applications, which has led to the development of TW with environmentally-responsive optical properties. Chromic TWs have seen significant development, particularly in the areas of temperature-responsive thermochromic (TC), electrically-responsive electrochromic (EC), and light-responsive photochromic (PC) functionalities. These composites are capable of varying their visible optical properties (i.e., transmittance, reflectance, color and haze) t in response to one or several external stimulus[78]. In addition to potential glazing and broader architectural applications, these mechanically-robust, energy-efficient, potentially colorful, stimuli-responsive TW, could readily find applications in smart packaging, anti-counterfeit materials, intelligent optical sensors, temperature indicators, smart switches as well as energy storage and conversion. However, an issue with chromic filler inclusion into TW is that it can (slightly) increase the haze of the composite – the higher the chromic material loading, the greater the haze, while particle size effects are also important [79]. Thus, there is an elected trade-off between the enhancement of chromic properties and haze, depending on particular applications [80].

The TC TW can be obtained via directly impregnating the wood scaffold with TC polymers, such as poly(N-isopropylacrylamide)(PNIPAM), which is known for its variable visible transmittance. The transition temperature of PNIPAM is also known as the lower critical solution temperature (LCST~32 ^oC). Below the LCST, PNIPAM is visually transparent due to the highly structured hydration shell resulted from strong hydrogen bonding. As the temperature increases, hydrogen bonding weakens, leading to phase separation, in which PNIPAM chains are dehydrated and aggregated into a tightly packed globular conformation[81]. As a result, PNIPAM becomes visually opaque. Wang et al. prepared thermochromic TW based on PNIPAM[82]. The in situ fibrillation of cellulose microfibrils in delignified wood was achieved by TEMPO-mediated oxidation[83], yielding TO-wood. The TO-wood was strengthened via hydrochloric acid induced nanoscale aggregation between cellulose microfibrils, obtaining A-TO-wood. PNIPAM was infiltrated into TO-wood and A-TO-wood, creating a TC TW hydrogel. The transmittance (Fig. 7a) of TO-wood/PNIPAM (~85.8%, 2mm) is higher than that of A-TO-wood/PNIPAM (~64.5%, 2mm) due to aggregation of the cellulose microfibrils, while their mechanical properties showed the opposite trend. The A-TO-wood/PNIPAM (~845kPa) showed a much higher strength compared to TO-wood/PNIPAM (~317kPa) due to the stiffening of cell walls by acid treatment (Fig. 7b). More interestingly, A-TO-wood/PNIPAM and TO-wood/PNIPAM sharply changed from transparent to white when the temperature was increased from 20 to 40 ^oC (Fig. 7c),

while the pure PNIPAM remained translucent, indicating a lower solar modulation capacity. The complete opacity of A-TO-wood/PNIPAM and TO-wood/PNIPAM can be attributed to scattering effects at the interface between the hydrophilic cellulose microfibrils and the hydrophobic PNIPAM when the temperature is above LCST.

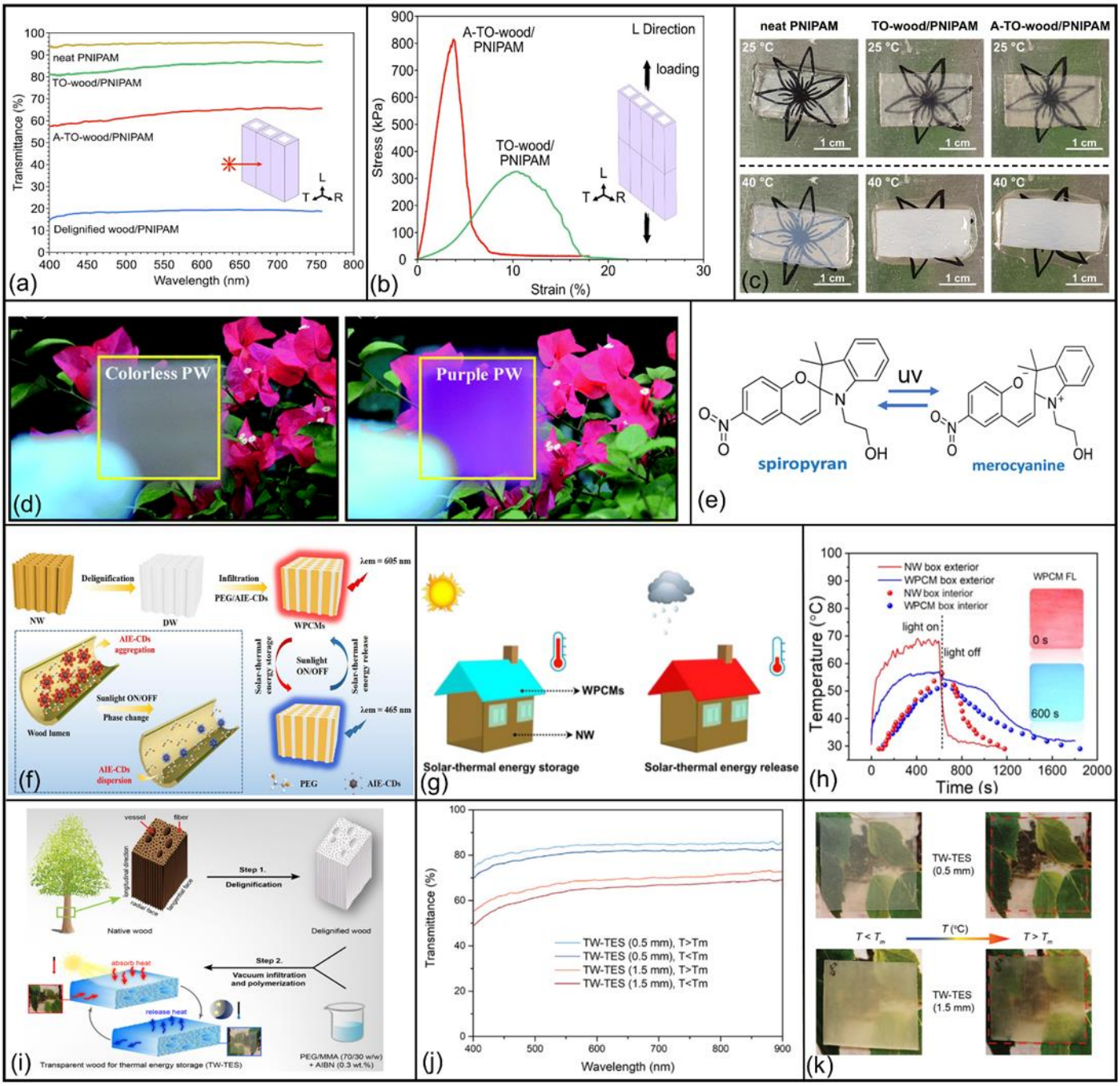

Figure. 7 Examples of chromic TW. (a-c), Reproduced with permission, Copyright 2021, Elsevier[82]: (a)Total optical transmittance of neat PNIPAM, delignified wood/PNIPAM, TO-wood/PNIPAM and A-TO-wood/PNIPAM hydrogels; (b) Typical tensile stress–strain curves of TO-wood/PNIPAM and A-TO-wood/PNIPAM composite hydrogels in longitudinal direction; (c) Photos of samples at different temperatures to show the thermochromic behaviors. (d-e), Reproduced with permission, Copyright 2019, Royal Society of Chemistry[84]: (d)Images of colorless PW and purple PW with flowers; (e) The UV induced reversible chemical structural changes between spiropyran and merocyanine; (f-h), Reproduced with permission, Copyright 2021, Elsevier[85]: (f) Schematic diagram of TW-PCM construction and thermochromic mechanism; (g) Demonstration of TW-PCM as the energy saving roof; (h) Temperature-time curves TW-PCM compared to

natural wood during the simulation; (i-k), Reproduced with permission, Copyright 2019, American Chemical Society[54]: (i) Schematic representation of the two-step preparation of TW-TES applications; (j) Optical transmittance of TW-TES at below and above the melting temperature (T_m) of PCM in the visible spectrum range; (k) Images of TW-TES under different temperatures showing the reversible opaque to transparent changes.

Apart from temperature, changes to optical properties can also be induced by light. In 2019, Wang *et al* experimentally demonstrate TW-PC with photo-switching of transmittance in the visible light region [84]. The TW-PC was obtained by infiltration of the PC material 3′,3′-dimethyl-6-nitro-spiro[2H-1-benzopyran-2,2′-indoline]-1′-ethanol (DNSE) and pre-polymerized methyl methacrylate (MMA). The color tuning properties (i.e., a vibrant purple-to-colorless change under light illumination, as shown in Fig. 7d), results from the chemical structure switching (spiropyran to merocyanine, Fig. 7e) of DNSE under UV light. Liu *et al*, in 2021, formed fluorescent TW-TC based composite (phase change materials) PCMs (TW-TC-PCM) by encapsulating PEG (as the PCM) and aggregation-induced emission carbon dots (AIE-CDs; acting as the TC and photothermal materials, in Fig. 7f) [85]. The aim of exploring this system was to develop an intelligent visual color change monitoring system for improved energy utilization in solar-thermal energy conversion and storage. The TW-PCM underwent a solid-liquid transformation that promoted AIE-CD's dispersion thus changing fluorescence properties and allowing real-time and visually capture, convert, and store solar energy via fluorescent TC and photothermal conversion processes (Fig. 7g) – the AIE-CDs emitted blue fluorescence in the dispersion state (solar-thermal energy release) and red AIE in the aggregation state (solar-thermal energy storage). The TW-PCM possessed great solar-thermal conversion capacity due to the strong and broad solar light absorption behaviors of AIE-CDs. TW-PCM also exhibited a high latent heat of fusion (160.8 J/g), favorable stability over 150 heat–cool cycles, thermal stability <210 °C and good shape stability. The TW-PCM device contributed to the decrease of the box exterior in the simulation (Fig. 7h), indicating its potential for energy-saving buildings.

Another chromic TW via PCMs combination was conducted by Montanari *et al*, though it was originally for looking into thermal energy storage (TES) systems within TW [54]. Mesoporous TW structures are ideal supporting, non-leaking carriers for PCMs, ensuring shape stability during the thermal cycle. A shape-stabilized 70/30 (w/ w) PEG/PMMA-based PCM was encapsulated into a delignified wood substrate (Fig. 7i). TW-TES combines large latent heat (~76 J/g) with switchable and reversible optical transparency due to the phase change of PEG. During the heating process, as the PEG melts, optical transmittance increases by 6% and reaches 68% for a 1.5 mm thick TW-TES (Fig. 7j & 7k). Characterization of the thermal energy regulation performance shows that the prepared TW-TES composite is superior to normal silica glass due to a combination of good heat-storage and thermal insulation properties, implying a great potential in energy-saving buildings. Very recently, Montanari et al[86] achieved significant progress on TW-based TES system. A fully bio-based TES system was prepared within TW by selecting bio-based polymer (PLIMA) and bio-based PCM (1-dodecanol). The resulting TW-based TES system also exhibited excellent heat storage properties and temperature-dependent optical transmittance.

Samanta *et al*, in 2021, demonstrated a temperature- and UV-inducible, dual-stimuli-responsive chromic TW for reversible control of optical properties (in addition to lowered haze, improved transmittance and color change capability, Fig. 8b) [87]. In this case, the UV-polymerized solvent-free thiol and ene monomers containing chromic components (comprising a mixture of TC and PC systems) were infiltrated into the wood scaffold (Fig. 8a). The independent optical properties of individual chromic components were retained in the compositional mixture, allowing for enhancement of the absolute optical transmission to four times above the phase change temperature. Thus, at 20 °C, the TW-TC substrate was opaque, while at 35 °C, the substrate became clear. Likewise, upon exposure to 260 nm UV light, a pink tinge was adopted by the substrate, which

accompanied both the high and low temperature transitions (Fig. 8c). Such a dual TC-PC response under different conditions potentially allows for discrimination of light against temperature, as well as retention of privacy. For example, the transmission at 550 nm could be reduced by 11−77% when exposed to UV by changing the concentration of chromic components. These durable reversible optical properties were demonstrated by multiple cycling testing, while the individual PC and TC properties were non-reactive to each other. In addition, the chromic TW composites showed reversible energy absorption capabilities for thermal energy storage applications and demonstrated an enhancement of 64% in the tensile modulus; comparable to a native thiol–ene polymer.

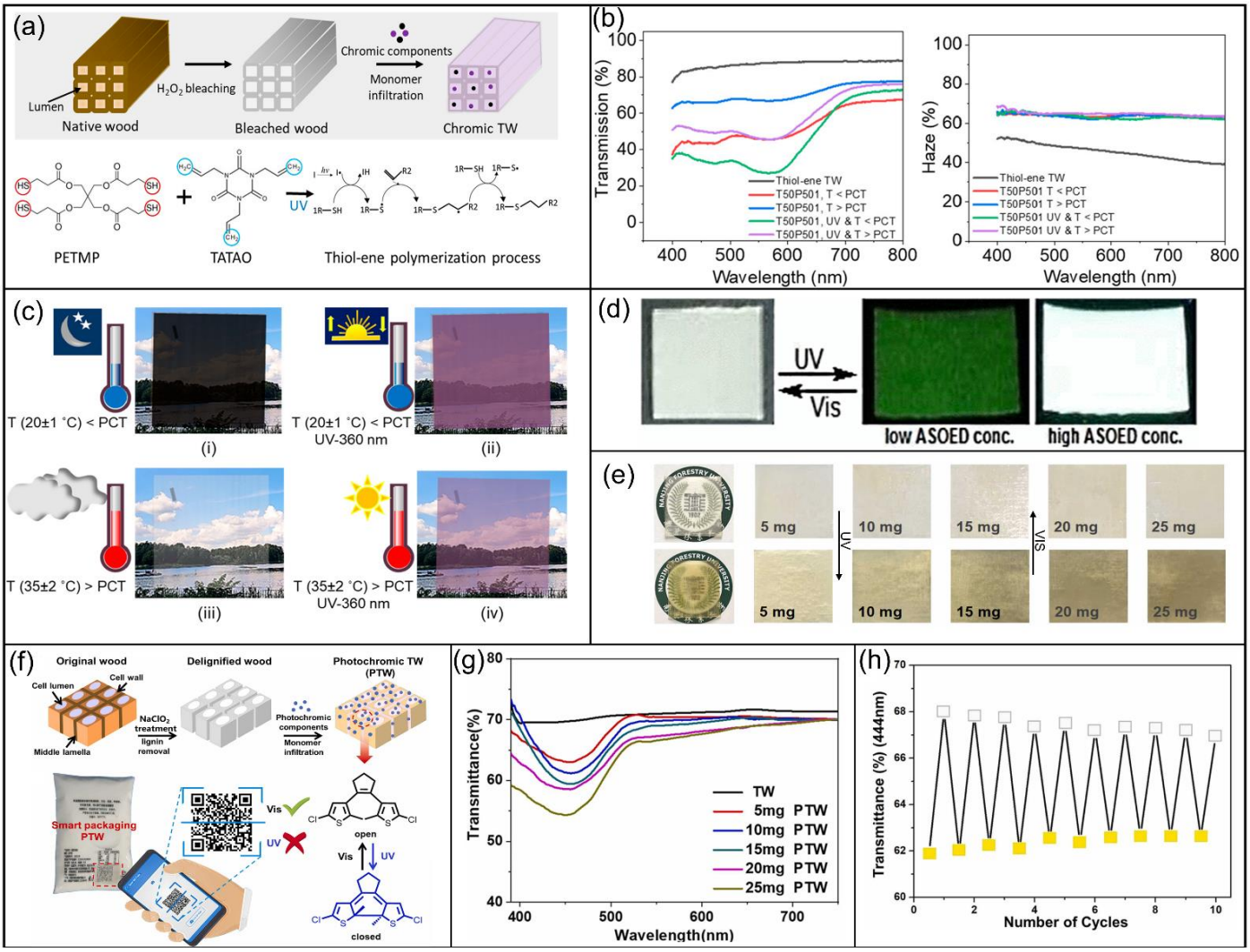

Figure. 8 Demonstration of chromic TW. (a-c), Reproduced with permission, Copyright 2021, American Chemical Society [87]: (a) Fabrication steps for chromic TW and schematic sketch for representation of the polymerization process; (b) Transmission and haze curves of chromic TW on exposure to various conditions of temperature and/or UV mimicking external climatic conditions; (c) Images demonstrating visual change in transmission and color of chromic TW under different conditions; (d) Photographs of photochromic transparent wood under visible light and UV light at different ASOED concentrations. Reproduced with permission, Copyright 2021, American Chemical Society [88]; (e-h), Reproduced with permission, Copyright 2022, Elsevier [89]: (e) The reversible color changes of the PTW with different concentrations of DTE under UV and visible light irradiation; (f) The fabrication process of the PTW and its potential smart packaging applications; (g) The transmittance spectra of TW and PTW under irradiation with 254 nm UV light; (h) The transmittance of PTW (25 mg) at 444 nm after cyclic test through UV (λ = 254 nm) and visible light irradiation.

Al-Qahtani *et al* developed PC and fluorescent TW with a color switching ability in the UV and visible spectrum regions, in 2021 [88]. The fluorescent and TW-PC were generated through addition of methyl methacrylate (MMA) and a photoluminescent Ln-doped aluminium strontium oxide ($SrAl_2O_4:Eu^{2+}$, Dy^{3+}; ASOED) pigment characterized by good photo- and thermal stability. This ASOED phosphor was dispersed without aggregation in pre-polymerized MMA and then subsequently, within the TW framework. A color change from colorless in visible light, to a green colored substrate under UV-irradiation was observed (Fig. 8d), while a photoluminescence absorption signal was also observed at 365 nm and two related emission signals at 433 and 517 nm (Fig. 8d). This demonstrates that the generated transparent luminescent wood exhibited improved UV protection, while showing fast and reversible PC responses to UV light without fatigue.

Most recently, in 2022, Liu *et al* reported on a photochromic TW (PTW) by impregnating PMMA and UV/visible light switchable dithienylcyclopentene-based photochromic dye (1,2-bis(5-chloro-2-methylthiophen-3-yl) cyclopent-1-ene, DTE) fillers into the wood scaffold(Fig. 8f) [89]. The transmittance and the color of the PTW were switchable – a reversible yellow-to-colorless change – under UV and visible light excitation due to a change from the closed-ring (induced by UV light) to the open-ring form (induced by visible light), of DTE (Fig. 8e & 8g). Moreover, the PTW exhibited UV shielding performance, favorable thermal and mechanical properties, as well as excellent transmittance stability (Fig. 8h), comparable to standard TW.

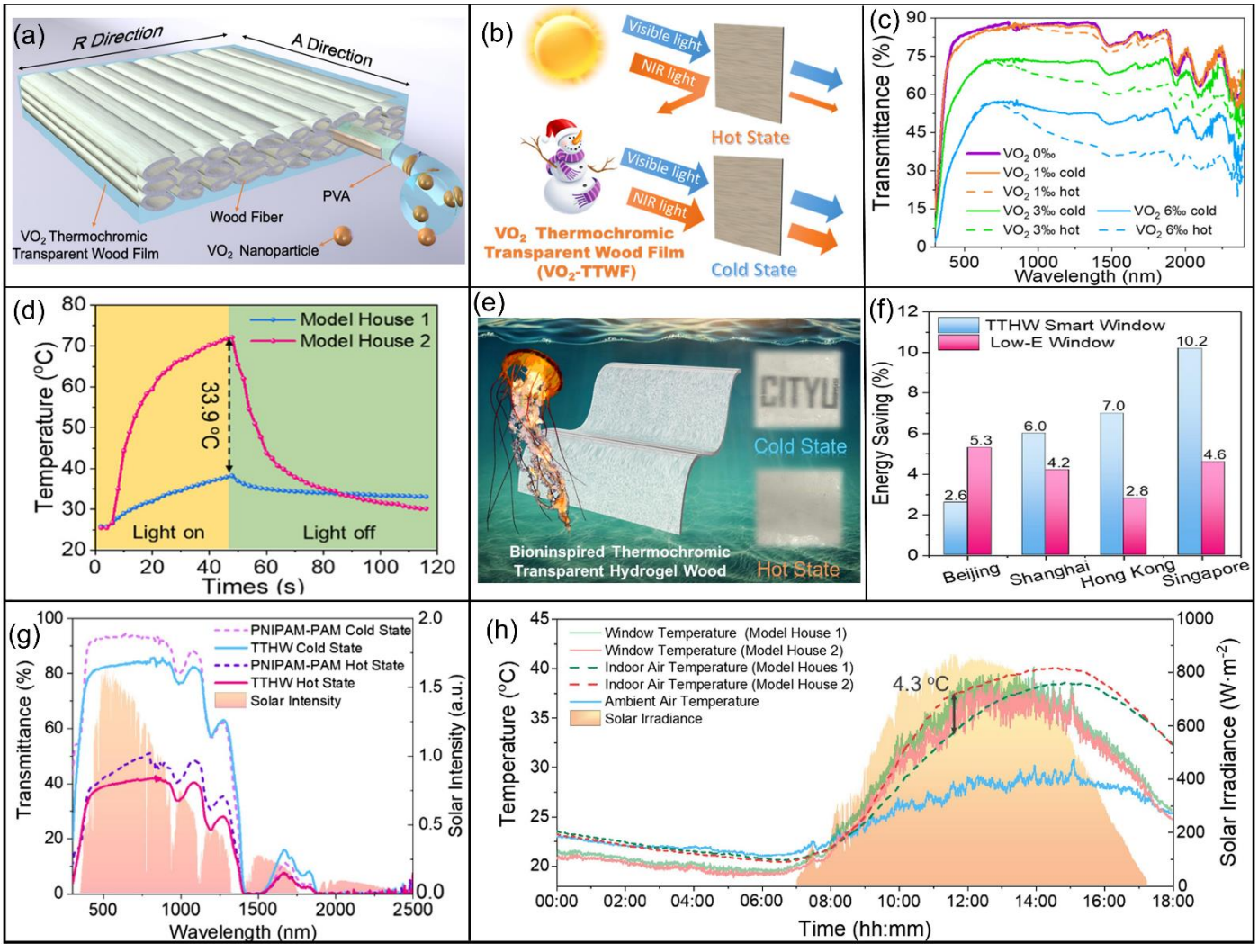

Figure. 9 Demonstrations of chromic TW in infrared range. (a-d), Reproduced with permission, Copyright 2021, American Chemical Society[90]: (a)Schematic illustration of VO_2-TTWF structure; (b) Schematic

illustration of the working states of VO_2-TTWF under different temperatures; (c) The optical transmittance spectra of VO_2-TTW under different temperatures; (d) curves of indoor air-temperature profile in model house 1 equipped with VO_2-TTWF and model house 2 equipped with pure glass; (e-h), Reproduced with permission, Copyright 2021, Elsevier[91]: (e) Images of thermochromic TW under different temperature; (f) Energy saving potential of the TTHW smart window and low-E window compared with the ordinary window; (g) Transmittance spectrum of PNIPAM-PAM hydrogel and TTHW at the cold and hot states; (h) Temperature profiles of the model house field test on the 22nd October 2020 in Hong Kong.

The concept of "chromic" for TW can also extend beyond the visible wavelength range (400 - 800 nm). Liu *et al*, in 2021, fabricated a smart window by impregnating polyvinyl alcohol (PVA) and W-Doped VO_2 Nanoparticles into the wood scaffold (Fig. 9a) [90]. This W-doped VO_2 TW (VO_2-TTWF) showed excellent mechanical and thermal properties (130.6 MPa of tensile strength along the wood growth direction, 0.29 W/(m·K) of thermal conductivity along the perpendicular direction to the wood fibers), as well as excellent solar modulation ability based on temperature change (Fig. 9b). Moreover, the as prepared VO_2-TTWF shows promising luminous transmittance (T_{lum} = 50.5%) and solar regulation capability (ΔT_{sol} = 3.4%), as shown in Fig. 9c. The solar regulation capability results from the intrinsic reversible phase change from a metal (hot state) to an insulator (cold state) across the critical-transition temperature (26.9 ^{o}C). Though the field test did not prove the advantage of solar modulation capability, it showed a desirable temperature reduction (Fig. 9d) compared to conventional glass window due to the infrared shielding ability.

In the same year, Liu also reported another type of TW-wood aerogel, which also showed chromic characteristics in the infrared range [91]. The wood aerogel was prepared by infiltrating Poly(N-isopropylacrylamide) (PNIPAM) into the delignified wood (Fig. 9e). Due to the thermochromic nature of PNIPAM, the wood aerogel showed high luminous transmittance (T_{lum} = 82.7%) under the transition temperature (i.e., 22.9 °C), while when the temperatures were above the transition temperature, it exhibited low luminous transmittance (T_{lum} = 39.8%), indicating a higher solar modulation (ΔT_{sol} = 38.1%) compared to their previous report (Fig. 9g). Model tests and energy-saving simulations suggested that the wood aerogel can reduce the indoor air temperature by 4.3 °C and offer up to 10.2% energy savings compared to quartz glass windows (Fig. 9f & 9h). In these two report the thermochromic characteristic of TW was reflected by the solar modulation capability rather than the usually encountered color changes.

To date, chromically-responsive TW systems are the most intensively reported area of functionalized TW systems. Such reported performance parameters also compare well with alternative substrates with a longer history of development, e.g., PC solar transmittance decreases from 57% to 7.5% in under three minutes [92]. However, speed and transition efficiencies still need further refinement, for example, the considerable improvements required with respect to haze control and transmission offset upon chromic filler material loading. Nevertheless, developments in this area show great promise for improving on best-reported values, especially in architectural and glazing applications, where both capital costs savings (due to reduced cooling requirements), as well as savings from lowered energy costs, offer tangible real-world benefits, if realized.

3.3 Conductive Transparent Wood

TW substrates hold potential for various applications such as flexible electronic devices, tactile sensors, and wearable devices due to their strong mechanical performance, potential flexibility, high transmittance, and low surface roughness. However, TW is intrinsically insulating, and so, achieving electrical conductivity is crucial for its use in these applications.

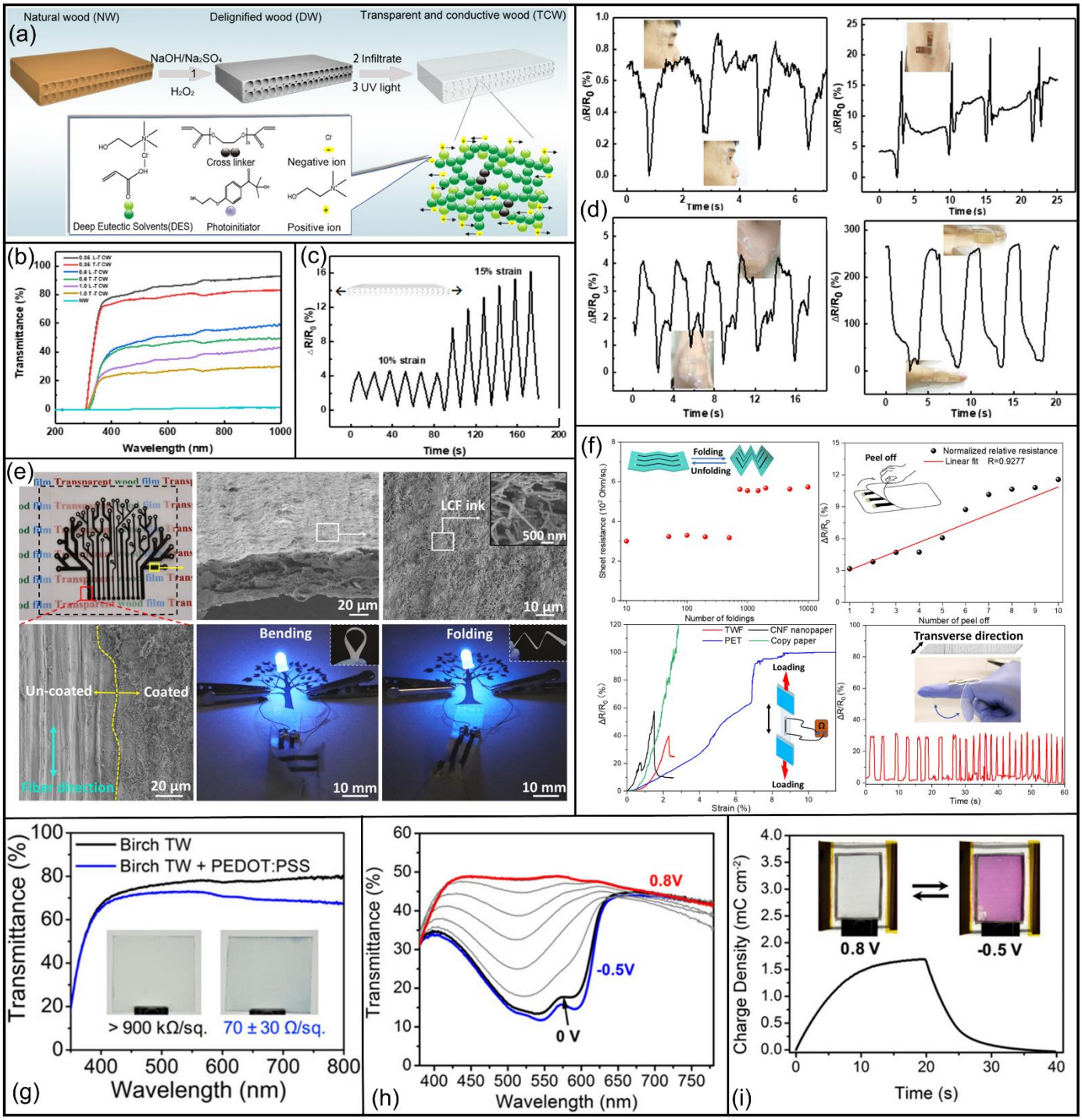

Figure .10 Examples of conductive TW. (a-d), Reproduced with permission, Copyright 2019, American Chemical Society[93]: (a) Fabrication process of TCW and the polymerization mechanism of the impregnating polymer; (b) Transmittance spectrum of the NW and TCW for transverse and longitudinal direction; (c) Resistance-time curves of TCW at different strains (10 and 15%); (d) Demonstration of TCW as train/touch sensors to monitor human activities (eye blinking, throat swallowing, knees bending, and finger bending); (e & f), Reproduced with permission, Copyright 2020, American Chemical Society [94]: (e)Electrical performance, flexibility, and structural surface characterization of the TWF flexible electronics; (f) Sheet resistance of the flexible film electronics versus folding–unfolding cycles. Normalized relative resistance variation as a function of number of peel-off repeats, applied strain and time during 90 °folding, respectively. (g-i), Reproduced with permission, Copyright 2018, Wiley-VCH [66]:(g) Visible transmittance of birch TW with and without the PEDOT:PSS coating. Inset images show the uncoated (left) and coated (right) substrates with their corresponding sheet resistances. (h) Transmittance spectral changes of the magenta-to-clear TW ECD

from −0.5 to 0.8 V. (i) Charge density versus time for 20 s potential square-wave pulses and photographs of the device in its colorless (0.8 V) and colored (−0.5 V) states;

In addition to established conductive materials like PEDOT:PSS, deep eutectic solvents (DES) have also shown promise for achieving conductive substrates. DES are low-temperature mixtures composed of H-bond acceptors (e.g., quaternary ammonium salts) and H-bond donors (e.g., carboxylic acids, polyols), in a certain molar ratio. The advantages of such mixtures include their relatively low cost, that they are often made through green manufacturing routes, as well as their biodegradability, biocompatibility and non-toxicity [95]. Compared with other established TW fillers, the polymerizable DES can be solidified in the delignified wood template simply through irradiation under UV light for short time periods. Wang *et al* reported on stretchable, electrically conducting, TW sensors in 2019 [93]. Such sensors were achieved by combining conductive polymers with polymerizable DES (PDES) – acrylic-acid (AA)/choline chloride (ChCl) – that were used as backfilling agents and in situ photopolymerized under UV-light for a few seconds, in the delignified wood (Fig. 10a). The filling agents inhabiting the channels and pores were chosen because of their low Young's modulus and high stretchability. This resulted in TW composites with high visible light optical transparency (transmittance of 90%, Fig. 10b), good stretchability (strain up to 80%), and relatively high electrical conductivity (0.16 S/m). The beneficial properties were thought to result from the retained cellulose orientation and strong interactions between the cellulose-rich template and PDES. Furthermore, these conductive TWs exhibited excellent sensing behaviors to strain/touch (Fig. 10c), even at low strain, implying that they could be readily used for the detection of weak pressures such as human being's subtle bending-release and other similar activities (Fig. 10d).

In 2020, Fu *et al* reported on the creation of a fully wood-based flexible electronics circuits where a strong, flexible and conductive-TW film substrate was printed with a lignin-derived carbon nanofibers conductive (LCF) ink [94]. The first step involved removal of lignin and hemicellulose from wood, followed by collapse of the cell walls, into a compressed, thin, transparent film. This process preserved the original alignment of the cellulose nanofibers (NF) and promotes their binding. Then, the high-carbon content lignin was electrospun and then carbonized into conductive carbon fibers, which were in turn blended with amyloid fibrils, taking advantage of their strong dispersive and adhesive properties, in order to formulate amyloid/lignin-derived carbon fibers (LCF)-based conductive ink. The LCF were randomly oriented and overlapped to form an electrically conductive, interconnected network that enables long distance electron transport with minimal reduction of electrical properties.

The resultant TCW substrate was flexible while remaining strong in the fiber (i.e., longitudinal) direction with a Young's modulus and a tensile strength of 49.9 GPa and 469.9 MPa, respectively, i.e., making it stronger than most engineering materials, such as petroleum-based plastics and alloys. It was also able to withstand various types of deformations such as knotting, rolling, twisting, and bending without sustaining any obvious cracks or damage, e.g., when wrapped around a 5 mm radius cylindrical object, a shape recovery of ~95% was observed. Further, when the printed circuit was bent or folded, it could still activate a blue light-emitting diode (LED), Fig. 10e. In terms of stability to flexibility, there were negligible changes after 500 cyclic folding/unfolding tests, an ~80% increase in resistance after 1000 cycles, and then relative stability for the remaining cycles up to 10,000 cycles. With the strain increases from 0% to 1%, the randomly oriented protein fibrils/LCF fibers network was rearranged leading to a relative resistance increase of LCF on TCW of ~5%. At 2% deformation strain, the relative resistance change rose to 40% (Fig. 10f). These data suggest that TCW/LFC sensors have better electro-mechanical performance than other substrates due to an absence of strain deformation at low loading and strong adhesion to the ink. A proof-of-concept durable strain sensor for bending testing was attached to the hand, on the joint between the second and the third index phalanges, with

the finger repeatedly bent at 90° then straightened. The normalized relative resistance changed with an amplitude of 30% and varied in synchrony with the finger movement. Similarly, an 8% variation in relative resistance change was observed in the longitudinal direction.

The desirable conductivity of TW can also be achieved by conductive polymer coatings. Lang et al, explored the fabrication of color-changing electrochromic devices (ECD) based on conductive TW substrates for energy-saving smart windows and roofing, in 2018 [66]. PEDOT:PSS was blade coated on the TW surface with a thickness of 140 nm. Despite the coating's excellent conductivity, the inherent transmittance has been slightly reduced (Fig. 10g). Then, highly conducting TW based electrodes were solution-processed with a post-treatment of 1M p-toluene sulfonic acid (*p*TSA) dissolved in ethylene glycol (EG) at room temperature, which increased the conductivity to 1200 S/cm and provided a conductive potential window of −0.7 to 0.8 V versus Ag/Ag^+ – a similar redox response as on ITO (−0.5 to 0.8 V). The resultant TW-based ECD showed a vibrant magenta-to-colorless on-demand switching contrast of 38 Δ%T (ΔE*=43.2) and a highly color neutral bleached state without the need for chemical or electrochemical peroxidation (Fig. 10h & 10i). The process required low energy and power inputs of 3 mWh/m at 2 W/m^2 to switch due to a high coloration efficiency (590 cm^2/C), low driving voltage (0.8 V), and the small charge required to switch the device between its colored and bleached states (1.7 mC/cm^2, 0.02 $\mu Ah/m^2$). Electrochemical impedance analysis revealed that small changes in capacitance and ion diffusion occurred at potentials less than −0.5 V versus Ag/Ag^+, which resulted in faster coloration than bleaching for the magenta-to-clear ECP (ECP-Magenta) films and ECD. The TW substrates also exhibited improved strength and toughness compared to neat PMMA or glass.

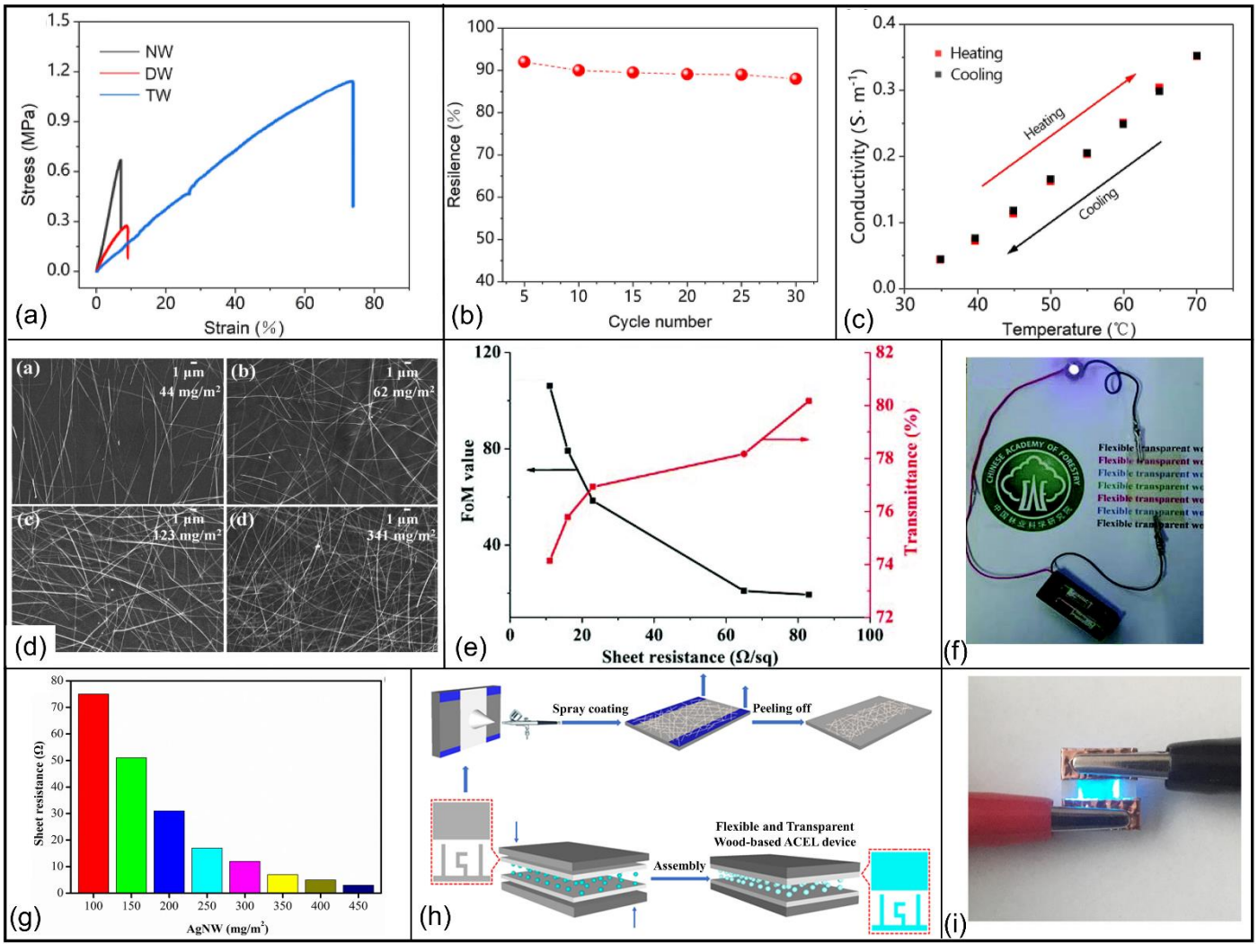

Figure. 11 Demonstrations of conductive TW. (a-c), Reproduced with permission, Copyright 2021, Elsevier[96]: (a)Stress–strain curves of NW, DW (delignified wood) and TW; (b) Resilience of the TW at different cycle numbers measured under 40% strain; (c) The conductivity variation of TW within one cycle of heating and cooling; (d-f), Reproduced with permission, Copyright 2018, Royal Society of chemistry[97]: (d) SEM micrographs of AgNWs deposited on the TW with different area densities; (e) The figure of merit (FoM) value and transmittance curves versus sheet resistance; (f) Image of a lighting LED lighted up by the prepared conductive TW at natural state; (g-i), Reproduced with permission, Copyright 2019, American Chemical Society[98]: (g) Sheet resistance of AgNWs with different area densities; (h) Schematic diagram of the fabrication process of ACEL devices based on flexible conductive transparent wood; (i) Graphics of a light emitting devices based on conductive transparent wood.

Most recently, temperature-based TCW sensor systems were reported by Yang *et al* in 2021, via an alternative DES filler route, again involving AA/ChCl and a photo-initiated polymerization [96]. The resultant 2 mm thick TW composite could withstand physical deformation, with excellent stretchability (maximum tensile strain up to 73.9% and tensile stresses of 1.14 MPa), flexibility (Young's modulus of 3.3 MPa, i.e., readily deformable) and tensile resilience (a resilience of ~92% in the initial cycle, with minor drop-offs, at a constant strain of 40%, shown in Fig. 11a & 11b). Moreover, this TW also had relatively good electrical conductivity (0.04 S/m and a high degree of stability under cycling, as compared to the pure PDES value of 0.15 S/m, at a 0.5 V applied voltage) and good optical properties (visible light transmittance of 72% for a 1.5 mm thick sample, albeit with high optical haze). Electrical conductivity in this system is thought to be facilitated by the free movement of positive and negative ions provided by ChCl in DES. The TCW also has certain electrical conductivity and temperature sensing properties that arise when it is placed in an external electric field-tests found that as the temperature increased, the resistivity decreased linearly within the temperature range of a heat–cool cycle (30-70 °C), as shown in Fig. 11c. Such responsivity was found to be stable, and noise-free, for each condition across multiple heat-cool cycles. Thus, the composite has great potential as a temperature sensor.

Besides impregnating such conductive polymers, the conductive TW can also be obtained through surface coating. Tang *et al,* in 2018, prepared conductive flexible TW films by directly depositing silver nanowires (AgNWs) on TW surface using the Meyer technique (Fig. 11d) [97]. The relationships between the sheet resistances and the area density of the nanowire network were well investigated. As the increase of the area density, the sheet resistance can be lowered to 11 Ω/sq, which was evidently comparable to that of the traditional transparent and conductive oxide (ITO) (10 Ω/sq). Though, the transmittances show a opposite with the increase of area density, the transmittance at 550 nm was as high as 75-80%, which is acceptable for visual purpose (Fig. 11e). The final product was successfully used to light a light-emitting diode even after 100 100 cycles of bending, showing excellent stability (Fig. 11f). Similarly, in 2019, Zhang *et al* reported a much lower sheet resistance (3 Ω/sq, shown in Fig. 11g) and a desirable transmittance (~80 % at 800 nm) through spraying AgNWs on TW substrate [98]. The low sheet resistance was stable during 500 bending tests indicating an excellent reliability. A flexible alternating current electroluminescent (ACEL) device based on the as prepared conductive TW was assembled by sandwiching a luminescent layer between two conductive TW (Fig. 11h). The device showed a maximum value of 18.36 cd/m^2 at a voltage of 220 V (frequency at 1k Hz) in terms of luminance (Fig. 11i). Also, the device exhibited e promising waterproofing properties and excellent durability to withstand external impacts and unexpected damages.

While conductive TW substrates have shown good progress, there are still many advances required to compete with, for example, the established transparent conducting oxide (TCO) substrates (i.e., indium-tin-oxide, fluorine-tin-oxide, among others) which show conductivity values of the order of 1 x 10^3 to 1 x 10^4

S/cm – many orders of magnitude higher than the best-reported TCW to-date [98-99]. However, TCO tend to be hard-surface based application (e.g., glass, steel), and so, the flexibility of TW offers alternative application routes with such novel combinations of materials properties, based on further conductive-TW advances in future.

3.4 Shape Memory Transparent Wood

Shape memory polymers (SMP) are able to memorize and hold temporary, deformed shapes (i.e., via a shape fixity process) and then revert to their original geometries (i.e., shape recovery) via controlled application of external stimuli (e.g., heat, light and magnetic fields) [100]. The preparation of TW-based SMP (TW-SMP) was seen as a challenge initially, due to the requirement of an impregnating polymer that possessed both stimuli-responsive shape-memory properties, as well as a RI that could suitably match the wood substrate. However, such functional TW-SMP would otherwise afford great scope in applications spanning temperature sensors, heat storage, and light-transmitting structural materials. Generally, the shape memory function in TW can be obtained by impregnation of vitrimers.

Vitrimers are a group of reversible, covalently cross-linked polymers derived from thermosetting polymers, with epoxy vitrimers being the first reports and most thoroughly investigated of the family. They consist of molecular networks that can dynamically rearrange their topology through thermally-activated bond-exchange reactions, without changing their cross-link density. Thus, they behave as thermosets below the glass transition temperature (T_g) but become elastomeric above a particular topology freezing point (T_v); when $T_v > T_g$ they exhibit macroscopic flow and viscoelastic fluid behavior [101]. Thus, these systems can combine the mechanical properties of thermosets, with the reprocessability of thermoplastics, while also affording self-healing, and reshaping [102]. Epoxy vitrimers, when used as the polymer filler for TW, are thus able to impart stimuli-responsive, shape-memory, reprogramming, and shape-recovery properties due to the dynamic rearrangements possible under thermal stimulus.

Using the exchangeable covalent transesterification networks of such epoxy vitrimers (Fig. 12a), Wang *et al* made the first report of TW-SMP purely for shape-memory testing, in 2021 [103]. This TW-SMP composite exhibited a cooling-induced shape fixing and heating-induced shape recovery behavior and possessed programmable stimuli-responsive abilities. The transmittance and haze of the resultant TW, at 2 mm thickness, were approximately 60% and 95%, respectively (with slight variation between transverse and longitudinal arrangements, Fig. 12b). As illustrated in Fig. 12c, excellent shape manipulation abilities were obtained including shape-memory, shape-fixation, shape recovery (85%), shape-(re-)programming, shape-erasing, and the management of the arbitrary transformation between the original shape and permanent shape, was obtained, which would broaden the scope of designing future intelligent and advanced functional TW-based thermal-adaptive SMP materials.

Wang *et al*, followed up their 2021 report, with a 2022 advance that increased upon the original T_g (considered a low 30 °C), and further characterized the optical and thermal management properties [104]. The resultant materials had improved mechanical properties thought to be partly due to the highly aligned cellulose fibers of the wood scaffold. Again, epoxy vitrimers were used, with the resultant thermal adapt TW-SMP possessing stiffness at low temperature and flexibility at high temperatures, while also exhibiting high haze and transmittance (approximately 60% and 95%, respectively, Fig. 12d), solid-state plasticity and shape-manipulation capability under thermal stimuli (Fig. 12e). The shape recovery ratios of TW-SMP were as high as 86.7% (transverse) and 94.4%, (longitudinal) respectively. Most importantly, the shape-management capability of TW-SMP enables unique light guiding, directional scattering effects, and tunable transmitted light intensity distribution, potentially allowing for a uniform and consistent daylight distribution (Fig. 12e).

Additionally, the resultant TW possesses great thermal insulation properties - the thermal conductivities of TW-SMP were 0.3002 W/(m·K) (transverse) and 0.2898 W/(m·K) (longitudinal), respectively, which are at least one-third that of common silica glazing glass. All these characteristics make TW-SMP a promising candidate for green, energy-efficient, and advanced and intelligent building materials in 3D applications.

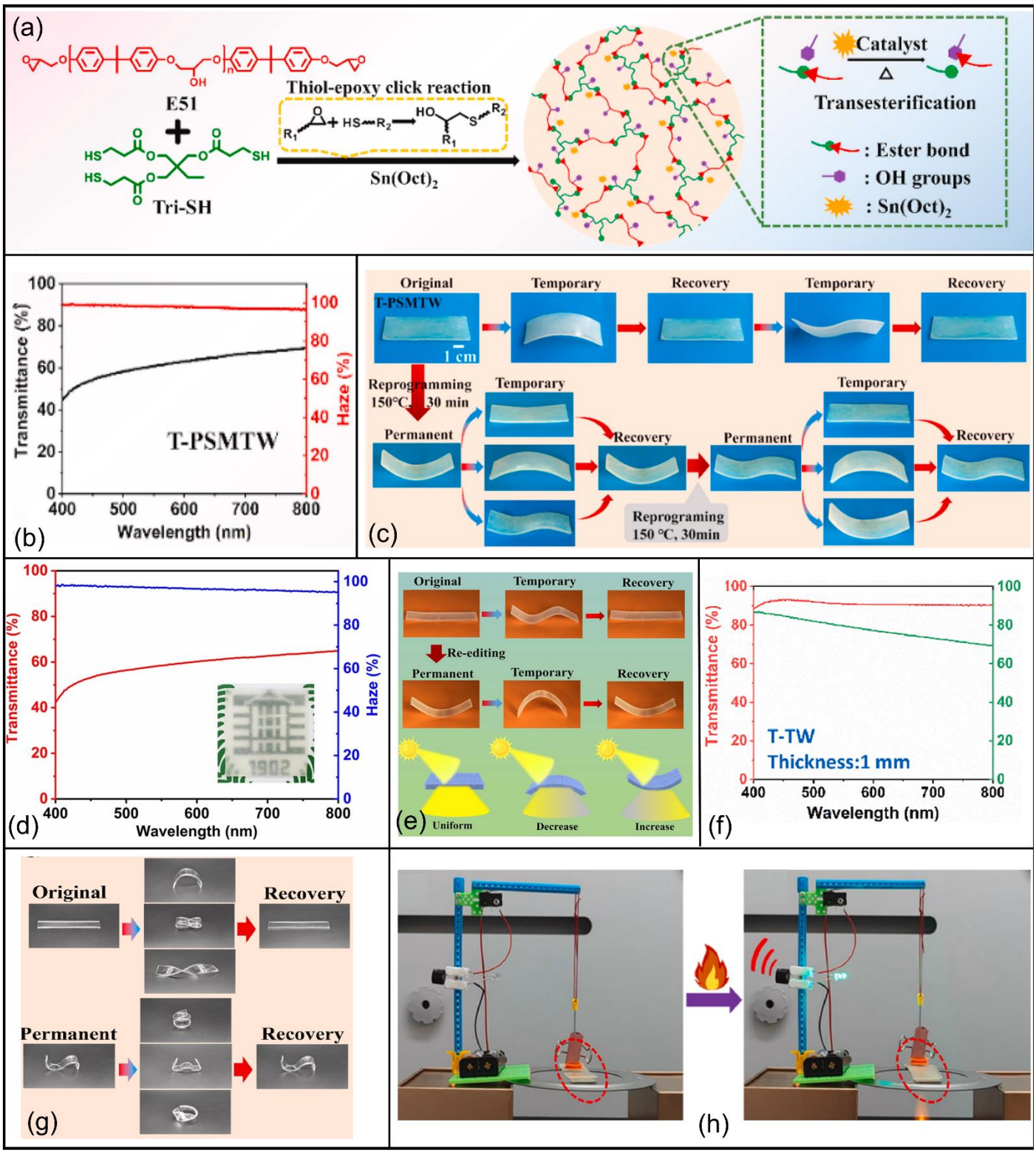

Figure. 12 Demonstrations of shape-memory TW. (a-c), Reproduced with permission, Copyright 2021, Elsevier[103]: (a) Reaction and transesterification mechanism of epoxy-based vitrimers; (b) Transmittance and haze spectra of PSMTW; (c) Photographs of the programmable shape-memory performance of the T-PSMTW;

(d & e), Reproduced with permission, Copyright 2022, Springer Nature [104]: (d) Transmittance and haze spectra of T-ESMTW; (e) Schematic diagrams of the editable shape-memory behavior of ESMTW and its light guiding effect; (f-h), Reproduced with permission, Copyright 2022, Elsevier. [105]: (f) Transmittance and haze of T-TW with thicknesses of 1mm; (g) Digital photo of the reconfigurable shape-memory performance of PTU; (h) Demonstration of the resultant TW for fire alarm applications.

In addition to structural applications, the shape memory characteristics of TW can also be used for fire alarms. A smart shape-reconfigurable TW was fabricated by infiltrating polythiourethane covalent adaptable networks (PTU CANs) into the delignified wood scaffolds by Wang *et al* [105]. The transmittance and haze of TW with thicknesses of 1 mm were 91% and 78%, respectively (Fig. 12f). The fracture strength, elastic modulus, and toughness of TW were 9.45 MPa, 767.31 MPa, and 82.47 kJ/m^3, respectively. Due to the solid-state plasticity and shape-memory behaviors of PTU CANs, the resulting TW exhibited reconfigurable shape-memory performance (Fig. 12g), which allowed the use of a smart actuator for the design of a fire alarm system. The high temperature resulting from a fire triggers deformation of functional TW to its permanent shape, leading to the connection of the closed-circuit switch, triggering the alarm (Fig. 12h). This demonstrated the potential of functional TW for intelligent building applications.

The TW-SMP reports to-date are extremely promising, with properties that compare well with established and more comprehensively researched SMP systems (e.g., polyurethane-based foams where reported toughness values of >800 J/m^3) [106]. Acrylic-based composite, and cyanate ester-based SMP systems also exhibit toughness, tensile strength and elastic modulus values that are also comparable to TW-SMP [107]. However, for real-world application in potential medical (mainly external uses) or industrial (usually non-load bearing) applications, among others, further developments are required, such as faster recovery speeds (down to the order of seconds), as well as the ability to extract such properties from thicker TW substrates.

3.5 Flame-Retardant Transparent Wood

The inherent flammability of wood-based systems poses serious fire risks as well as the follow-on dangers of critical injury and even fatalities. This danger is also true for standard TW substrates, which normally use flammable polymer impregnates to satisfy their optical transparency requirements. As such, it is critical to develop additives or coatings that can ameliorate these inherent flammability risks if TW-substrates are to realistically have applications in future. Such investigations should build on the strong foundation of flame-retardant (FR) timbers to-date.

The flammability process is complex, involving multiple different parameters, such as time to ignition, rate of flame spread, rate of heat release, flame extinction, flaming droplets, smoke/toxic gas evolution as well as its relative composition. Thus, flame retardants (FR) tend to interfere with one or more of these flammability parameters in order to minimize ignitability, as well as any consequent flame spread and gas evolution, to help e.g., increase the time available for occupants to exit an enclosed space. Such FR mechanisms of action include enhanced char formation, dilution and/or displacement of oxygen away from the flame vicinity, alteration of substrate thermal properties, inhibition of chain reactions, as well as minimization of volatile gas formation, among others [108].

FR treatments are typically either coated onto the surface of the wood, or impregnated into the wood structure, most frequently via a vacuum-pressure process [109]. While halogenated (usually bromine-based) FR are considered the most mature, such materials have fallen out of favor due to toxicity issues. Alternative additives currently used include those based on boron, nitrogen, phosphorous, and/or silicon, as well as various intumescent FRs, among a whole host of investigated systems [110]. The fire resistance of such modified woods is usually significantly improved, as indicated by increased limiting oxygen index (LOI) values and cone

calorimeter characterizations – the most widely used bench-scale fire test method. Some of such FR enhancements have also been explored for TW, i.e., FR-TW.

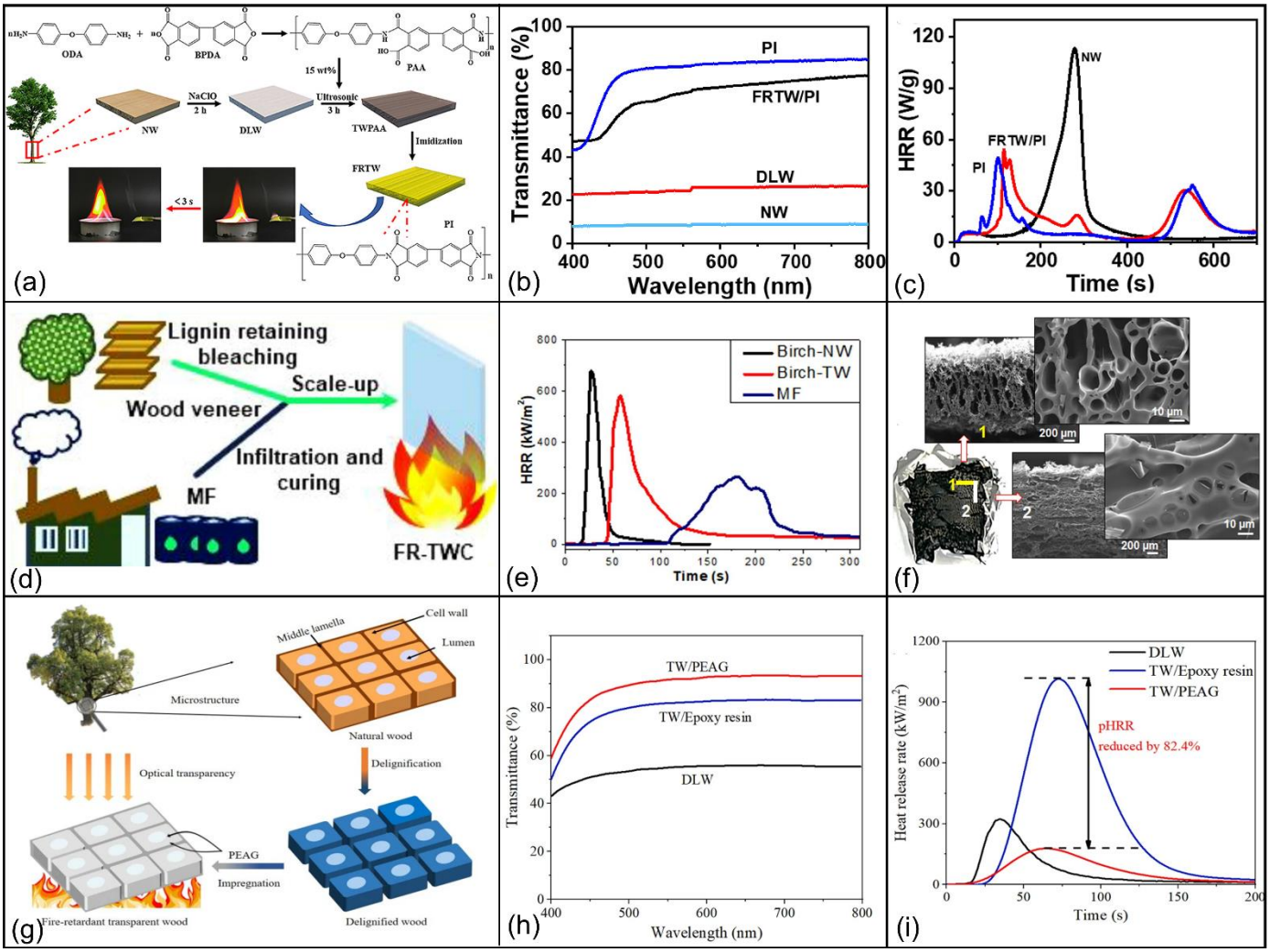

Figure.13 Examples of flame-retardant TW. (a-c), Reproduced with permission, Copyright 2020, Elsevier.[111]: (a) Schematic illustration of the preparation for the FRTW/PI composites; (b) Optical transmittance of NW, DLW, FRTW/PI and PI films; (c) HRR curves for NW, FRTW/PI and neat PI film; (d-f), Reproduced with permission, Copyright 2022, Elsevier [56]: (d) Schematic illustration preparation process of FR-TW based on melamine formaldehyde (MF); (e)HRR curves of birch-NW, birch-TW and MF; (f) SEM images of char residues of birch-TW after cone test; (g-i), Reproduced with permission, Copyright 2022, Springer Nature [52]: (g) The fabrication process of FRTW; (h) Transmittance spectra of DLW, TW/Epoxy resin, and TW/PEAG; (i) HRR curves for DLW, TW/Epoxy resin, and TW/PEAG.

By introducing the impregnating polymer with intrinsic flame retardancy, FR-TW composites can be obtained. As shown in Fig. 13a & 13b, Chen *et al* incorporated polyimide (PI) into delignified wood (DW) slices and obtained both yellowish and FR-TW having a transmittance of 75% at 750 nm, which is comparable to neat PI film (83%) [111]. These substrates self-extinguished within 2 s after leaving the fire source, while exhibiting an enhanced mechanical strength of 169 MPa (Young's modulus 2.11 GPa) compared to natural wood. The microscale combustion calorimetry indicated that the resultant peak heat release rate (PHRR) for FRTW was 53.9 W/g, showing a significantly reduction compared to that (113.1 W/g) of NW (Fig. 13c). The authors attributed such decrease in PHHR to the formation of char residue in the combustion process. Samanta *et al* selected another polymers with inherent flame retardancy – melamine formaldehyde (MF) resin as the impregnating polymer to prepared FR-TW (Fig. 13d) [56]. The as prepared FR-TW showed a desirable

transmittance of 68-74% at 550 nm with an improved tensile strength (60 MPa) compared to neat MF. The infiltration of MF can substantially improve the char forming ability of TW, showing excellent self-extinguishing effect similar to that of MF resin. According to the cone calorimeter test (50 kW/m^2 heat flux), the prepared TW presented a lower peak heat release rate (PHRR~590 kW/m^2) compared to the native birch (688 kW/m^2), and a reduction 84% in total smoke release (TSR) was in comparison with pure MF resin (Fig. 13e). The porous char layer (Fig. 13f) formed from the decomposition of the surface layer might be responsible for the improved fire safety. Chu *et al* prepared a FR-TW via incorporating polyethylene glycol phosphate ester (PEAG)) into DW (Fig. 13g) [52]. Fig. 13h presents a TW/PEAG transmittance of 93% that is higher than that of TW/epoxy resin (82%) and DW (55%). It exhibited a haze of 98%, providing uniform indoor light and enhanced visual comfort with privacy well-protected when being used as windows and roofing in buildings. When exposed to a butane flame continuously, the TW/PEAG was ignited after 150 s and self-extinguished fast within 60 s, whereas the TW/epoxy resin was burnt off within 220 s. In the cone calorimetry test (50 kW/m^2), the PHRR of TW/PEAG was 82.4% (Fig. 13i) less than that of TW/epoxy resin, demonstrating significantly improved fire resistance. The strength of TW/PEAG was reported as high as 153.6 MPa, although this result is not entirely convincing given the abnormal tensile curve shape.

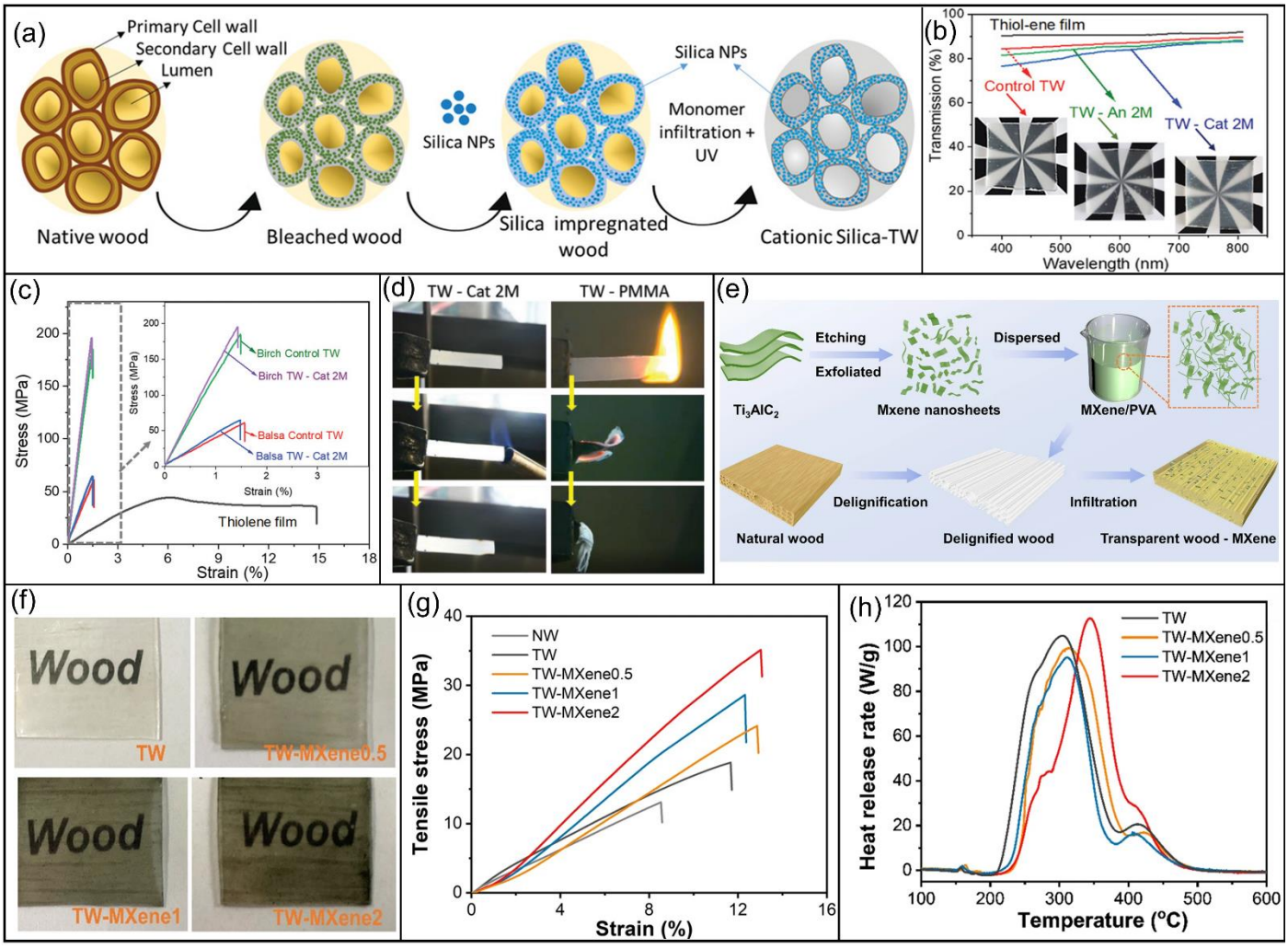

Figure.14 Demonstrations of flame-retardant TW. (a-d), Reproduced with permission, Copyright 2022, Wiley-VCH [112]: (a) Illustration of silica infiltration and formation mechanism of TW biocomposites; (b) Transmittance and haze spectra of silica TW composites; (c) Stress–strain curves of TW composites and neat thiol-ene films; (d) Snapshots from flammability test; (e-h), Reproduced with permission, Copyright 2022, Springer Nature[113]: (e) Fabrication process of TW-MXene; (f) Digital photo of TW with different MXene

concentrations; (g) Stress–strain curves of NW, TW, and TW-MXene composites; (h) HRR curves of TW and TW-MXene composites.

The FR-TW system can also be obtained by the combination of specific flame retardants with normal polymers. Samanta *et al* prepared TW-FR with silica nanoparticle (SiNP; ~30 nm, carrying positive charge) infused into nanostructured cell walls at pH 8.5 (Fig. 14a) [112]. They bleached birch wood veneer instead of delignification, to retain 80% of lignin, and then impregnated the wood slice with thiols and allyl monomers, which were cured under 365 nm UV lamps for 4 min. When 4.8 wt.% cationic SiNP were infused into bleached wood cell walls, they reduced the TW (28 wt.% wood + 67 wt.% resin) transmittance at 550 nm by only 5% (Fig. 14b), despite having a lower RI (RI = 1.45) than thio-ene resin (1.56) and wood substrate (1.54). Despite the decrease in transmittance, the silica NPs enhanced the mechanical properties slightly (Fig. 14c). The addition of 18 wt.% silica to the bleached wood changed its burning behaviors (Fig. 14d), by reducing the flame propagation rate and increasing the final residue from 11% up to 33%, to provide physical barrier effect to mass and heat transfer in flame. In the cone calorimeter test, TSR of the TW was reduced by 23% via silica addition, while its time to ignition was increased by 15s. However, the addition of silica had little effect on the heat release rate and tensile property of TW.

Che's group reported on the addition of delaminated Ti_3C_2Tx (MXene; two-dimensional transition metal carbides or nitrides [114]) into polyvinyl alcohol (PVA)-based TW(as illustrated in Fig. 14e) [113]. When the concentration of MXene was increased from 0.5% to 2%, the visible transmittance was moderately reduced (Fig. 14f). Addition of MXene helped to improve the UV resistance and tensile strength of TW (Fig. 14g). The obtained TW-MXene is much less dense than glass, very flexible and lightweight, making it convenient to transport and install. The thermal conductivity of TW-MXene was 0.31 W/(m·K), slightly higher than that of TW (0.22 W/(m·K)) but much lower than that of glass (1.1 W/(m·K)). Besides, the presence of 1% MXene endowed TW with a 9.3% reduction in PHRR (Fig. 14h). This increased flame retardancy can be ascribed to a barrier effect of the continuous char layer.

Despite many reports on transparent flame-retardant coatings[115], to date, there are seemingly no reports on FR coating on TW substrates. As such, transparent FR coatings for TWs are likely to be fruitful avenues of exploration in future. The development of reliable TW-FR systems is a critical bottleneck that must be suitably addressed before TW can be considered a realistic material for commercial and industrial use. Several reports show promising developments of TW-FR, while encouragingly coinciding with an improvement in mechanical properties. This is heartening as on occasion, conventional FR treatments on wood can result in degraded strength properties due to one or a combination of chemicals treatment, high-temperature treatments and/or treatment approaches. Thus, further improvements that can be reliably reproduced and safely used in real-world applications, are critical in future FR-TW reports.

3.6 Electromagnetic Interference Shielding Transparent Wood

Data and information exchanges based on wireless communication technology are increasingly prevalent, thanks to the rapid development of communication technology, and the fifth-generation of communication technology is likely to accelerate such trends. Though advanced wireless communication technology will likely bring indispensable convenience to our lives, the electromagnetic interference caused by the intensive information exchanges utilizing such systems is an issue that must be considered for ensuring the stability and security of electronic devices [116]. Though various electromagnetic interference (EMI) shielding materials have been developed, the role of transparency was often underestimated. However, the rapid expansion of advanced electronic devices, such as aerospace equipment, artificial skin and wearable devices, raise the need

of optical transparency [117].TW-based EMI shielding systems have the potential to meet the needs of such transparent EMI systems.

The first EMI shielding TW (EMI-TW) report was seemingly by Cho *et al* in 2020[118]. The electromagnetic properties of epoxy-balsa TW were measured by a dielectric resonator. Upon the introduction of epoxy, the dielectric constant of TW was increased from 1.706 (NW) to 3.344 on average, while the loss tangent showed the opposite trend, dropping from 0.0913 to 0.0548. The electromagnetic wave transmission/reflection of TW (ITO as a top layer) were both simulated and measured, with good agreement between both sets of results (Fig. 15a). This indicated that TW has the potential to be an eco-friendly electromagnetic shielding material.

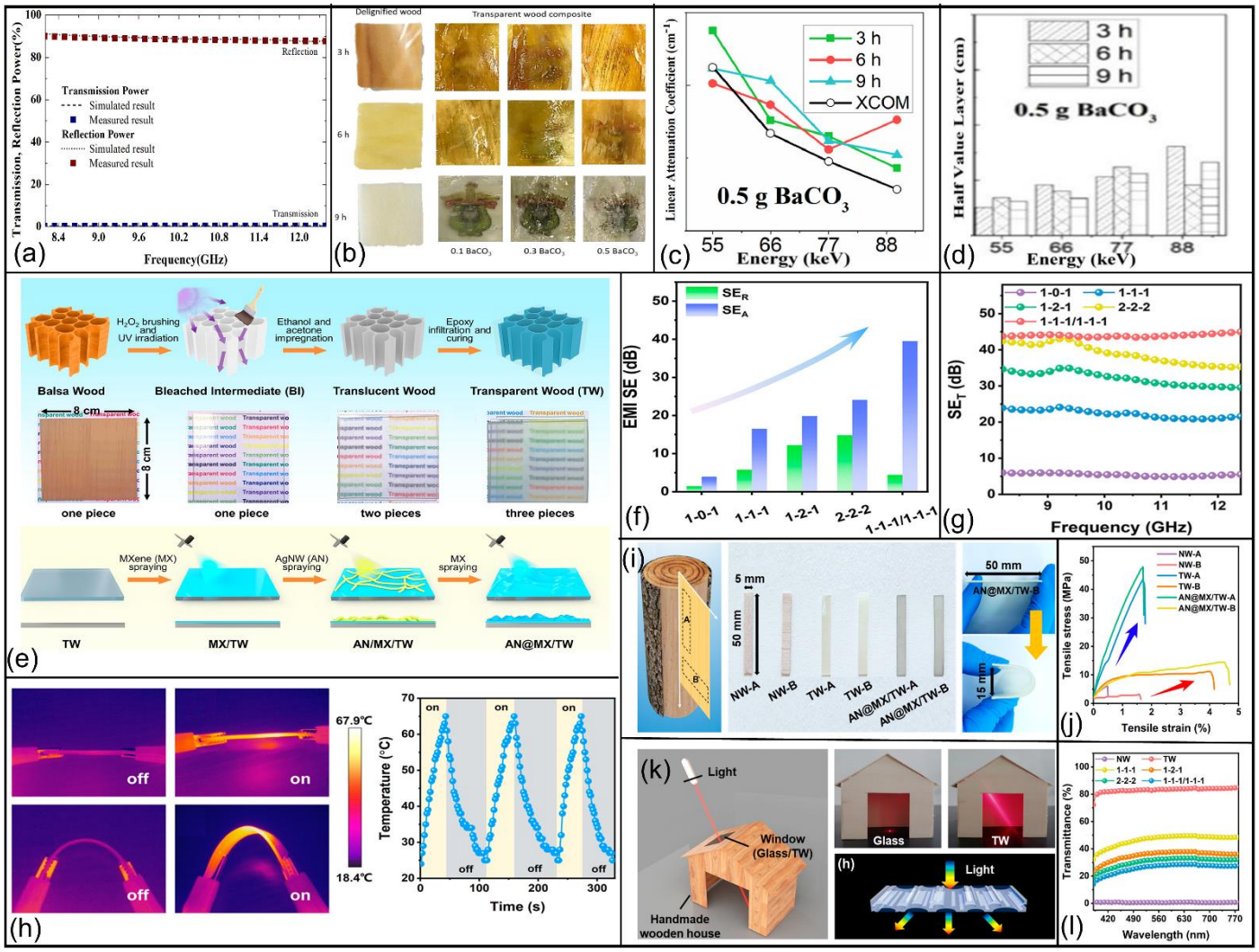

Figure. 15 Examples of EMI shielding TW. (a) Electromagnetic transmission/reflection power of transparent wood with ITO layer, Reproduced with permission, Copyright 2020, Wiley-VCH[118]; (b-d), Reproduced with permission, Copyright 2022, Elsevier. [119]: (b)Digital photos of PVA/Gelatin/$BaCO_3$/wood composite film; The experimental value of linear attenuation coefficient (μ) of the prepared composite film with 0.5 g $BaCO_3$; (d) Half value layer of the prepared composite film with 0.5 g $BaCO_3$; (e-l), Reproduced with permission, Copyright 2022, American Chemical Society[120] : (e) Schematic diagram of fabricating TW and sandwiched AN@MX/TW composites; (f) Average of SE_R and average of SE_A; (g) Dependence of EMI SE_T on frequency; (h) Infrared thermography images of AN@MX/TW composite under straightening and bending at 10 V and its thermal response under circulating current at 10 V; (i) Digital images of tensile test samples showing the

excellent flexibility; (j) Tensile strength of NW, TW, and AN@MX/TW composites; (k) Digital images and principled illustration of scattering phenomena in glass and TW; (l) Visible transmittance spectra of NW, TW, and AN@MX/TW composite.

A more recent report by Muhammad *et al*, explored the functionality of X-ray radiation shielding based on TW[119]. The PVA/gelatin/$BaCO_3$/TW composite was prepared by sandwiching the delignified wood between the shielding solutions (Fig. 15b). The as prepared composites showed considerable visible transparency. Upon addition of 0.5 g of $BaCO_3$ the TW composite achieved the highest linear attenuation coefficient of ~1.37 cm^{-1} at 55 keV due to the dominant photoelectric interaction between photons and absorber materials (Fig. 15c). The half value layer (HVL) was calculated from the linear attenuation coefficient and was shown in Fig. 15d. Upon addition of 0.5 g $BaCO_3$, the sample exhibited the lowest HVL, suggesting an excellent radiation shielding capacity. Overall, the PVA/gelatin/$BaCO_3$/TW composite also holds promise for X-ray radiation shielding applications.

Another EMI-TW structure was reported in 2022 by Chen et al[120]. The EMI-TW was fabricated through sandwiching TW between silver nanowire (AgNW)@MXene composites (Fig. 15e). As shown in Fig. 15l, although the transmittance was relatively low (28.8%), considerable increases in tensile strength were achieved (47.8 MPa, an increase of 9.6%, Fig. 15j). The shielding effectiveness by absorption (SE_A), and shielding effectiveness by reflection (SE_R) both gradually increased with the increasing silver coating layer (Fig. 15f). The average of EMI shielding effectiveness (SE_T) reached 44.0 dB in the frequency of 8-12.4 GHz Fig. 15g). The excellent shielding effectiveness mainly resulted from the absorption and multiple reflections of EWs in the gaps of the 2D MXene sheets reflection. The electrical heating induced by its conductivity had a short response time (40s for heating and ∼60s for cooling, as shown in Fig. 15h) regardless of the shape (straight or bent). When such TW composites were used as windows, a brighter indoor environment was achieved due to the intensive light scattering effect, resulting from the intrinsic high haze of TW (Fig. 15k). This ensures a broad range of future practical applications.

3.7 Aesthetic Transparent Wood

Though the energy, thermal and optical performance of building envelopes is of great importance, aesthetic considerations are also a critical cultural need for human beings and for improving the likelihood of adoption of any eventual products[121]. While TW for energy saving applications have been intensively studied, TW for aesthetic purposes have been less explored. Unlike the various applications covered in previous sections, which are derived from external functional additives (e.g., ATO, VO_2, flame retardants, MXene, Ag nanowires, etc.), TWs for aesthetic purpose have been fabricated through delicate intrinsic structural design by researchers.

The aesthetic TW was reported by Mi *et al* in 2020 [122]. Two types of aesthetic wood orientations (perpendicular and parallel) were fabricated by selectively removing the lignin in early wood areas while preserving the lignin in late wood areas. This allows partial preservation of the annual growth rings of douglas fir wood even after the polymer infiltration (Fig. 16a). As shown Fig.16b, the TW with growth ring patterns showed excellent overall transmittance, despite differences between early wood (~86%) and late wood (~68%). More interestingly, different patterns can be realized by stacking multiple layers of aesthetic TW. Due to the high haze of TW, aesthetic TW has great potential for light guiding and anti-glare applications. Combined with the preserved growth rings patterns, aesthetic TW ceilings combine unique visual beauty with a potentially more efficient indoor lighting (Fig. 16c). The prepared aesthetic TW also showed excellent thermal insulation properties due to the low thermal conductivity. The unique combination of mechanical, optical properties combined with the aesthetic characteristics make such TW a promising candidate for energy

efficient applications with additional aesthetic function. Similarly, Zhou *et al*, also prepared TW with Turing (growth rings) patterns by completely removing lignin in early wood area and partially reserving lignin in the late wood area [123]. This results in the different area transmittance (high in early wood and low in late wood area, Fig.16d). The prepared TW also exhibited desirable heat-shielding capacity as well as remarkable UV blocking ability (Fig. 16e). More interestingly, the prepared TW showed high latent heat (25.30 J/g), which might help mitigate indoor temperature changes.

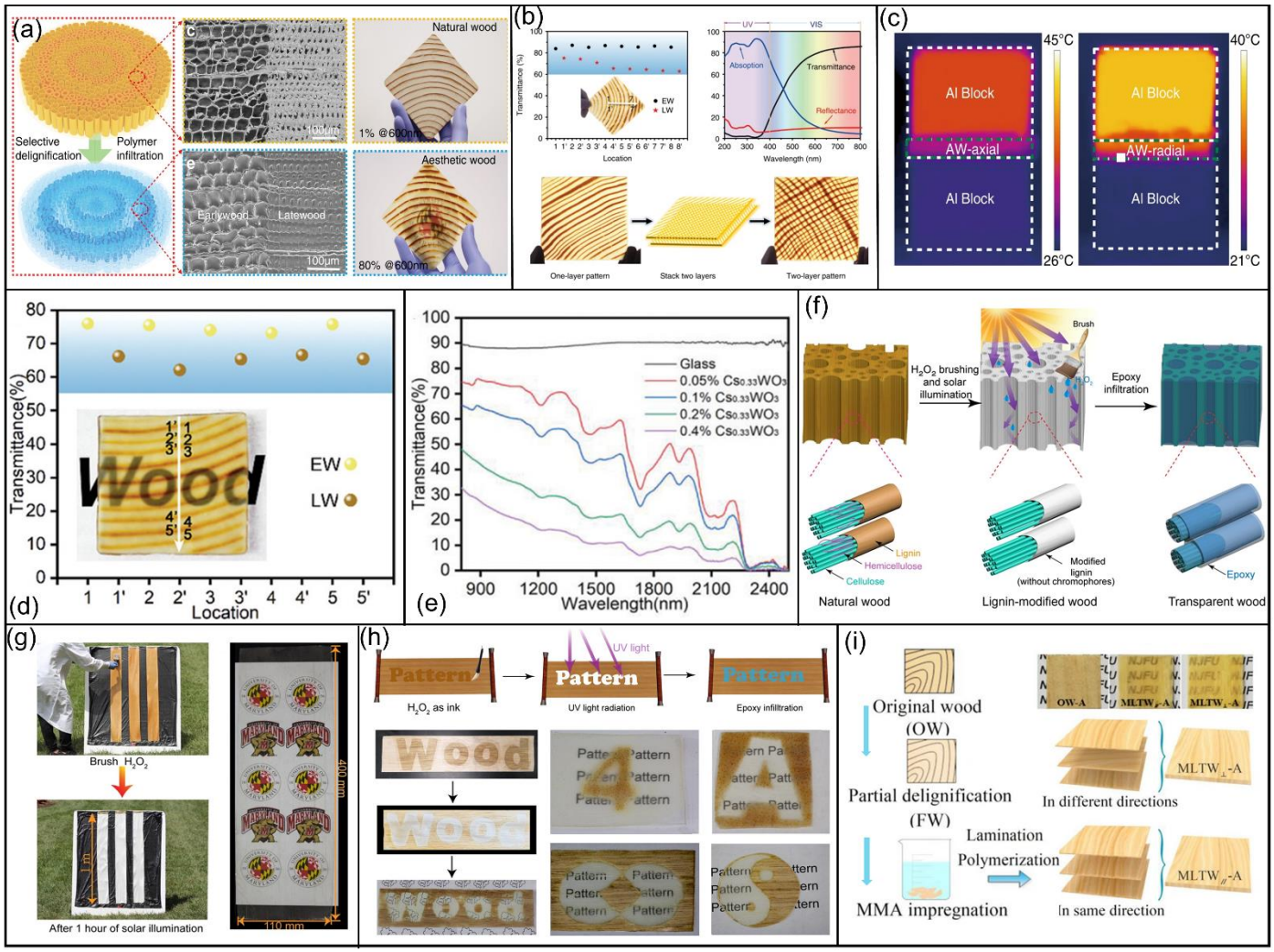

Figure. 16 Examples of Aesthetic TW. (a-c), Reproduced with permission, Copyright 2020, Springer Nature[122]:(a)Schematic procedures for fabricating aesthetic wood with annual growth rings (left), cross-sectional SEM images of natural wood and dense aesthetic wood-R microstructures after polymer filling (middle), and photos of large size aesthetic wood-R (right); (b) The transmittance in the EW and LW of obtained aesthetic wood and the illustration of novel patterns via stacking; (c)Thermal insulating performance of the aesthetic wood; (d & e), Reproduced with permission, Copyright 2022, Wiley-VCH [123]: (d)The visible transmittance at 750 nm in EW and LW area of the TP-TW; (e) The transmittance of TW-$Cs_{0.33}WO_3$ composites in the near-infrared range; (f-h), Reproduced with permission. Copyright 2021, American Association for the Advancement of Science[43]: (f)Illustration of the solar-assisted chemical brushing method; (g) The outdoor fabrication of lignin-modified wood with a length of 1 m and a digital photo of a piece of large transparent wood (400 mm by 110 mm by 1 mm); (h) Schematic and experiments demonstration for aesthetic wood with different patterns; (i) The fabrication process of MLTW and digital photos to showing its natural color and texture, Reproduced with permission, Copyright 2021, Springer Nature[63].

Preserving the intrinsic growth ring is not the only way to fabricate TW with unique patterns. Xia *et al*, prepared patternable TW through a solar-assisted chemical brushing approach [43]. Before H_2O_2 brushing, a trace amount of NaOH (10 wt.%) was applied to the wood surface, aiding the modification process (Fig.16f). Upon UV illumination, the lignin in the brushed areas of wood was modified (i.e., light-absorbing chromophore removal). However, due to lignin-retention in the unbrushed areas of the wood scaffold, its tensile strength (20.6 MPa) was 50 times higher than that of lignin-removed wood (0.4 MPa). This process also possesses potential for large-scale fabrication; 400 mm x 110 mm x 1 mm TW sheets were obtained by such processes (Fig. 16g). In such a manner, TW with different patterns (including "WOOD", "4", "A" and "Tai Ji" pattern) could be obtained (Fig. 16h) to cater to human aesthetic preferences. Besides these two methods, preserving the original texture and color may be another way to achieve aesthetic purpose. Wu *et al*, designed multi-layered transparent wood (MLTW) with natural wood color and texture by impregnating a partially delignified wood scaffold with PMMA [63]. The resultant MLTW holds potential for home decoration and furniture design (Fig. 16i).

Overall, for practical building applications, aesthetics needs to be considered in addition to the technical performances. Products without artistic consideration or aesthetic appeal will not be selected by architects or consumers, despite any admirable technical parameters. Thus, it is of great significance to find the balance between aesthetics and performance in building envelopes to increase their likelihood of adoption.

4. Potential Applications

Since its inception, TW has been designed as a structural material for building applications due to its excellent mechanical, optical and thermal performance. Though the building envelop is still the main expected application for TW, the application area has been extended to many other fields owing to the vast array of extra functionalities. Thus, the application of TW can be broadly divided into two categories: building and optoelectronic devices.

4.1 Building Applications

The use of nature-based materials intrinsically reduces the impacts of manufacturing on the broader environment. Green building materials enable construction of energy-efficient structures that could help decarbonize urban areas and achieve net-zero carbon buildings, whilst also producing sustainable structures that are stronger, more functional and longer-lasting (often outlasting their established counterparts) [124]. Intriguingly, such new materials will also enable the exploration of new design, architecture and construction directions, most likely for light discrimination purposes in the first instance [125].

Conventional building materials and their often energy-inefficient nature make the building industry (both commercial and residential) one of the most energy-intensive sectors on this planet. For example, siliceous glass is the established material for use in building windows for light transmission. However, it suffers from high thermal conductivity (~1.0 W/(m·K)) and is brittle in the event of failure, resulting in unwanted substantial energy loss/gain and potential safety issues. The reflecting and glazing effect of glass not only causes visual discomfort but also results in lower working efficiency, poor emotional well-being, and even occasional traffic accidents [44]. Moreover, the glass manufacturing industry is estimated to emit more than 60 million tons of CO_2 per year [126]. Thus, it is of great significance to promote the green transition of the building industry in terms of materials and energy consumption. Functional TW may play an important role in this anticipated transition due to its optical, mechanical and thermal properties as well as greater sustainability.

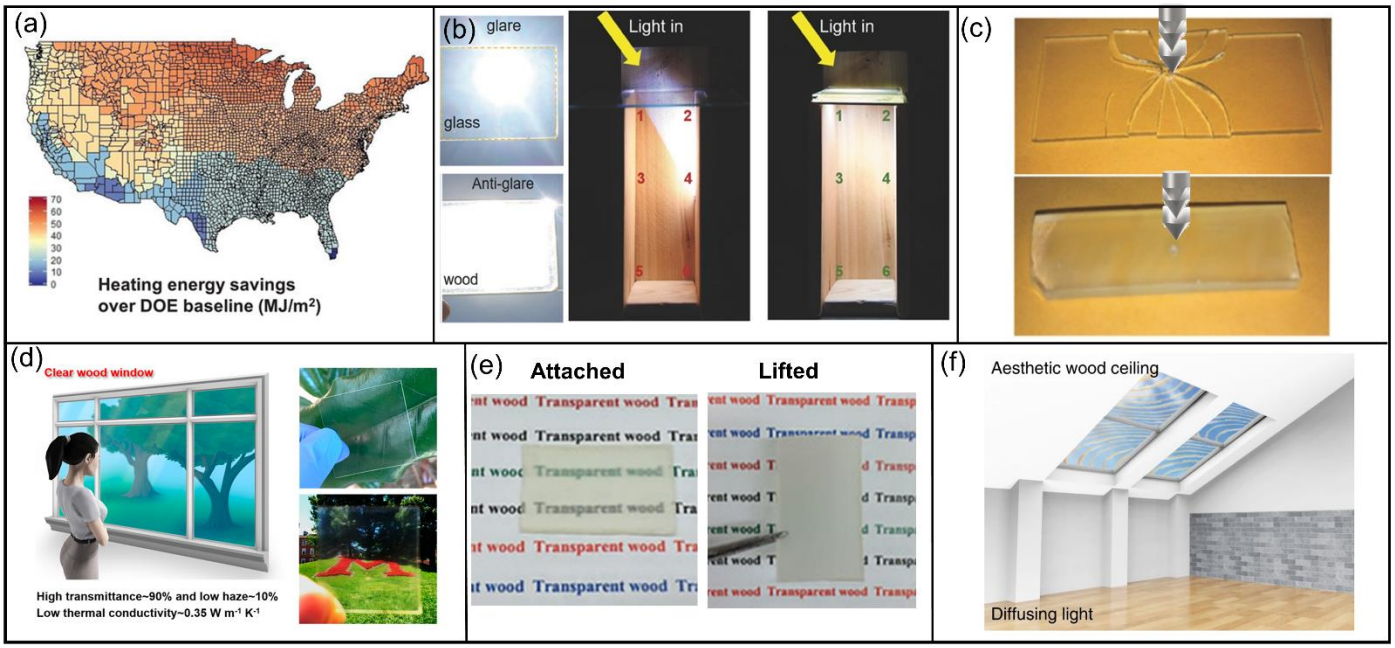

Figure.17 (a) The heating energy savings pattern for the continental U.S. over the DOE baseline, Reproduced with permission, Copyright 2020, Wiley-VCH[49]; (b & c), Reproduced with permission, Copyright 2016, Wiley-VCH[44]: (b) Photographic showing the anti-glare effect and light guide effect of TW; (c) The impact

test of a piece of standard glass and a transparent wood composite of similar thickness; (c) Photographic showing the anti-glare effect and light guide effect of TW; (d) Schematic illustration of the clear wood and its digital images, Reproduced with permission, Copyright 2019, American Chemical Society[55]; (e) Digital photo showing the privacy protection potential of TW, Reproduced with permission, Copyright 2017, Wiley-VCH[42]; (f) The schematic scene shows the light distribution and aesthetic appeal inside a building, Reproduced with permission, Copyright 2020, Springer Nature[122].

TW has been considered one of the most promising green building material candidates for the following reasons: (1) The thermal insulating properties. (2) The ability of visible light guiding and high haze. (3) High toughness. (4) Sustainability. The inherent low thermal conductivity (~0.19 W/(m·K)) of TW makes it a promising candidate for energy saving applications, allowing for lower energy consumptions than conventional glass. The energy saving simulation suggests that TW, when used in double-pane windows with air filling the intervening gap, can provide energy savings compared to the baseline set by the US Department of Energy (DOE). The savings are estimated to be 38 and 23 $MJ \cdot m^{-2}$ per year in old and new buildings, respectively (Fig. 17a) [49]. TW can be used for glazing materials in buildings for visual clarity (low haze) or privacy protection (high haze). The light guide effect of TW enables uniform illumination with enhanced visual comfort (Fig. 17b), while avoiding the glaring effect of common glass (Fig. 17b). Moreover, the potential safety issues of common glass arising from intrinsic brittleness can be avoided due to the high ductility of TW. As shown in the Fig. 17c, after a sudden impact, common glass break into shattered pieces, posing serious safety concerns. Due to its high toughness, transparent wood only bends and splits rather than shattering into sharp pieces, dispelling the safety concern associated with common glass [44]. TW can serve dual purposes as windows, providing both visual clarity and privacy protection, depending on the level of haze. Low-haze TW can be achieved by complete delignification (NaClO) and interfacial design [48-49, 55]. TW with a 10% haze was obtained from NaClO delignification process, indicating a great potential of replacing common glass for visual clarity (Fig.17d). While the high-haze TW with a haze of 75% and a transmittance of 83%, obtained from alkaline/H_2O_2 lignin modification, allows for normal lighting and personal privacy protection (Fig. 17e) [42]. The aesthetic appeal of building envelopes is also a fundamental cultural need for human beings. This can be accomplished through structural design and lamination. As discussed in section 3.7, TW with various patterns, such as letters and the symbol of *TaiJi*, can be obtained via the solar-assisted chemical (H_2O_2) brushing method[43]. By taking advantage of the gradient distribution of lignin between late and early natural wood, aesthetic TW with visually appealing patterns resembling the natural growth rings of trees can be obtained[122-123]. More complicated patterns can be obtained by laminating several layers of TW. Such aesthetically pleasing TWs were showcased as a patterned ceiling installation in a museum or gallery, creating a uniformly illuminated indoor environment (Fig. 17f). From the point view of sustainability, the wood scaffold can be regarded as renewable and biodegradable, and the fabrication process involves less energy consumption as compared to glass making. It is more promising to note that impregnated resins and functional components are transitioning towards more environmentally friendly materials, such as biomass-derived PLIMA, biodegradable PVA and renewable 1-dodecanol[41, 49, 86, 127]. According to the cradle-to-gate life-cycle assessment, the fully bio-based TW system offers higher sustainability benefits (approximately 40% lower environmental indicator metrics) when compared to conventional transparent panels like PMMA and PC [86].

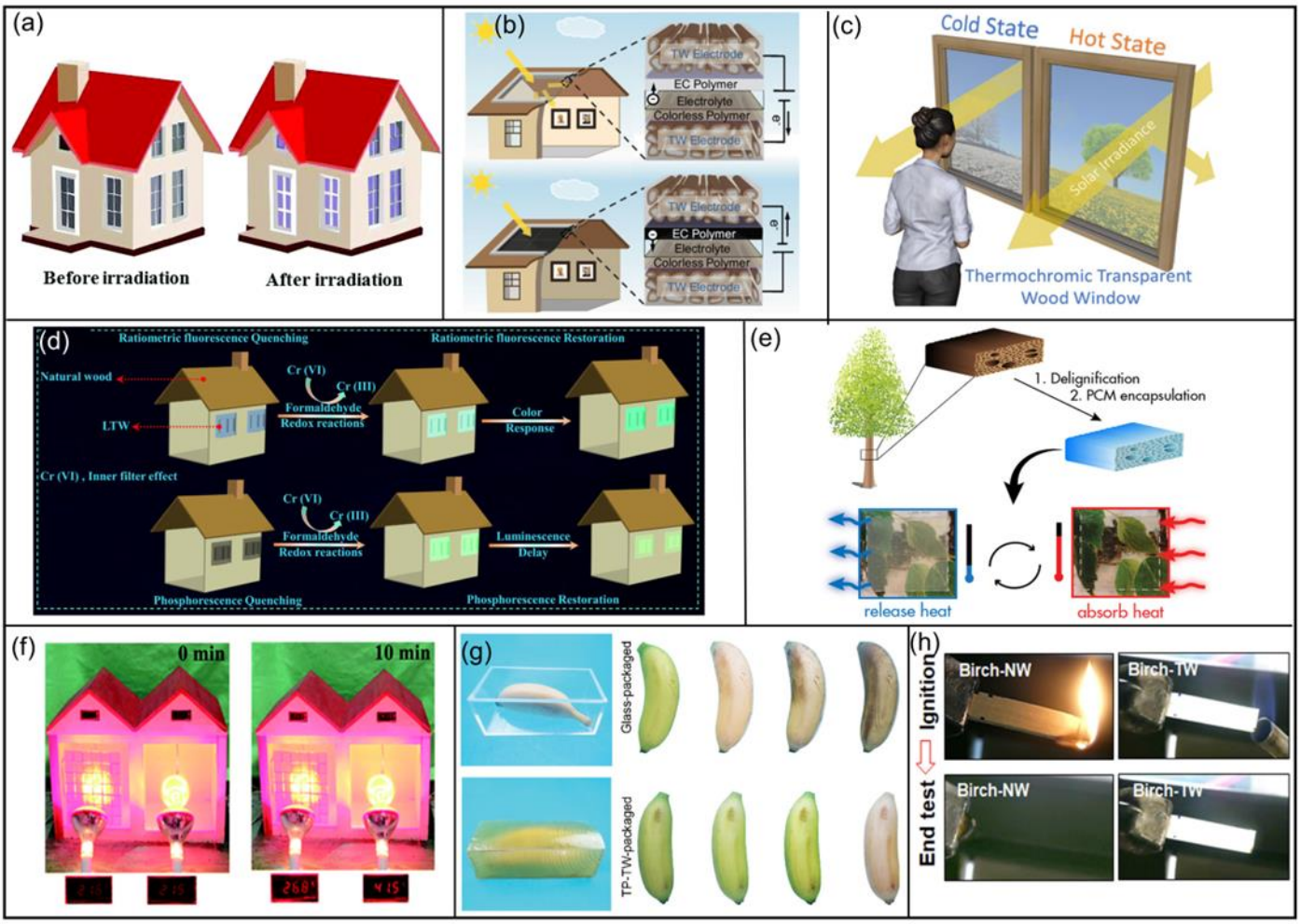

Figure.18 (a) Schematic of TW windows on building before irradiation and after irradiation, Reproduced with permission, Copyright 2019, Royal Society of chemistry [84]; (b) Demonstration of electrochromic TW for smart windows and roofs, Reproduced with permission, Copyright 2018, Wiley-VCH [66]; (c) The schematic illustration of thermochromic TW for smart windows, Reproduced with permission, Copyright 2021, American Chemical Society[90]; (d) Schematic of the TW based gas sensor for detection of FA gas, Reproduced with permission, Copyright 2020, American Chemical Society [128]; (e) Schematic illustration of TW for energy storage and release at different temperatures, Reproduced with permission, Copyright 2019, American Chemical Society [54]; (f) Images of model houses to show the temperature change after 10 min's simulate solar radiation, Reproduced with permission, Copyright 2017, Royal Society of chemistry [9a]; (g) Photo of glass-packaged (upper) and TP-TW-packaged (lower) banana after different treatment durations of solar radiation, Reproduced with permission, Copyright 2022, Wiley-VCH [123]; (h) Flammability test snapshots in horizontal and vertical direction, Reproduced with permission, Copyright 2022, Elsevier [56].

Extra functionalities boost the potential of TW in building application. Photochromic- [84], electrochromic- [116c], thermochromic- [9b, 96], luminescent- [128-129], thermal energy storage/release- [54, 130], NIR shielding- [9a, 9c], and UV-protective-TW [123, 129a] both have enhanced its the application value in some aspects. Specifically, the implementation of photochromic TW as windows would enhance the aesthetic appeal by introducing color changes (Fig. 18a), while also reducing total light exposure through UV absorption[84]. Similarly, the electrochromic TW also shows unique color changes behaviors and holds great promise for energy-efficient smart windows and roofs (Fig. 18b) [66]. Thermochromic TW, enabled by VO_2, allows for low/high NIR transmissions at high/low temperatures, providing considerable solar modulation [9b, 90]. This enables the use of TW as smart windows (Fig. 18c), providing improved indoor temperature control and,

consequently, reduced indoor energy consumption. Luminescent TW, obtained from impregnating multicolor lignin-derived carbon dots (CDs) and poly(vinyl alcohol) (PVA) into wood scaffold, provides dual-channel, real-time, and visual detection of formaldehyde gas (Fig. 18d) when used as windows [128]. Thermal energy storage TW absorbs heat at high temperatures (above the melting temperatures of the polyethylene glycol (PEG) polymers), and releases heat at low temperature (below the crystallization temperature of PEG polymers), allowing TW better to regulate indoor temperature when used as energy-saving windows (Fig. 18e) [54]. By blocking the majority of near infrared, NIR shielding TW reduces the indoor temperature increase caused by solar radiation (as shown in Fig. 18f). Therefore, NIR shielding TW is expected to further enhance the energy efficiency of buildings by reducing the cooling loads during hot hours [112]. UV radiation is imperceptible to the human eye, yet it poses a potential hazard and can inflict damage to various indoor items, including furniture and interior displays. Consider the common glass packaged banana, which showed signs of rotting on the exterior after 3 h of simulated solar radiation [123]. In contrast, the banana packaged with UV protective TW remained relatively fresh due to its thermal management and UV-blocking capabilities (Fig. 18g). The use of UV-protective TW creates a relatively UV-free environment, which is advantageous for prolonging the service life of indoor items. Despite the promising potential of TW in building applications, the issues of fire safety must be resolved before practical implementation can be achieved. The flammability of TW raises safety concerns regarding its practical application. To address these concerns, flame retardants or intrinsic flame-retardant polymers can be impregnated into wood scaffolds to increase the fire safety of TW [52, 56, 111-113, 131], but this may compromise the optical properties. For example, by selecting melamine formaldehyde as the impregnating polymer, the MF based TW showed excellent self-extinguishing performance (Fig. 18h).

4.2 Optoelectronic Devices

The intensive use of petroleum-based and non-renewable materials in optoelectronic devices, as well as the constant (i.e., frequently annual) output of updated product variants is having a huge detrimental impact on the environment, both in terms of waste as well as raw materials consumption. The transition towards sustainable materials for device components is a pressing need, prompting researchers and engineers to shift their focus to materials with high sustainability characteristics. TW substrates, prepared from sustainable processes and materials, offer great potential to replace all-plastic-based substrates in optoelectronic devices due to their high transparency/haze, potential flexibility, and electrical conductivity (when combined with suitable additives or architectures).

As discussed in *Section 3.3*, Zou et al. explored the AgNWs coating on TW by the Meyer technique. The prepared AgNWs coated TW exhibited a sheet resistance of 11 $\Omega \cdot sq^{-1}$ [97]. Similarly, flexible conductive TW was prepared by spraying coating with AgNWs, showing a much lower sheet resistance of 3 $\Omega \cdot sq^{-1}$ [98]. Both of the as-prepared conductive TW successfully lit up an LED (Fig.19a). Based on the flexible conductive TW, an alternating current electroluminescent (ACEL) system was successfully prepared by sandwiching a luminescent layer between two conductive electrodes, showing stable light-emitting stability even after partial destruction (Fig. 19b). Based on this research, Zhang et al. further fabricated thermal-resistant ACEL device [132]. The thermal expansion coefficient of TW (~$4\times10^{-6}K^{-1}$) substrate was much lower than that of others commonly used plastics (PET~$86\times10^{-6}K^{-1}$, Epoxy~$77\times10^{-6}K^{-1}$), providing higher light-emitting stability. The device also exhibited high humidity resistance and water resistance, indicating its great potential as a high-temperature-resistant ACEL device (Fig. 19c). Moreover, various patterns, such as mushroom, square, and trees, can be fabricated via controlling the shape of the top electrode substrate (Fig. 19d).

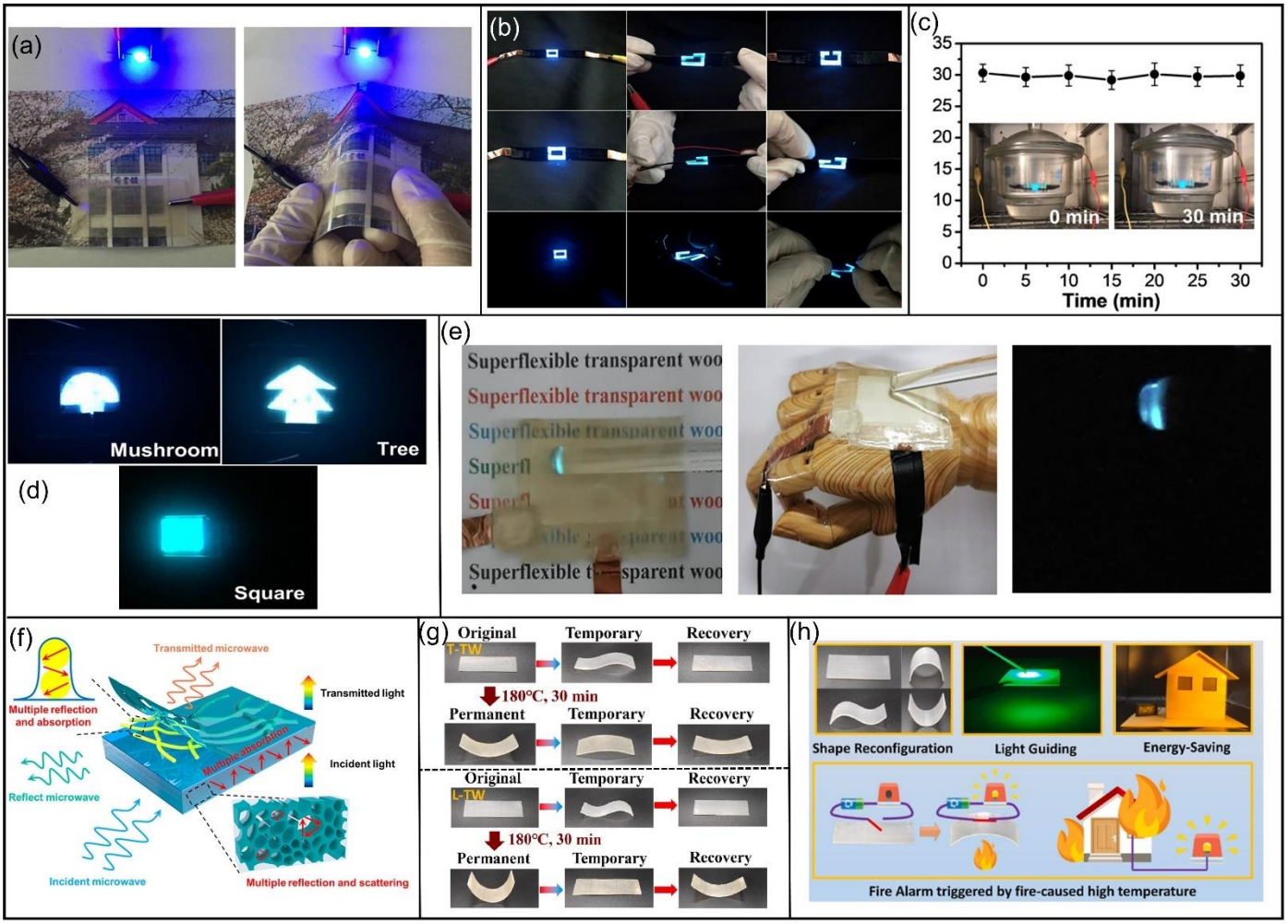

Figure.19 (a & b), Reproduced with permission, Copyright 2019, American Chemical Society [98]: (a) Photos of lighting up a LED using conductive TW under normal and bending states; (b) Photo to show the light-emitting stability after partial destruction,; (c & d), Reproduced with permission, Copyright 2019, American Chemical Society [132]:(c) Luminance changes of the TW based ACEL device under high temperature and humidity conditions; (d) Three different illumination patterns of the TW based ACEL[132]; (e) The electroluminescence of electronic skin on a flat surface and the surface of prosthesis, Reproduced with permission, Copyright 2022, Elsevier[10a]; (f) Schematic illustration of the working mechanism of the EMI shielding TW, Reproduced with permission, Copyright 2022, American Chemical Society[120]; (g & h), Reproduced with permission, Copyright 2022, Elsevier[105]: (g) Reconfigurable shape-memory performance of TW in two directions; (h) Schematic illustration of the fire alarm design.

TW based sensors have also been developed due to high sustainability and flexibility at low thickness. In 2020, Fu *et al.* reported on the creation of fully wood-based flexible electronics circuits using a strong, flexible and conductive TW film substrate was printed with a lignin-derived carbon NF conductive ink [94]. A hand-held TW based strain sensor based on such electronics circuits was successfully demonstrated, showing variation in relative resistance with individual finger movement (i.e., bending and straightening). Another demonstration was reported by Wang et al, where the as prepared conductive TW showed excellent sensing behaviors to strain/touch, even at low strain, implying that they could be readily used for the detection of weak pressures such as subtle bodily bend-release actions and other similar activities. In addition to strain sensors,

TW based temperature sensor was reported by Yang *et al.* in 2021, via an alternative DES filler route, involving AA/ChCl and a photo-initiated polymerization [96]. The conductivity of the flexible TW showed a monotonic increase or decrease when the temperature was raised or lowered, indicating a great potential for temperature sensing (Fig. 11c). Recently, a super flexible TW was prepared by impregnating biocompatible and flexible poly(ethylene glycol) diacrylate into a wood scaffold [10a]. The TW-based electrodes were prepared by depositing AgNWs ink on the surface of TW. A pressure sensor was then produced by sandwiching a pyramidal microstructure layer with stimuli-responsive behavior between two TW-based electrodes. The resultant wood-based e-skin exhibited exceptional electroluminescent response within the range of pressures (0 ~ 150 kPa) that are perceived as painful by humans (Fig. 19e). Apart from these applications, TW can also be used for electromagnetic interference (EMI) shielding applications. A TW based EMI shielding composite was fabricated by sandwiching TW between (AgNW)@MXene composites (Fig. 19f) [120]. A shape memory TW was prepared by infiltrating the polythiourethane covalent adaptable networks (PTU CANs) into the wood scaffold[105]. The prepared TW showed unique reconfigurable shape-memory performance (Fig. 19g). More interestingly, a fire alarm system was designed based on the shape memory behavior of TW, providing effective warning signs in case of fire (Fig. 19h).

The high haze and transmittance of TW also make it a promising alternative for a diffusely-transmitting solar cells (Fig. 6). For TW-PV, Zhu *et al.* first demonstrated that TW can be used for GaAs solar cells in 2016, where an 18% efficiency improvement versus bare GaAs cells (i.e., conversion efficiency of 14.41%) was obtained due to the high optical transmittance (~90%) and concurrent high haze (~80%) over a broad wavelength range between 400-1100 nm [73]. Another TW based solar cell demonstration was reported by Li et al., a power conversion efficiency of 16.8% was achieved with good long-term stability [74]. The enhanced power conversion may be attributed to reduced light reflection and increased light scattering. These two reports seemingly are the only TW-based solar cell demonstrations to-date, although the promising results ensure that many more will likely follow.

Overall, the optical, mechanical and thermal properties of TW make it a potential substitute for building envelopes in energy-efficient buildings and glazing applications. The extra functionalities (i.e., solar control, chromic, shape memory and conductive, etc.) enabled by various fillers or coating allows TW being used in other advanced applications, such as smart buildings, flexible optoelectronics, sensors, energy conversion and storage devices, EMI shielding and novel fire alarm. The integration of both structural and functional design in the development of TW is expected to broaden its application scope.

5. Summary and Outlook

Transparent wood (TW), one of the most promising contemporary wood-based materials for both commercial and research investigation, shows high optical transmittance and clarity (although the clarity is distance-dependent). It is made by selectively removing or modifying much of the lignin (i.e., delignification or lignin modification), then substituting with a suitable, refractive index-matched polymer. Extra functionalities combined with the intrinsic advantage of TW may extend the TW to other advanced applications. Developments into functional TW are still in the early stages, but it is a nascent area with enormous potential. We have covered seven of the most developed areas of functionalized TW in this review spanning; i) solar control; ii) chromically-responsive, iii) electrically-conductive, iv) shape-memory active; v) flame-retardant; vi) electromagnetic interference shielding; and vii) aesthetic, and their potential applications based on such functionalities.

Despite the various advantage of TW-based materials, several challenges still exist in the fabrication process. Problems that need to be addressed in the production of TW composites include the fact that the discoloration process is currently performed on a lab scale, which results in the production of small, low-thickness materials. High-throughput methods that can rapidly, efficiently and inexpensively prepare mechanically-robust, large-size TW-based systems on a large-scale, are required. To enable more widespread adoption, the current limitations of TW thickness, which currently only allows for thicknesses of the order of millimeters in most cases, need to be overcome. Another scale-up issue is the variable nature of wood properties due to its structural inconsistencies, whereas real-world application will require products with more stable performance and much narrower tolerance band of performance variation. There are seemingly no possible ways to address such structural variation in starting materials. But the variations in resultant products might be solved by strict quality management or directly turning the focus to high level of customization. Besides, the chemicals used in the manufacturing procedures is also a concern. Although the chemicals used for functionalization process may be largely different, those used in the fabrication process of TW substrates are quite similar (i.e., discoloration and impregnation phase). As discussed in Section 2.2, the chemicals and solvent used for delignification/lignin-modification and impregnating polymers are the main source of chemicals waste. To-date, there appear to be no reported discoloration or impregnating methods that entirely comply with green chemistry manufacturing principles. Most of the chemicals, polymers and solvent used for the fabrication are wasted without recycling. For example, during the impregnating process, only a small part of the polymer would be infiltrated into the wood scaffold, while much of the polymer is wasted. Another example is that lignin, which is otherwise removed and discarded in the TW formation process, is itself a great focus of research currently, due to the ability to convert it into high value products (e.g., fuels or bio-based composites) for many other fields. Therefore, the recycling of the lignin might a possible way to help achieve a closed-loop production cycle. Overall, a green mass production route that generate the minimal wastes and maximize the use of feedstock deserves more attention for future explorations.

In addition to manufacturing issues, the life cycle measurement, dimensional stability and further functional integration of such TW-based materials require more attention. TWs have usually been designed with a view to eventual outdoor and thermal applications. The impregnating polymers and additives are usually prone to environmental degradation when exposed to natural and thermal conditions, especially when UV light and a hot-humid environment are involved. To date, there seemingly are few reports exploring the life span of TW based materials under extreme conditions. Thus, there are also requirements for improvements in certain other properties of wood to be made, e.g., novel wood properties including UV-resistant, flame retardance, IR-reflective, thermal-stable, and anti-fungal, etc. Such improvements are required for extended life cycles, improved safety and enhanced physico-mechanical property requirements. The dimensional

stability of TW substrates is also a crucial factor for fabrication and real-world applications. Though introduction of impregnating polymers may overcome the moisture-dependent swelling and shrinkage of natural wood, the curing deformation and the resultant internal stress imbalances may cause dimensional instability and irreversible deformation. Such dimensional instability, particularly for coating processes, might result in the cracking of the coating layer and in extreme cases, the complete loss of functional efficacy. While various functionalities were achieved through either functional fillers or coating as reported in this review, the integration of multiple functionalities has rarely been reported to-date. This is an important next development step because in many cases, a sole functionality improvement may not be able to meet the practical applications requirements. For instance, solar control TW holds significant potential for building applications. However, before practical application, it is important to consider fundamental requirements for building safety, such as fire safety.

Overall, functional TWs, based on functional fillers, coatings or intrinsic structural design, will provide the biggest opportunity for maximizing the extraordinary potential and returns of all such bio-based materials. Functional TWs have a clear value proposition across a multitude of factors, including energy efficiency and operational savings with respect to architectural applications. Longer-term, such substrates will likely find use in the vast and expanding optoelectronic devices fields. We expect that the nascent and growing field of coated TW and TW composites to promise many exciting developments spanning various fields, including smart/energy-efficient buildings, optoelectronics, energy conversion, sensors, e-skins, and actuators, in years ahead.

Acknowledgements: All authors would like to thank the Hong Kong Environment and Conservation Fund (Grant code: ECF 107/2020, P0034081), and PolyU (1-BBCB) for funding.

Consent for publication: All authors agree to the submission and publication of article materials.

Conflicts of Interest: There are no known conflicts to declare.

Biographies:

Hu Xin received his B.S. (2018) in polymer material science and engineering from Changzhou university. He obtained his M.S. (2021) degrees in material science and engineering from Chongqing University. Currently, he is a PhD candidate at The Hong Kong Polytechnic University under the supervision of Dr Fei Bin and Dr Nuruzzaman Noor. His research focuses on functional transparent wood, flame retardant polymer, as well as their advanced applications in energy-efficient and high fire safety buildings.

Rujun YU received B.Eng. from School of Materials and Engineering, Sun Yat-sen University, Guangzhou, China in 2021. He is currently working toward the MPhil degree in School of Fashion & Textile, Hong

Kong Polytechnic University under the supervision of Dr Fei. His research interests include biobased composites, shape memory polymers and polymer synthesis.

Nuruzzaman Noor received his EngD in Materials Science in 2014 at University College London (UCL), under the supervision of Prof Ivan Parkin. This was followed in 2014–2015 with the pursuit of an EPSRC postdoctoral fellowship at UCL, focusing on the use of chemical vapour deposition (CVD) variants for functional thin films synthesis. In 2016, he started as a Research Assistant Professor at The Hong Kong Polytechnic University. Currently, his main research interests include; i) Sonochemical coatings and synthesis routes, and; ii) Transparent wood-based bio-composites and coatings.

Bin Fei, Associate Professor of School of Fashion & Textile, Hong Kong Polytechnic University, got B.S. from Dept. Appl. Chemistry, Chinese University of Science & Technology in 1996 and Ph.D. from Changchun Institute of Applied Chemistry, Chinese Academy of Sciences in 2003. With more than two decades experience in polymer and composites research, currently, Dr. Fei has been engaged in fundamental and applied research of bio-composites, energy devices, flame retardant, and energy saving.

References

[1] a) F. Wang, J. D. Harindintwali, Z. Yuan, M. Wang, F. Wang, S. Li, Z. Yin, L. Huang, Y. Fu, L. Li, S. X. Chang, L. Zhang, J. Rinklebe, Z. Yuan, Q. Zhu, L. Xiang, D. C. W. Tsang, L. Xu, X. Jiang, J. Liu, N. Wei, M. Kästner, Y. Zou, Y. S. Ok, J. Shen, D. Peng, W. Zhang, D. Barceló, Y. Zhou, Z. Bai, B. Li, B. Zhang, K. Wei, H. Cao, Z. Tan, L.-b. Zhao, X. He, J. Zheng, N. Bolan, X. Liu, C. Huang, S. Dietmann, M. Luo, N. Sun, J. Gong, Y. Gong, F. Brahushi, T. Zhang, C. Xiao, X. Li, W. Chen, N. Jiao, J. Lehmann, Y.-G. Zhu, H. Jin, A. Schäffer, J. M. Tiedje, J. M. Chen, *The Innovation* **2021**, 2, 100180; b) I. Ambat, V. Srivastava, M. Sillanpää, *Renewable and Sustainable Energy Reviews* **2018**, 90, 356; c) I. Coxhead, *World Development* **2007**, 35, 1099.

[2] D&R International Ltd, *2011 Buildings Energy Data Book, U.S. Department of Energy* **2012**.

[3] a) L. Pokrajac, A. Abbas, W. Chrzanowski, G. M. Dias, B. J. Eggleton, S. Maguire, E. Maine, T. Malloy, J. Nathwani, L. Nazar, A. Sips, J. i. Sone, A. van den Berg, P. S. Weiss, S. Mitra, *ACS Nano* **2021**, 15, 18608; b) L. D. Anadon, G. Chan, A. G. Harley, K. Matus, S. Moon, S. L. Murthy, W. C. Clark, *PANS* **2016**, 113, 9682; c) S. H. Ali, *Nature Materials* **2018**, 17, 1052; d) THE 17 GOALS, https://sdgs.un.org/goals, accessed.

[4] a) M. E. Puettmann, J. B. Wilson, *Wood and Fiber Science* **2005**, 18; b) D. Kretschmann, *Wood handbook : wood as an engineering material: chapter 5. Centennial ed. General technical report FPL ; GTR-190. Madison, WI : U.S. Dept. of Agriculture, Forest Service, Forest Products Laboratory* **2010**, 5.1; c) E. Toumpanaki, D. U. Shah, S. J. Eichhorn, **2021**, 33, 2001613.

[5] a) S. Johnsson, E. Andersson, P. Thollander, M. J. E. Karlsson, *Energy* **2019**, 187, 115919; b) T. Li, Y. Zhai, S. He, W. Gan, Z. Wei, M. Heidarinejad, D. Dalgo, R. Mi, X. Zhao, J. Song, J. Dai, C. Chen, A. Aili, A. Vellore, A. Martini, R. Yang, J. Srebric, X. Yin, L. Hu, *Science* **2019**, 364, 760; c) J. Huang, B. Zhao, T. Liu, J. Mou, Z. Jiang, J. Liu, H. Li, M. Liu, *Advanced Functional Materials* **2019**, 29, 1902255; d) H. Zhu, W. Luo, P. N. Ciesielski, Z. Fang, J. Y. Zhu, G. Henriksson, M. E. Himmel, L. Hu, *Chemical Reviews* **2016**, 116, 9305; e) G. Chen, T. Li, C. Chen, W. Kong, M. Jiao, B. Jiang, Q. Xia, Z. Liang, Y. Liu, S. He, L. Hu, *ACS Nano* **2021**, 15, 11244; f) Q. Xia, C. Chen, Y. Yao, S. He, X. Wang, J. Li, J. Gao, W. Gan, B. Jiang, M. Cui, L. Hu, *Advanced Materials* **2021**, 33, 2001588.

[6] X. Wang, T. Zhan, Y. Liu, J. Shi, B. Pan, Y. Zhang, L. Cai, S. Q. Shi, *ChemSusChem* **2018**, 11, 4086.

[7] a) S. Iwamoto, A. N. Nakagaito, H. Yano, M. Nogi, *Applied Physics A* **2005**, 81, 1109; b) M. Nogi, H. Yano, *Adv Mater* **2008**, 20, 1849.

[8] a) L. A. Berglund, I. Burgert, *Advanced Materials* **2018**, 30, 1704285; b) H. Cai, Z. Wang, D. Xie, P. Zhao, J. Sun, D. Qin, F. Cheng, *Journal of Forestry Research* **2021**, 32, 1779.

[9] a) Z. Yu, Y. Yao, J. Yao, L. Zhang, Z. Chen, Y. Gao, H. Luo, *Journal of Materials Chemistry A* **2017**, 5, 6019; b) L. Zhang, A. Wang, T. Zhu, Z. Chen, Y. Wu, Y. Gao, *ACS Applied Materials & Interfaces* **2020**, 12, 34777; c) Z. Qiu, Z. Xiao, L. Gao, J. Li, H. Wang, Y. Wang, Y. Xie, *Composites Science and Technology* **2019**, 172, 43.

[10] a) Q. Tang, M. Zou, L. Chang, W. Guo, *Chemical Engineering Journal* **2022**, 430, 132152; b) X. Hu, Y. Zhang, J. Zhang, H. Yang, F. Wang, F. Bin, N. Noor, *Renewable Energy* **2022**, 193, 398.

[11] a) Y. Li, Q. Fu, X. Yang, L. Berglund, *Philosophical Transactons of The Royal Society A: Mathematical, Physical and Engineering Sciences* **2018**, 376, 20170182; b) Y. Li, E. Vasileva, I. Sychugov, S. Popov, L. Berglund, *Advanced Optical Materials* **2018**, 6, 1800059.

[12] J. Zhang, A. Koubaa, Y. Tao, P. Li, D. Xing, *Current Forestry Reports* **2022**, 8, 333.

[13] J. Wang, J. G. Zhu, *Frontiers in Chemistry* **2021**, 9, 747385.

[14] S. Zhu, S. Kumar Biswas, Z. Qiu, Y. Yue, Q. Fu, F. Jiang, J. Han, *Progress in Materials Science* **2023**, 132, 101025.

[15] a) X. Shan, J. Wu, X. Zhang, L. Wang, J. Yang, Z. Chen, J. Yu, X. Wang, *Cell Reports Physical Science* **2021**, 2, 100654; b) J. Li, C. Chen, J. Y. Zhu, A. J. Ragauskas, L. Hu, *Accounts of Materials Research* **2021**, 2, 606; c) F. Jiang, T. Li, Y. Li, Y. Zhang, A. Gong, J. Dai, E. Hitz, W. Luo, L. Hu, *Adv Mater* **2018**, 30, 1703453.

[16] S. Fink, *Holzforschung* **1992**, 46, 403.

[17] Y. Li, Q. Fu, S. Yu, M. Yan, L. Berglund, *Biomacromolecules* **2016**, 17, 1358.

[18] M. Zhu, J. Song, T. Li, A. Gong, Y. Wang, J. Dai, Y. Yao, W. Luo, D. Henderson, L. Hu, *Adv Mater* **2016**, 28, 5181.

[19] U. G. K. Wegst, H. Bai, E. Saiz, A. P. Tomsia, R. O. Ritchie, *Nature Materials* **2015**, 14, 23.

[20] J. F. Katers, A. J. Snippen, M. E. Puettmann, *Forest Products Journal* **2012**, 62, 289.

[21] U. P. Agarwal, *Planta* **2006**, 224, 1141.

[22] R. Pettersen, *The Chemistry of Solid Wood. In Advances in Chemistry Series* **1984**, (Book 207) 57.

[23] a) J. Fahlén, L. Salmén, *Journal of Materials Science* **2003**, 38, 119; b) H. Yano, A. Hirose, S. Inaba, *Journal of Materials Science Letters* **1997**, 16, 1906.

[24] M. P. Ansell, in *Wood Composites*, DOI: https://doi.org/10.1016/B978-1-78242-454-3.00001-9 (Ed: M. P. Ansell), Woodhead Publishing **2015**, p. 3.
[25] C. Chen, Y. Kuang, S. Zhu, I. Burgert, T. Keplinger, A. Gong, T. Li, L. Berglund, S. J. Eichhorn, L. Hu, *Nature Reviews Materials* **2020**, 5, 642.
[26] J. Blomberg, B. Persson, A. Blomberg, *Wood Science and Technology* **2005**, 39, 339.
[27] B. J. Zobel, J. P. Van Buijtenen, *Wood variation: its causes and control*, Springer Science & Business Media, **2012**.
[28] F. Bertaud, B. Holmbom, *Wood Science and Technology* **2004**, 38, 245.
[29] A. Konstantinov, A. Lomunov, T. N. Iuzhina, G. Gray, *Problems of Strength and Plasticity* **2018**, 80, 555.
[30] a) Y. Wu, Y. Wang, F. Yang, *Frontiers in Materials* **2021**, 8, 633345; b) Q. Fu, M. Yan, E. Jungstedt, X. Yang, Y. Li, L. A. Berglund, *Composites Science and Technology* **2018**, 164, 296.
[31] a) M. H. Ramage, H. Burridge, M. Busse-Wicher, G. Fereday, T. Reynolds, D. U. Shah, G. Wu, L. Yu, P. Fleming, D. Densley-Tingley, J. Allwood, P. Dupree, P. F. Linden, O. Scherman, *Renewable and Sustainable Energy Reviews* **2017**, 68, 333; b) R. Parthasarathi, G. Bellesia, S. P. S. Chundawat, B. E. Dale, P. Langan, S. Gnanakaran, *The Journal of Physical Chemistry A* **2011**, 115, 14191.
[32] D. Hepworth, J. Vincent, G. Stringer, G. Jeronimidis, *Philosophical Transactions. Series A, Mathematical, Physical, and Engineering Sciences* **2002**, 360, 255.
[33] a) S. Antonsson, P. Mäkelä, C. Fellers, M. E. Lindström, *Nordic Pulp & Paper Research Journal* **2009**, 24, 409; b) N. Soltani, A. Bahrami, M. I. Pech-Canul, L. A. González, *Chemical Engineering Journal* **2015**, 264, 899.
[34] a) Y. Kamijo, M. Sugino, T. Miyanishi, *Japan Tappi Journal* **2015**, 69, 1125; b) in *Forest Products and Wood Science An Introduction*, DOI: https://doi.org/10.1002/9780470960035.ch5, Wiley **2011**, p. 79.
[35] H. R. Milner, A. C. Woodard, in *Sustainability of Construction Materials (Second Edition)*, DOI: https://doi.org/10.1016/B978-0-08-100370-1.00008-1 (Ed: J. M. Khatib), Woodhead Publishing **2016**, p. 159.
[36] a) X. Qin, Y. Lu, H. Xiao, W. Zhao, *Polymer Engineering & Science* **2013**, 53, 827; b) K. Li, X. Ni, Q. Wu, C. Yuan, C. Li, D. Li, H. Chen, Y. Lv, A. Ju, *Advanced Fiber Materials* **2022**, 4, 631; c) Z. Sun, Y. Lu, R. Wang, C. Yang, *Journal of Applied Polymer Science* **2021**, 138, 50247; d) B. Kasal, *Wood formation and properties| mechanical properties of wood*, In book: Encyclopedia of Forest Sciences **2004**.
[37] a) K. Freudenberg, *Journal of Chemical Education* **1932**, 9, 1171; b) L. Salmén, *Cellulose* **2022**, 29, 1349; c) R. Javier-Astete, J. Jimenez-Davalos, G. Zolla, *PLoS One* **2021**, 16, e0256559; d) J. Wang, E. Minami, H. Kawamoto, *Journal of Wood Science* **2020**, 66, 41; e) N. Zhang, S. Li, L. Xiong, Y. Hong, Y. Chen, *Modelling and Simulation in Materials Science and Engineering* **2015**, 23, 085010.
[38] Y. Wu, J. Wu, F. Yang, C. Tang, Q. Huang, *Polymers* **2019**, 11, 776.
[39] a) G. Buschle-Diller, X. D. Yang, R. Yamamoto, *Textile Research Journal* **2001**, 71, 388; b) P. Bajpai, A. Anand, P. K. Bajpai, *Biotechnology annual review* **2006**, 12, 349; c) G. K. Gupta, R. K. Kapoor, P. Shukla, in *Microbial Enzymes and Biotechniques: Interdisciplinary Perspectives*, DOI: 10.1007/978-981-15-6895-4_3 (Ed: P. Shukla), Springer Singapore, Singapore **2020**, p. 43.
[40] D. Huang, J. Wu, C. Chen, X. Fu, A. H. Brozena, Y. Zhang, P. Gu, C. Li, C. Yuan, H. Ge, M. Lu, M. Zhu, L. Hu, Y. Chen, **2019**, 31, 1903270.
[41] C. Montanari, Y. Ogawa, P. Olsén, L. A. Berglund, *Advanced science* **2021**, 8, 2100559.
[42] Y. Li, Q. Fu, R. Rojas, M. Yan, M. Lawoko, L. Berglund, **2017**, 10, 3445.
[43] Q. Xia, C. Chen, T. Li, S. He, J. Gao, X. Wang, L. Hu, *Science Advances* **2021**, 7, eabd7342.
[44] T. Li, M. Zhu, Z. Yang, J. Song, J. Dai, Y. Yao, W. Luo, G. Pastel, B. Yang, L. Hu, *Advanced Energy Materials* **2016**, 6, 1601122.
[45] H. Chen, C. Montanari, R. Shanker, S. Marcinkevicius, L. A. Berglund, I. Sychugov, *Advanced Optical Materials* **2022**, 10, 2102732.
[46] U. Müller, M. Rätzsch, M. Schwanninger, M. Steiner, H. Zöbl, *Journal of Photochemistry and Photobiology B: Biology* **2003**, 69, 97.
[47] Y. Li, X. Yang, Q. Fu, R. Rojas, M. Yan, L. Berglund, *Journal of Materials Chemistry A* **2018**, 6, 1094.
[48] M. Höglund, M. Johansson, I. Sychugov, L. A. Berglund, *ACS Applied Materials & Interfaces* **2020**, 12, 46914.
[49] R. Mi, T. Li, D. Dalgo, C. Chen, Y. Kuang, S. He, X. Zhao, W. Xie, W. Gan, J. Zhu, J. Srebric, R. Yang, L. Hu, *Advanced Functional Materials* **2020**, 30, 1907511.
[50] J. Qin, X. Li, Y. Shao, K. Shi, X. Zhao, T. Feng, Y. Hu, *Vacuum* **2018**, 158, 158.
[51] C. Montanari, P. Olsén, L. A. Berglund, *Green Chemistry* **2020**, 22, 8012.
[52] T. Chu, Y. Gao, L. Yi, C. Fan, L. Yan, C. Ding, C. Liu, Q. Huang, Z. Wang, *Advanced Composites and Hybrid Materials* **2022**, 5, 1821.
[53] J. Wu, Y. Liang, C. Xia, X. Ma, B. Fei, Y. Wu, S. Ge, J. Lu, J. Li, Z. Xia, *Advanced Materials Technologies* **2023**, 8, 2200704.

[54] C. Montanari, Y. Li, H. Chen, M. Yan, L. A. Berglund, *ACS Applied Materials & Interfaces* **2019**, 11, 20465.
[55] C. Jia, C. Chen, R. Mi, T. Li, J. Dai, Z. Yang, Y. Pei, S. He, H. Bian, S.-H. Jang, J. Y. Zhu, B. Yang, L. Hu, *ACS Nano* **2019**, 13, 9993.
[56] P. Samanta, A. Samanta, C. Montanari, Y. Li, L. Maddalena, F. Carosio, L. A. Berglund, *Composites Part A: Applied Science and Manufacturing* **2022**, 156, 106863.
[57] in *American Society for Testing and Materials*, West Conshohocken 2000.
[58] H. S. Yaddanapudi, N. Hickerson, S. Saini, A. Tiwari, *Vacuum* **2017**, 146, 649.
[59] H. Chen, A. Baitenov, Y. Li, E. Vasileva, S. Popov, I. Sychugov, M. Yan, L. Berglund, *ACS Applied Materials & Interfaces* **2019**, 11, 35451.
[60] a) K. E. O. Foster, R. Jones, G. M. Miyake, W. V. Srubar, *Composites Science and Technology* **2021**, 208, 108737; b) J. Zhou, W. Xu, *Journal of Materials Science* **2022**, 57, 5825.
[61] S. Reinelt, M. Tabatabai, N. Moszner, U. K. Fischer, A. Utterodt, H. Ritter, *Macromolecular Chemistry and Physics* **2014**, 215, 1415.
[62] a) E. Vasileva, H. Chen, Y. Li, I. Sychugov, M. Yan, L. Berglund, S. Popov, *Advanced Optical Materials* **2018**, 6, 1800999; b) E. Vasileva, A. Baitenov, H. Chen, Y. Li, I. Sychugov, M. Yan, L. Berglund, S. Popov, *Opt. Lett.* **2019**, 44, 2962.
[63] Y. Wu, J. Zhou, F. Yang, Y. Wang, J. Wang, J. Zhang, *Journal of Materials Science* **2021**, 56, 8000.
[64] a) C. Montanari, P. Olsén, L. A. Berglund, *Frontiers in Chemistry* **2021**, 9; b) J. Pang, A. Baitenov, C. Montanari, A. Samanta, L. Berglund, S. Popov, I. Zozoulenko, *Advanced Photonics Research* **2021**, 2, 2100135.
[65] Y. Wang, Y. Wu, F. Yang, L. Yang, J. Wang, J. Zhou, J. Wang, *Wood Science and Technology* **2022**, 56, 669.
[66] A. W. Lang, Y. Li, M. De Keersmaecker, D. E. Shen, A. M. Österholm, L. Berglund, J. R. Reynolds, *ChemSusChem* **2018**, 11, 854.
[67] E. Jungstedt, S. Östlund, L. A. Berglund, *Composites Science and Technology* **2022**, 225, 109492.
[68] J. H. Arehart, University of Colorado at Boulder, **2017**.
[69] a) Y. Wang, X. Zhang, X. Ding, P. Zhang, M. Shu, Q. Zhang, Y. Gong, K. Zheng, X. Tian, *Composites Part B: Engineering* **2020**, 199, 108267; b) K. Uetani, K. Takahashi, R. Watanabe, S. Tsuneyasu, T. Satoh, *ACS Applied Materials & Interfaces* **2022**, 14, 33903.
[70] W. A. Mehdi, A. A. Mehde, M. Özacar, Z. Özacar, *International journal of biological macromolecules* **2018**, 117, 947.
[71] P. Bisht, K. K. Pandey, H. C. Barshilia, *Polymer Degradation and Stability* **2021**, 189, 109600.
[72] H. Guo, D. Klose, Y. Hou, G. Jeschke, I. Burgert, *ACS Applied Materials & Interfaces* **2017**, 9, 39040.
[73] M. Zhu, T. Li, C. S. Davis, Y. Yao, J. Dai, Y. Wang, F. AlQatari, J. W. Gilman, L. Hu, *Nano Energy* **2016**, 26, 332.
[74] Y. Li, M. Cheng, E. Jungstedt, B. Xu, L. Sun, L. Berglund, *ACS Sustainable Chemistry & Engineering* **2019**, 7, 6061.
[75] LONGi, At 26.81%, LONGi sets a new world record efficiency for silicon solar cells, https://www.longi.com/en/news/propelling-the-transformation/, accessed.
[76] a) H. Helmers, E. Lopez, O. Höhn, D. Lackner, J. Schön, M. Schauerte, M. Schachtner, F. Dimroth, A. W. Bett, *physica status solidi (RRL) - Rapid Research Letters* **2021**, 15, 2100113; b) T. Shan, X. Qi, *Infrared Physics & Technology* **2015**, 71, 144; c) G. E. Arnaoutakis, J. Marques-Hueso, A. Ivaturi, K. W. Krämer, S. Fischer, J. C. Goldschmidt, B. S. Richards, *Opt. Express* **2014**, 22, A452.
[77] Y. Wang, S. R. Kavanagh, I. Burgués-Ceballos, A. Walsh, D. O. Scanlon, G. Konstantatos, *Nature Photonics* **2022**, 16, 235.
[78] C. G. Granqvist, P. C. Lansåker, N. R. Mlyuka, G. A. Niklasson, E. Avendaño, *Solar Energy Materials and Solar Cells* **2009**, 93, 2032.
[79] a) C. Haratoka, R. A. Yalcin, H. Erturk, *Solar Energy* **2022**, 241, 637; b) N. A. Fleer, K. E. Pelcher, K. Nieto, E. J. Braham, J. Zou, G. A. Horrocks, Y. Naoi, S. W. Depner, B. J. Schultz, J. Amano, D. G. Sellers, S. Banerjee, in *ACS omega*, Vol. 3, 2018, 14280.
[80] L. Zhao, E. Strobach, B. Bhatia, S. Yang, A. Leroy, L. Zhang, E. N. Wang, *Opt. Express* **2019**, 27, A39.
[81] L. Tang, L. Wang, X. Yang, Y. Feng, Y. Li, W. Feng, *Progress in Materials Science* **2021**, 115, 100702.
[82] S. Wang, H. Chen, K. Li, S. Koskela, L. A. Berglund, Q. Zhou, *Composites Part A: Applied Science and Manufacturing* **2022**, 154, 106757.
[83] K. Li, S. Wang, H. Chen, X. Yang, L. A. Berglund, Q. Zhou, *Adv Mater* **2020**, 32, 2003653.
[84] L. Wang, Y. Liu, X. Zhan, D. Luo, X. Sun, *Journal of Materials Chemistry C* **2019**, 7, 8649.
[85] Y. Liu, H. Yang, Y. Wang, C. Ma, S. Luo, Z. Wu, Z. Zhang, W. Li, S. Liu, *Chemical Engineering Journal* **2021**, 424, 130426.
[86] C. Montanari, H. Chen, M. Lidfeldt, J. Gunnarsson, P. Olsén, L. A. Berglund, *Small* **2023**, n/a, 2301262.

[87] A. Samanta, H. Chen, P. Samanta, S. Popov, I. Sychugov, L. A. Berglund, *ACS Applied Materials & Interfaces* **2021**, 13, 3270.
[88] S. Al-Qahtani, E. Aljuhani, R. Felaly, K. Alkhamis, J. Alkabli, A. Munshi, N. El-Metwaly, *Industrial & Engineering Chemistry Research* **2021**, 60, 8340.
[89] L. Liu, G. Zhu, Y. Chen, Z. Liu, L. Donaldson, X. Zhan, H. Lian, Q. Fu, C. Mei, *Industrial Crops and Products* **2022**, 184, 115050.
[90] S. Liu, C. Y. Tso, H. H. Lee, Y. W. Du, K. M. Yu, S.-P. Feng, B. Huang, *ACS Applied Materials & Interfaces* **2021**, 13, 22495.
[91] S. Liu, C. Y. Tso, Y. W. Du, L. C. Chao, H. H. Lee, T. C. Ho, M. K. H. Leung, *Applied Energy* **2021**, 297, 117207.
[92] a) C. G. Granqvist, in *Nanotechnology in Eco-efficient Construction (Second Edition)*, DOI: https://doi.org/10.1016/B978-0-08-102641-0.00020-7 (Eds: F. Pacheco-Torgal, M. V. Diamanti, A. Nazari, C. G. Granqvist, A. Pruna, S. Amirkhanian), Woodhead Publishing **2019**, p. 467; b) M. Hočevar, S. Bogati, A. Georg, U. Opara Krašovec, *Solar Energy Materials and Solar Cells* **2017**, 171, 85; c) Y. Cui, Y. Ke, C. Liu, Z. Chen, N. Wang, L. Zhang, Y. Zhou, S. Wang, Y. Gao, Y. Long, *Joule* **2018**, 2, 1707.
[93] M. Wang, R. Li, G. Chen, S. Zhou, X. Feng, Y. Chen, M. He, D. Liu, T. Song, H. Qi, *ACS Applied Materials & Interfaces* **2019**, 11, 14313.
[94] Q. Fu, Y. Chen, M. Sorieul, *ACS Nano* **2020**, 14, 3528.
[95] J. Wu, Q. Liang, X. Yu, Q.-F. Lü, L. Ma, X. Qin, G. Chen, B. Li, *Advanced Functional Materials* **2021**, 31, 2011102.
[96] L. Yang, Y. Wu, F. Yang, W. Wang, *Journal of Materials Research and Technology* **2021**, 15, 5396.
[97] Q. Tang, L. Fang, Y. Wang, M. Zou, W. Guo, *Nanoscale* **2018**, 10, 4344.
[98] T. Zhang, P. Yang, Y. Li, Y. Cao, Y. Zhou, M. Chen, Z. Zhu, W. Chen, X. Zhou, *ACS Sustainable Chemistry & Engineering* **2019**, 7, 11464.
[99] a) S. C. Dixon, D. O. Scanlon, C. J. Carmalt, I. P. Parkin, *Journal of Materials Chemistry C* **2016**, 4, 6946; b) C. Sotelo-Vazquez, N. Noor, A. Kafizas, R. Quesada-Cabrera, D. O. Scanlon, A. Taylor, J. R. Durrant, I. P. Parkin, *Chemistry of Materials* **2015**, 27, 3234; c) A. Kafizas, N. Noor, C. J. Carmalt, I. P. Parkin, *Journal of Materials Chemistry C* **2013**, 1, 6335; d) A. Kafizas, N. Noor, P. Carmichael, D. O. Scanlon, C. J. Carmalt, I. P. Parkin, *Advanced Functional Materials* **2014**, 24, 1758.
[100] a) B. Kumar, N. Noor, S. Thakur, N. Pan, H. Narayana, S.-c. Yan, F. Wang, P. Shah, *ACS Omega* **2019**, 4, 15348; b) M. D. Hager, S. Bode, C. Weber, U. S. Schubert, *Progress in Polymer Science* **2015**, 49-50, 3; c) L. Sun, W. M. Huang, Z. Ding, Y. Zhao, C. C. Wang, H. Purnawali, C. Tang, *Materials & Design* **2012**, 33, 577; d) J. Hu, S. Zhu, R. J. Young, Z. Cai, L. Li, J. Han, N. Pan, *Journal of Materials Chemistry A* **2017**, 5, 503; e) M. Behl, M. Y. Razzaq, A. Lendlein, *Adv Mater* **2010**, 22, 3388; f) M. Behl, A. Lendlein, *Materials Today* **2007**, 10, 20.
[101] a) Y. Yang, Y. Xu, Y. Ji, Y. Wei, *Progress in Materials Science* **2020**, 120, 100710; b) F. I. Altuna, C. E. Hoppe, R. J. J. Williams, *Polymers* **2018**, 10, 43.
[102] a) J. Zheng, Z. M. Png, S. H. Ng, G. X. Tham, E. Ye, S. S. Goh, X. J. Loh, Z. Li, *Materials Today* **2021**, 51, 586; b) T. X. Wang, H. M. Chen, A. V. Salvekar, J. Lim, Y. Chen, R. Xiao, W. M. Huang, *Polymers* **2020**, 12, 2330; c) J. Joe, J. Shin, Y. S. Choi, J. H. Hwang, S. H. Kim, J. Han, B. Park, W. Lee, S. Park, Y. S. Kim, D. G. Kim, *Advanced science* **2021**, 8, e2103682.
[103] K. Wang, Y. Dong, Z. Ling, X. Liu, S. Q. Shi, J. Li, *Composites Science and Technology* **2021**, 207, 108690.
[104] K. Wang, X. Liu, Y. Dong, Z. Ling, Y. Cai, D. Tian, Z. Fang, J. Li, *Cellulose* **2022**, 29, 7955.
[105] K. Wang, T. Zhang, C. Li, X. Xiao, Y. Tang, X. Fang, H. Peng, X. Liu, Y. Dong, Y. Cai, D. Tian, Y. Li, J. Li, *Composites Part B: Engineering* **2022**, 246, 110260.
[106] A. D. Easley, M. B. B. Monroe, S. M. Hasan, A. C. Weems, J. Frederick, D. J. Maitland, *Journal of Applied Polymer Science* **2019**, 136, 47268.
[107] a) T. Ware, K. Hearon, A. Lonnecker, K. L. Wooley, D. J. Maitland, W. Voit, *Macromolecules* **2012**, 45, 1062; b) Z. Tang, J. Yang, J. Gong, X. Zhang, S. Chen, Q. Wang, T. Wang, J. Zhang, Y. Zhang, *Reactive and Functional Polymers* **2021**, 166, 104982.
[108] R. M. Nussbaum, *Journal of Fire Sciences* **1988**, 6, 290.
[109] a) L. A. Lowden, T. R. Hull, *Fire Science Reviews* **2013**, 2, 4; b) Z.-P. Deng, T. Fu, X. Song, Z.-L. Wang, D.-M. Guo, Y.-Z. Wang, F. Song, *Polymers* **2022**, 14, 3944; c) C. Fan, Y. Gao, Y. Li, L. Yan, D. Zhu, S. Guo, C. Ou, Z. Wang, *Wood Science and Technology* **2022**, DOI: 10.1007/s00226-022-01415-9.
[110] a) B. Tawiah, B. Yu, W. Yang, R. K. K. Yuen, B. Fei, *Cellulose* **2019**, 26, 4629; b) X. Hu, H. Yang, Y. Jiang, H. He, H. Liu, H. Huang, C. Wan, *Journal of Hazardous Materials* **2019**, 379, 120793; c) X. Hu, M. Li, J. Yang, F. Liu, H. Huang, H. Pan, H. Yang, *Applied Clay Science* **2021**, 201, 105934.

[111] L. Chen, Z. Xu, F. Wang, G. Duan, W. Xu, G. Zhang, H. Yang, J. Liu, S. Jiang, *Composites Communications* **2020**, 20, 100355.
[112] A. Samanta, M. Höglund, P. Samanta, S. Popov, I. Sychugov, L. Maddalena, F. Carosio, L. A. Berglund, *Advanced Sustainable Systems* **2022**, 6, 2100354.
[113] L. Zhang, Y. Jiang, L. Zhou, Z. Jiang, L. Li, W. Che, Y. Yu, *Journal of Materials Science* **2022**, 57, 3348.
[114] X. Li, Z. Huang, C. E. Shuck, G. Liang, Y. Gogotsi, C. Zhi, *Nature Reviews Chemistry* **2022**, 6, 389.
[115] a) Z. Chen, P. Xiao, J. Zhang, W. Tian, R. Jia, H. Nawaz, K. Jin, J. Zhang, *Chemical Engineering Journal* **2020**, 379, 122270; b) W. Xing, P. Zhang, L. Song, X. Wang, Y. Hu, *Materials Research Bulletin* **2014**, 49, 1; c) X. Wang, J. Zhan, W. Xing, X. Wang, L. Song, X. Qian, B. Yu, Y. Hu, *Industrial & Engineering Chemistry Research* **2013**, 52, 5548; d) W. Xing, L. Song, G. Jie, X. Lv, X. Wang, Y. Hu, *Polymers for Advanced Technologies* **2011**, 22, 2123; e) B. Yu, Y. Tao, L. Liu, Y. Shi, H. Yang, G. Jie, S. Lo, Q. Tai, L. Song, Y. Hu, *RSC Advances* **2015**, 5, 75254.
[116] a) Z. Ma, X. Xiang, L. Shao, Y. Zhang, J. Gu, **2022**, 61, e202200705; b) H. Lv, Z. Yang, P. L. Wang, G. Ji, J. Song, L. Zheng, H. Zeng, Z. J. Xu, *Adv Mater* **2018**, 30, 1706343; c) F. Shahzad, M. Alhabeb, C. B. Hatter, B. Anasori, S. Man Hong, C. M. Koo, Y. Gogotsi, *Science* **2016**, 353, 1137; d) J.-M. Thomassin, C. Jérôme, T. Pardoen, C. Bailly, I. Huynen, C. Detrembleur, *Materials Science and Engineering: R: Reports* **2013**, 74, 211.
[117] a) H. Abbasi, M. Antunes, J. I. Velasco, *Progress in Materials Science* **2019**, 103, 319; b) J. Lipton, J. A. Röhr, V. Dang, A. Goad, K. Maleski, F. Lavini, M. Han, E. H. R. Tsai, G.-M. Weng, J. Kong, E. Riedo, Y. Gogotsi, A. D. Taylor, *Matter* **2020**, 3, 546; c) C. Liang, H. Qiu, P. Song, X. Shi, J. Kong, J. Gu, *Science Bulletin* **2020**, 65, 616.
[118] S.-S. Cho, S.-H. Song, I.-P. Hong, *Microwave and Optical Techology Letters* **2021**, 63, 2237.
[119] N. A. Muhammad, B. Armynah, D. Tahir, *Materials Research Bulletin* **2022**, 154, 111930.
[120] M. Cheng, M. Ying, R. Zhao, L. Ji, H. Li, X. Liu, J. Zhang, Y. Li, X. Dong, X. Zhang, *ACS Nano* **2022**, 16, 16996.
[121] a) M. C. Beardsley, *Metaphilosophy* **1970**, 1, 39; b) C. Zomer, A. Nobre, P. Cassatella, T. Reindl, R. Rüther, *Progress in Photovoltaics: Research and Applications* **2014**, 22, 744.
[122] R. Mi, C. Chen, T. Keplinger, Y. Pei, S. He, D. Liu, J. Li, J. Dai, E. Hitz, B. Yang, I. Burgert, L. Hu, *Nature Communications* **2020**, 11, 3836.
[123] J. Zhou, Y. Liu, Z. Yang, X. Wang, Y. Li, F. Liu, Z. Jiang, X. Sun, X. Li, Y. Zhao, C. Wang, S.-H. Ho, H. Yang, *Advanced Sustainable Systems* **2022**, 6, 2200132.
[124] a) S. M. Khoshnava, R. Rostami, R. Mohamad Zin, D. Štreimikienė, A. Mardani, M. Ismail, *International journal of environmental research and public health* **2020**, 17; b) L. Li, P. Wang, H. Wang, M. Zhang, *AASRI Procedia* **2012**, 3, 381; c) Y. Zhang, K. Shan, X. Li, H. Li, S. Wang, *Renewable and Sustainable Energy Reviews* **2023**, 171, 112991.
[125] a) M. Bechthold, J. C. Weaver, *Nature Reviews Materials* **2017**, 2, 17082; b) J. J. Kaschuk, Y. Al Haj, O. J. Rojas, K. Miettunen, T. Abitbol, J. Vapaavuori, *Adv Mater* **2022**, 34, 2104473.
[126] D. D. Furszyfer Del Rio, B. K. Sovacool, A. M. Foley, S. Griffiths, M. Bazilian, J. Kim, D. Rooney, *Renewable and Sustainable Energy Reviews* **2022**, 155, 111885.
[127] A. N. Subba Rao, G. B. Nagarajappa, S. Nair, A. M. Chathoth, K. K. Pandey, *Composites Science and Technology* **2019**, 182, 107719.
[128] Y. Liu, H. Yang, C. Ma, S. Luo, M. Xu, Z. Wu, W. Li, S. Liu, *ACS Applied Materials & Interfaces* **2020**, 12, 36628.
[129] a) A. Aldalbahi, M. E. El-Naggar, T. A. Khattab, M. Hossain, *Luminescence* **2021**, 36, 1922; b) Y. Li, S. Yu, J. G. C. Veinot, J. Linnros, L. Berglund, I. Sychugov, *Advanced Optical Materials* **2017**, 5, 1600834.
[130] R. Xia, W. Zhang, Y. Yang, J. Zhao, Y. Liu, H. Guo, *Journal of Cleaner Production* **2021**, 296, 126598.
[131] C. Fan, Y. Gao, Y. Li, L. Yan, Y. Zhuang, Y. Zhang, Z. Wang, *Journal of Applied Polymer Science* **2022**, 139, e52945.
[132] T. Zhang, P. Yang, M. Chen, K. Yang, Y. Cao, X. Li, M. Tang, W. Chen, X. Zhou, *ACS Applied Materials & Interfaces* **2019**, 11, 36010.